Passive Acoustic Monitoring of WEather Patterns in the Ocean

Collins, Melanie

Award date:
2011

Awarding institution:
University of Bath

ABSTRACT

Weather observations form a crucial part of meteorological forecasts and are also used as input to climate models and for monitoring long-term climate trends and changes. But coverage at sea is much less dense spatially and temporally, especially at high latitudes. Passive underwater acoustics has been established for several decades as a good and reliable tool to monitor the weather. The frequency spectra of different weather types have been well documented and acoustic disdrometers have been developed in several research environments. Nevertheless, many questions remain about the validity of some of these measurements, the best analysis approaches and the combination of different weather processes. This is particularly true in polar regions, where the loud and complex acoustics of ice-related processes adds to the difficulty of the task.

This thesis focuses on the analysis of a broadband dataset acquired in an Arctic fjord (Kongsfjord, Svalbard), in summer 2007. Taken at 6 locations from the mouth of the fjord to the glaciers at its termination, measurements cover the combination of varying levels of rain (from none to light rain), wind (from none to 11 km/h), ice (from none to growlers and bergy bits), shipping (from none to a large cruise ship) and animal activity (including whales and diving seabirds). The recordings covered frequencies from 100 Hz to 48 kHz. Principal-Components Analysis identified 3 distinct frequency bands mostly related to noise from wind, rain and ice. Laboratory-based tank experiments were conducted to assess the physical sources of these components (from 100 Hz to 100 kHz), confirming the acoustic role of ice and the relevance of the frequency bands identified by Principal-Component Analysis. These experiments also identified for the first time the role of higher (up to 45 kHz) acoustic frequencies in the identification of ice-related processes such as scraping, colliding and melting.

Principal-Component Analysis is shown to be a valuable and rigorous tool for identifying weather processes at sea, especially in complex combinations of wind, rain, ice and other factors. Analyses at frequencies higher than generally used also offer the potential of identifying specific processes associated to the melting of glaciers and icebergs. This has paved the way for field measurements at glaciers around Svalbard in summer 2009. The approach presented here is now considered by

the Meteorological Office (UK) for inclusion on operational present-weather sensors attached to moored or drifting buoys in polar and high-latitude regions in general.

ACKNOWLEDGMENTS

I would like to thank the Engineering and Physical Sciences Research Council for funding this project through a DTA grant. Their support was greatly appreciated.

I was told before embarking on my PhD that choosing 'the perfect supervisor' was the most important part. I could not have made a better choice than Philippe. He is a superb leader and his passion for his work is inspiring. Not only did he help to supervise my project, giving me guidance and always taking time to talk to me about work, but he always had time to chat about the work-leisure balance and his tips on tact and diplomacy were incredibly useful in my wedding-related dramas. So I would like to express my deepest gratitude to Philippe for sharing his knowledge with me and for teaching me some valuable life skills. Oh, and for always having a bizarre anecdote to reassure me that things could have been much worse. Please keep in touch with your funny stories and tips on how to be tactful.

I consider myself lucky to have been in a small but very friendly research group during my PhD. After moving to a smaller office with just two occupants instead of eight, which was less afflicted by the wind but with no radiators, I particularly enjoyed my long chats with Russell. Not only did he always have time to help with my Matlab issues but he probably supplied about half of the food I consumed over a couple of years (I'm really sorry for eating all of your Doritos, Russell, and I must confess that I quite often stole your food when you weren't around). I'm not entirely sure what you should normally expect from a fellow PhD student but I am grateful that Russell was always happy to spend his time with me, whether that was to help attack some ice blocks in the biology department's greenhouse, to feed the ducklings as a thesis-writing break, to go hunting for house moving boxes or just to daydream about cheeseburgers.

Having mentioned the biology department I must thank Ewan Basterfield for kindly responding to my plea and loaning me his freezers. They created some splendid blocks of ice and I hope I didn't make too much mess.

I would like to also thank all of the other members of the Department of Physics, particularly Charlene and Alexis, who were excellent lunch friends. Charlene was also kind enough to help paint my bathroom in return for some junk food, so extra thanks for that! My friends outside of university (especially Christine and Brown) have always been incredibly supportive and I appreciate their endless supplies of hospitality, cake, wine and jokes, it makes everything, from writing a thesis to putting up with a house-destroying crazy cat, more fun. And to my new friends at the Met Office – thank you for all the advice and words of encouragement.

Of course I must acknowledge the support of my family, who have never pressured me into choosing any career path except the one which makes me happy. At times, trying to save for (and organise) the wedding of the century and study full time felt like the hardest thing anybody had ever done, but the fact that I genuinely loved the work I was doing definitely made it an easier load to bear. And Meghan, I am amazed by your unfaltering belief that I am the coolest geek in the world and have a gnawing worry that one day my biggest fan will realise that I am a big incompetent doofus who trips over things which don't exist, stabs herself in the eye with mascara and quite often puts her clothes on inside out. Hopefully by the time you realise these things you'll have mastered the art of hiding your true feelings and I'll carry on living in blissful ignorance.

And finally, I thank my husband, Liam. I will be honest – one of my main hopes for university was to find a husband, and not only did I find a very good one but I had an incredible time and it has led to the job of my dreams. Thank you for making everything so much fun and for constantly humouring me that my infatuation with underwater acoustics is even a tiny bit interesting to you. Thank you also for so willingly preparing all of my meals – see the previous paragraphs regarding the cheeseburgers and Doritos for evidence that left to my own devices, my insides would have probably given up all hope in 2004. Thanks also for keeping Chloe from driving me completely insane. Chloe – I do not owe you any thanks for helping with this thesis as your paper-ripping and incessant wall-scratching drove me crazy. However, you are the cutest cat in the world so I will forgive you. Be warned though, if you chew up the bound copy of this thesis then you will never sleep on my bed again.

CONTENTS

LIST OF FIGURES

CHAPTER 2

CHAPTER 5

CHAPTER 6

LIST OF TABLES

CHAPTER 2

CHAPTER 3

CHAPTER 5

CHAPTER 1 – INTRODUCTION

1.1. RATIONALE

Weather observations form a crucial part of meteorological forecasts and are also used as input to climate models and for monitoring long-term climate trends and changes. Weather at sea is also an important part of flux exchanges between the ocean and atmosphere but despite advances in satellite imaging (e.g. Robinson (2004)), quantitative in-situ measurements of processes like rainfall are still hard to provide (e.g. Quartly (2010)).

A dense network of land-based observations exists, with operators ranging from national weather services to volunteers. However, at sea, the coverage of weather observations is much less dense, consisting of observations from moored and drifting buoys, volunteer observing ships, weather radars (close to shores) and satellite observations. These excel at giving an overall picture of the weather at a particular time over a large area, but their spatial and temporal resolution leave a requirement for extra observations. This is particularly true in polar regions, with poor spatial coverage from geostationary satellites and sparse temporal coverage from near-polar satellites. This is compounded by their frequent, dense cloud cover and the difficulty of *in situ* validation. Passive underwater acoustics has been established for several decades as a good and reliable tool to monitor the weather. The frequency spectra of different weather types have been well documented and acoustic disdrometers have been developed in several research environments. Nevertheless, many questions remain about the validity of some of these measurements, the best analysis approaches and the combination of different weather processes. This is particularly true in polar regions, where the loud and complex acoustics of ice-related processes adds to the difficulty of the task.

This thesis focuses on the analysis of a broadband dataset acquired in an Arctic fjord (Kongsfjord, Svalbard), in summer 2007. Taken at 6 locations from the mouth of the fjord to the glaciers at its termination, measurements cover the combination of varying levels of rain (from none to light rain), wind (from none to 11 $km.h^{-1}$), ice (from none to growlers and bergy bits), shipping (from none to a large cruise ship) and animal activity (including whales and diving seabirds). The recordings covered frequencies from 100 Hz to 48 kHz. Principal-Components Analysis identified 3 distinct frequency bands mostly related to noise from wind, rain and ice. Laboratory-based tank experiments were conducted to assess the physical sources of these components (from 100 Hz to 100 kHz), confirming the acoustic role of ice and the relevance of the frequency bands identified by Principal-Component Analysis. These experiments also identified for the first time the role of higher (up to 45 kHz) acoustic frequencies in the identification of ice-related processes such as scraping, colliding and melting.

Principal-Component Analysis is shown to be a valuable and rigorous tool for identifying weather processes at sea, especially in complex combinations of wind, rain, ice and other factors. Analyses at frequencies higher than generally used also offers the potential of identifying specific processes associated to the melting of glaciers and icebergs. This has paved the way for field measurements at glaciers around Svalbard in summer 2009. The approach presented here is now considered by the Meteorological Office (UK) for inclusion on operational present-weather sensors attached to moored or drifting buoys in polar and high-latitude regions in general.

1.2.THE ROLE OF UNDERWATER ACOUSTICS

Acoustic waves are frequently used to obtain measurements in water, since they suffer less attenuation than other methods, such as light. The applications of underwater acoustics are diverse, including imagery of the seabed topography, monitoring the ocean temperature and data transmission. While active acoustics, which involves sending a signal from a transmitter to a receiver, is often used to obtain information about specific targets, passive acoustics, which relies on the sound emitted by a target, is usually the most appropriate method for observing

weather-related noise underwater. Underwater acoustics can monitor weather patterns at sea which occur from below 1 kHz to 50 kHz, which corresponds to propagation distances from several kilometres to tens of kilometres.

1.3.PROJECT AIMS

Research published previously showed that underwater acoustics had been used to monitor weather patterns for several decades. Earlier work included research by Knudsen (1948) which showed how the frequency spectrum of the underwater noise caused by wind varied with the wind speed. Research had also been carried out by several authors into using underwater acoustics to determine the drop size distribution of rainfall (Nystuen 2001; Quartly 2001) and some findings discussed the underwater noise related to ice (Farmer and Xie 1989). Despite the numerous and detailed findings of other scientists, many publications had indicated where extra research was needed. Often, the experiments had not extended to frequencies above 50 kHz, particularly with experiments relating to noise from ice, where few documented experiments had considered frequencies above 10 kHz. When using underwater acoustics to investigate the drop size distribution, particular frequencies had been chosen as acoustic discriminants, but with disagreement between different authors as to the most appropriate frequencies to use. Therefore, after analysing a dataset containing noise from various weather types in an Arctic fjord, and several more obtained from tank experiments aimed to identify a more rigorous and repeatable method of selecting frequencies to use as acoustic discriminants, to separate weather processes from within a large dataset. The further experiments and analysis also aimed to investigate whether using higher frequencies in future observations would provide any beneficial information.

In summary, the project aims are:

- Review the acoustic contributions of specific weather patterns to ambient noise in the ocean and how they can be used in monitoring efforts, in particular in polar regions;
- Analyse a dataset acquired in the Arctic (Kongsfjord, Svalbard) in varied conditions and identify the different acoustic processes;

- Identify and distinguish the contribution of ice-related processes to the overall ambient noise

1.4.OVERVIEW OF THE THESIS

Chapter 2: Ambient noise underwater discusses the background to underwater acoustics and weather observations, particularly at sea, as well as sources of ambient noise underwater. The instruments used are discussed, as well as the propagation, attenuation and absorption of sound waves underwater. The acoustics of ice-related processes are described.

Chapter 3: Arctic field experiments discusses the measurements taken in the Arctic fjord and how they were analysed, as well as how previous similar experiments by other authors had been analysed and the results they had obtained.

Chapter 4: Field data analysis explains Principal Components Analysis and its potential applications, and describes its application to the Arctic dataset.

Chapter 5: Tank experiments and data analyses describes the tank experiments and the results obtained from their analysis. These results are compared to those obtained in the Arctic, and to those obtained by other authors, and their significance and potential implications are discussed.

Chapter 6: Discussion summarises the decisions made when analysing the data and designing the tank experiments. The relevance of the results obtained is discussed and suggestions are given as to their implications.

Chapter 6: Conclusions compares the results obtained during the course of the project to the initial aims and in doing so, summarises the main findings. Finally this chapter highlights future applications and extensions of this research.

CHAPTER 2 – AMBIENT NOISE UNDERWATER

2.1. UNDERWATER ACOUSTICS

2.1.1. BASICS

Acoustic waves are caused by a pressure change travelling from a source through a medium. They can be used to transmit information and are particularly good at this underwater, where other methods (e.g. light) are less effective due to attenuation. The use of acoustics underwater has become more and more popular in the last century and is well documented in textbooks such as Medwin and Clay (1998) and Lurton (2010). Underwater acoustics was used in both World Wars for submarine detection. In the early 1920s, it was first used to detect fish shoals. After their invention in the 1960s, sidescan sonars were able to provide acoustic images from the seabed, and in the 1970s the development of multibeam echosounders made producing these images much more efficient. Later, in the 1980s, sidescan imagery led to high-quality maps showing the topography of the seabed and its acoustic reflectivity. Offshore oil and underwater industries were interested in developing techniques for the positioning of ships or underwater vehicles, or for data transmission. Acoustic monitoring can be used to monitor the evolution of the average ocean temperature over large spatial and time frames, to provide information for global climate studies. There are some drawbacks to using underwater acoustics, though. The main ones are that there is a higher level of ambient noise than in air and there are often spurious echoes.

Several properties can be used to describe the acoustic wave:

- The amplitude of the movement of each particle around its equilibrium position.

- The particle velocity corresponding to the particle movement. In sea water the typical wave velocity is approximately 1500 m/s
- The frequency or period. Commonly used frequencies range from 10 Hz to 1 MHz (Blondel and Murton 1997; Lurton 2004; Lurton 2010).
- The resulting acoustic pressure, measured with hydrophones.

Acoustic waves are subject to attenuation as they propagate through water; significant sources of loss are geometric spreading and absorption of the energy by the medium (Figure 2.1). Large variations in acoustic pressures mean they are often measured in decibels (dB).

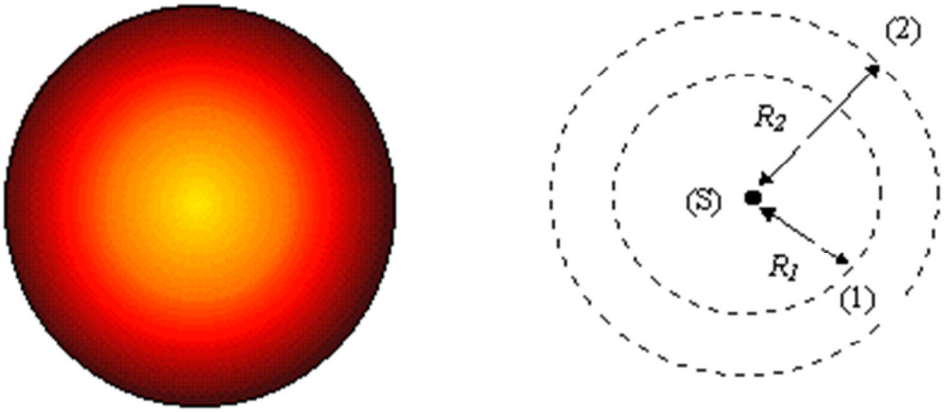

Figure 2.1: Spherical spreading from a point source (S). The energy received at two distances (eg R_1 and R_2) will be spread over spheres of increasing radii (1) and (2). From Lurton (2010).

If the path between source and receiver is sufficiently long, acoustic waves will generally reflect several times on the surface of the water and the seabed. Therefore the overall field detected at the receiver will consist in a direct path straight from the source to the receiver, as well as multiple paths which have undergone numerous reflections from the sides, bottom and surface. This effect is illustrated in Figure 2.2 (Lurton 2004).

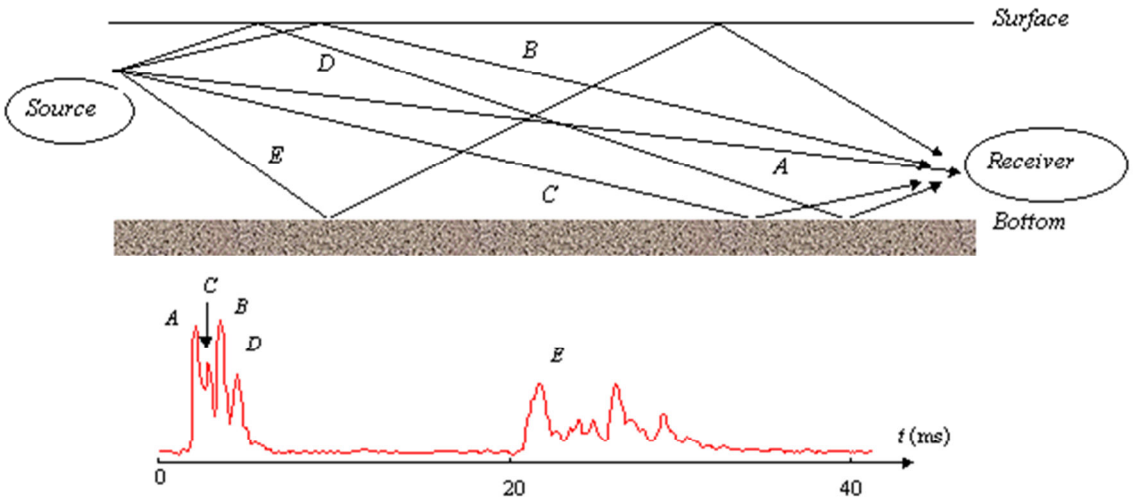

Figure 2.2: Sketch of possible propagation paths from an acoustic source to a receiver. (Top) multiple paths; (A) direct path, (B) reflection on the surface, (C) reflection on the bottom, (D) reflection on the surface and the bottom, (E) reflection on the bottom and surface. (Bottom) multiple paths shown in the reception of a single-pulse signal over time. From Lurton (2004).

The main limitations of underwater acoustics are the attenuation of sound waves over large distances and the slow propagation speed (compared to electromagnetic waves). It is also limited by the fact that the sound speed varies at different places, due to variations in the attenuation of the water and the way in which the sound waves propagate (see section 2.1.3). Moving targets and transmitters can also lead to frequency changes (Doppler effect) and the level of ambient noise caused by movements on the sea surface, volcanic and seismic activity, shipping, living organisms, wind, rain and many other factors, can mask the useful part of a signal. The marine environment is very important when considering the transmission of signals, and therefore modelling underwater acoustic propagation is a very active branch of underwater acoustics (Mccammon and Mcdaniel 1985; Buckingham 1987; Medwin et al. 1988; Medwin and Clay 1998).

Active acoustic monitoring

Underwater acoustics can be categorised into active and passive acoustics, where active acoustics uses reflections from targets to determine their locations, and passive acoustics identifies sources of noise using their acoustic signatures.

Active systems use a source and a receiver (or several) to analyse the echoes from particular targets. Active sonars transmit signals and receive echoes from a target then measure the time delay and use it to estimate the distance to the sonar. The signal is received on a suitable antenna (one or more hydrophones) to determine its angle of arrival, and further analysis can identify more of the target's characteristics, such as its speed or scattering amplitude. Figure 2.3 shows the principles of active acoustics. The acoustic field observed at the receiver will consist of both direct paths and multiple reflections.

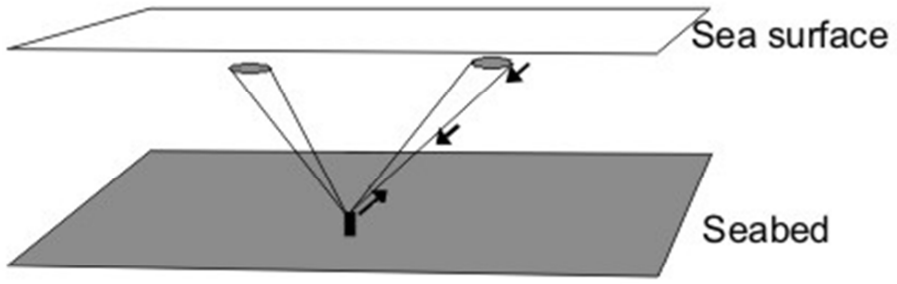

Figure 2.3: Diagram illustrating how active acoustics can be used to investigate the surface expression of weather processes: i.e. to be reflected from a target and then received at any other point in space. From Lurton (2004)

Combining series of measurements can provide a more complete view of the evolution in time and/or space of a phenomenon, for example by moving an upward-looking transducer to image a section of a water column. Figure 2.4 shows different measurements taken with an acoustic profiler looking upwards and measuring relative scattering strengths all the way to the sea surface. The heterogeneous structure of the surface waters, clearly visible, gives information about bubble content and surface agitation.

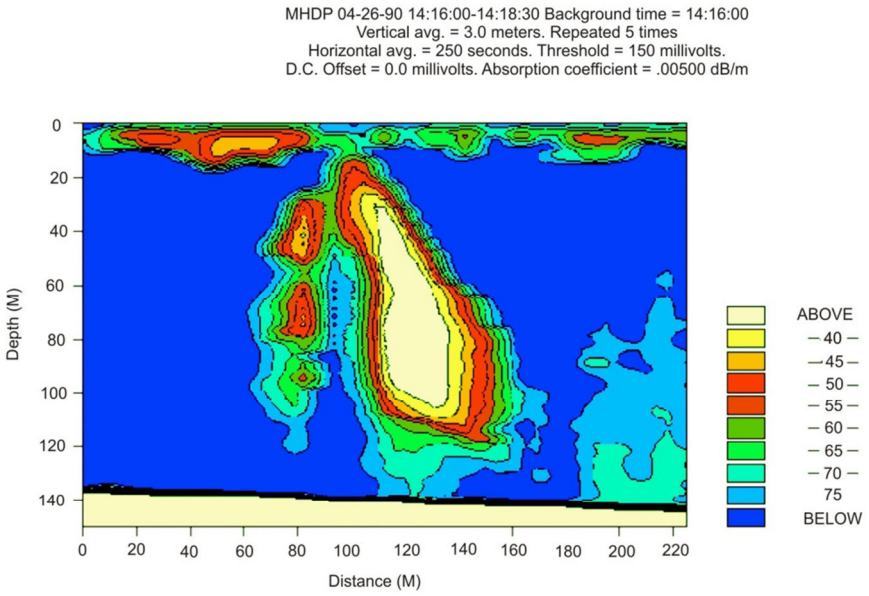

Figure 2.4: Example data obtained using active acoustics to image the water column. The yellow area in the centre is a shoal of fish, and the orange and green parts at the top show the heterogeneous structure of the surface water. The seabed is at -140 m. From NOAA: (http://www.aoml.noaa.gov/themes/CoastalRegional/cr_coastal_regional_adaptive_control.html)

Passive acoustic monitoring

Passive acoustics differs from active acoustics in that it does not use a transducer and receiver at separate locations, but instead relies on sound emitted from a target. This may be sound emitted from marine life, subsea (submarine) or surface (ship) vehicles, or from wind and rain. Passive acoustic techniques exploit the sea's natural sounds, combined with an understanding of physical processes, to determine which parameter caused the sound. Figure 2.5 illustrates the use of a hydrophone to listen to noise created by breaking waves and bubbles caused by wind.

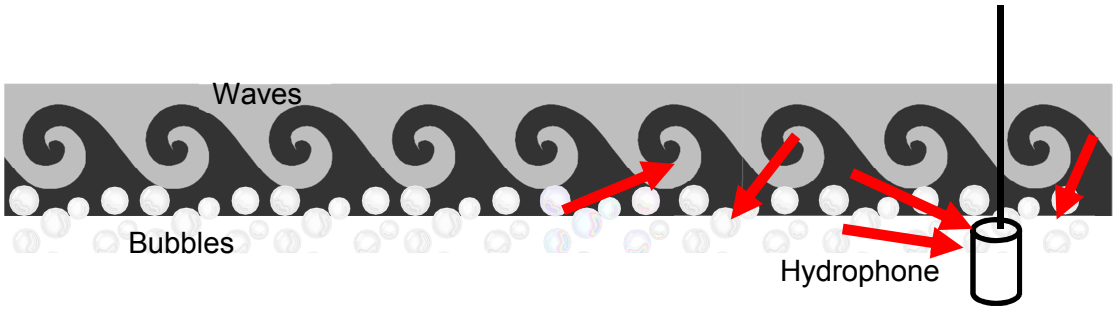

Figure 2.5: Passive acoustics – concept for listening to waves and bubbles caused by wind

Sometimes the target can be detected using a single hydrophone (Figure 2.5), or an array of hydrophones can be used. An array gives more detailed information about the source of the noise but is more costly and difficult to deploy and set up – the precise spacing between hydrophones is crucial. With an array of hydrophones, the angles of arrival will be measured in order to show the position of the target. If the array of hydrophones is linear, the system is limited in that the angles of arrival cannot be measured in both the horizontal and vertical planes. Passive acoustics is limited by its difficulty in measuring the distance between the sonar and a target. It is, however, possible to deduce this distance by using the phase shift or time delay between signals detected at different points on a linear array, yielding the length differences between the acoustic paths.

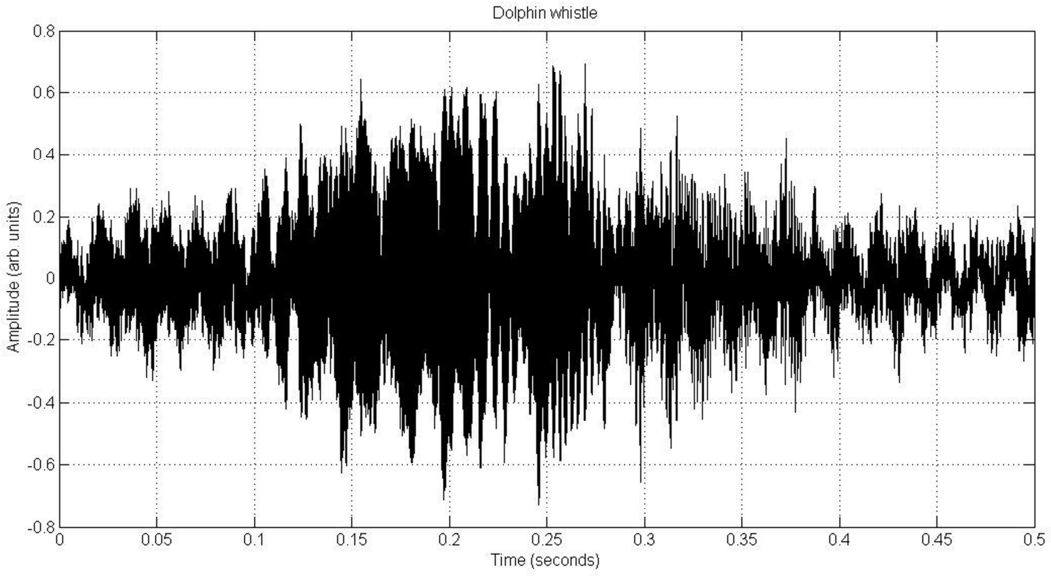

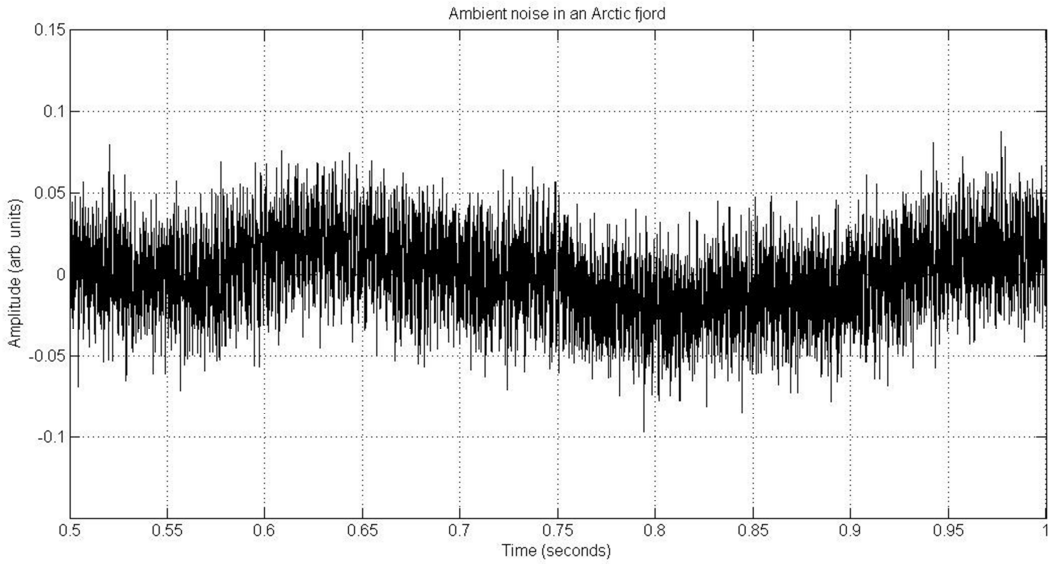

Figure 2.6. Typical time-domain observations obtained using passive acoustics. Top: a dolphin typical whistle, bottom: ambient noise in an Arctic fjord (Keogh and Blondel 2008). Note the dolphin whistle sound is more regular and structured whereas the ambient noise has short sharp spikes at irregular intervals.

Signals are often characteristic of a source (Figure 2.6). Trained operators are able to recognise a source of noise by listening to it, and in other cases, automated systems can analyse the spectrum of the received signal to identify the source after removing the background noise. Non-military applications include detecting rainfall (Nystuen 2001; Quartly 2001), studying bubbles in breaking waves (Medwin and Beaky 1989), analysing shipping (Gaul et al. 2007), tracking whales (Kipple and Gabriele 2003) and assessing sonar performance (e.g. (Ainslie 2010)).

2.1.2. PRESSURE, FREQUENCY AND VELOCITY

Generally acoustic signals are not instantaneous and therefore have a characteristic frequency. The wavelength is the spatial interval between two points in the medium undergoing the same vibration and in phase with each other. It is given by (Lurton 2010):

$$\lambda = \frac{c}{f} \tag{2.1}$$

Doppler effect

If a source and receiver, or a source and a target are displaced relative to each other, then the duration of the source-receiver paths changes and the apparent signal frequency after propagation changes, which is called the Doppler effect. The frequency variation δf created is given by (Lurton 2004);

$$\delta f = f_0 \frac{\upsilon_r}{c} \tag{2.2}$$

which is doubled for an echo on a target, due to the sound travelling both ways. Although the Doppler effect can make it difficult to process signals, it can be used to determine the speed of a moving object relative to the bottom or water column (Lurton 2010).

Sound velocity

Sound velocity varies with temperature, salinity and depth. Deeper than about 1000 m in open oceans and about 200 m in closed seas, it decreases in a stable manner with depth. Hydrostatic pressure makes sound velocity increase with depth linearly, roughly by 0.017 m/s for each metre downward. The salts dissolved in sea water also affect the velocity – in a large ocean basin the salinity is on average 35 p.s.u but can be quite different in closed seas, depending on the influence of evaporation or freshwater input. Furthermore, acoustic waves can be scattered by inhomogeneities such as bubble layers and fish, also altering the velocity and absorption of sound waves. If the resonant frequency of a portion of the bubble population is close to the frequency of the acoustic wave then the sound velocity can be significantly different from its value in sea water (Lurton 2010).

Often, the environment is approximately horizontally stratified so that the sound velocity only varies with depth, which simplifies the models of propagation processes. This variation is illustrated in Figure 2.7 (Lurton 2004)

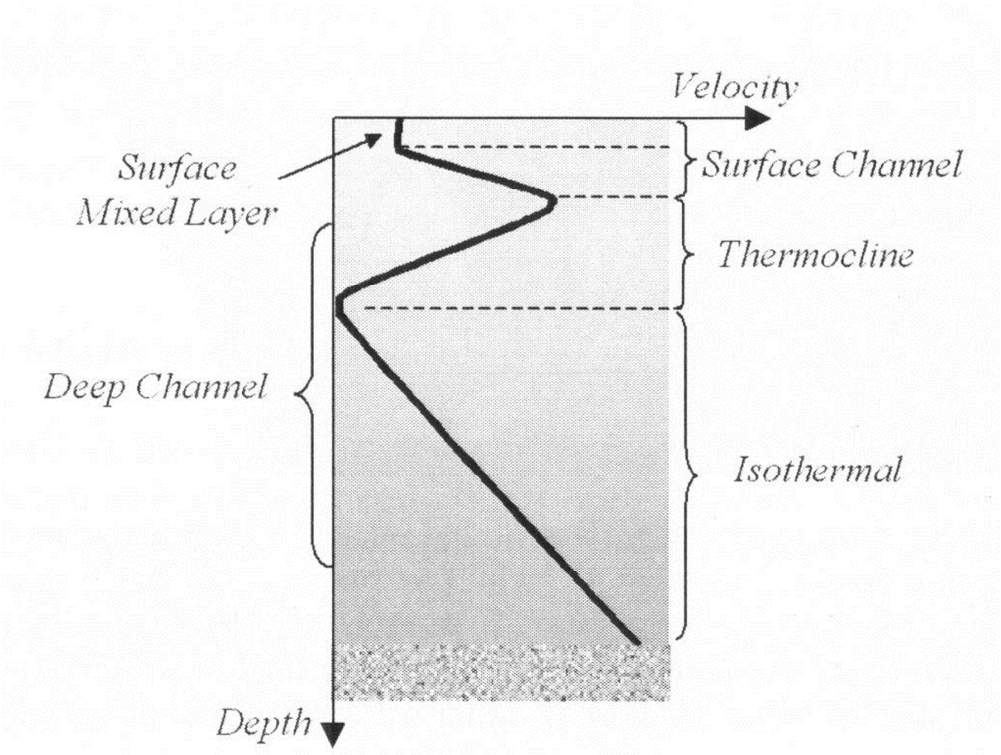

Figure 2.7: Elements of a typical sound-velocity profile. Sound velocity is represented on the *x*-axis, depth on the *y*-axis. From Lurton (2010).

At the interface between two homogeneous fluids with different sound velocities, the change in sound velocity induces specular reflections of the wave in medium 1 and refraction of the wave in medium 2. In medium 1 the reflection is along a direction symmetrical to the normal of the incidence point, and in medium 2 the angle of refraction is given by the Snell-Descartes law (Lurton 2010);

$$\frac{\cos \beta_1}{c_1} = \frac{\cos \beta_2}{c_2} \tag{2.3}$$

where β is the horizontal grazing angle (relative to the horizontal)

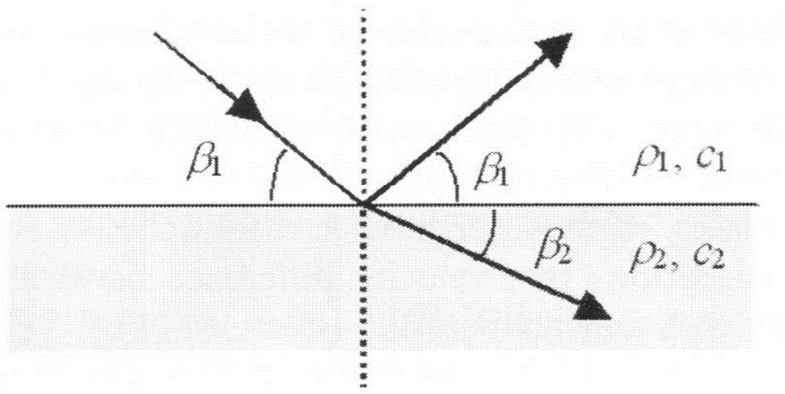

Figure 2.8 (Lurton 2010): Reflection and refraction of a plane wave, due to the change in sound velocity at the interface ($C_2 > C_1$).

and β_c is the critical angle for the interface – for angles smaller than this there is total reflection, so that transmission into medium 2 is not possible.

The Snell-Descartes law can be applied to a series of layers with constant velocities, and can then be used to describe the behaviour of a wave propagating in a medium where velocity varies with the co-ordinate *z*. If the layers of constant velocity are infinitely thin, the law can be expressed as (Lurton 2010):

$$\frac{\cos \beta(z)}{c(z)} = constant \tag{2.4}$$

2.1.3. PROPAGATION

Propagation of an acoustic wave decreases the amplitude of the signal due to geometrical effects and absorption, where absorption is related to the chemical properties of the medium (e.g. sea water). Due to the presence of two clearly-defined interfaces (e.g. the sea surface and the ocean floor) the propagation of the signal is often accompanied by multiple paths from reflections. The velocity of acoustic waves varies in the ocean with depth due to constraints on pressure and temperature, so that the paths of the sound waves can be deviated. The most efficient way to model the propagation of acoustic waves in water uses geometrical acoustics and the Snell-Descartes Law (Lurton 2004; Lurton 2010).

Acoustic waves are caused by a mechanical perturbation which propagates away from the source by compressions and dilations passing from one point to surrounding points due to the elastic properties of the medium. The rate of propagation is known as the velocity, which is determined by the mechanical properties of the medium. Acoustic waves are characterised by the amplitude of the movement of the particles in the medium about their equilibrium positions, by the corresponding particle velocity and by the resulting acoustic pressure (i.e. the variation around the average hydrostatic pressure). The propagation velocity *c* is given by (Lurton 2010);

$$c = \sqrt{\frac{E}{\rho}} \tag{2.5}$$

where ρ is the density of the medium and E is its elasticity modulus. In sea water *c* is approximately 1500 m/s depending on pressure, salinity and temperature (Lurton 2010).

The propagation of waves is described by the wave equation (Lurton 2010);

$$\Delta p = \frac{\partial^2 p}{\partial x^2} + \frac{\partial^2 p}{\partial y^2} + \frac{\partial^2 p}{\partial z^2} = \frac{1}{c^2(x,y,z)} \frac{\partial^2 p}{\partial t^2} \tag{2.6}$$

where *p* is the pressure of a wave propagating in the space *(x,y,z)* as a function of time *t* and *c(x,y,z)* is the local propagation velocity of the wave. **Δ** is the Laplacian operator ($\Delta = \nabla . \nabla = \nabla^2$) When the velocity is constant, *c(x,y,z)* = *c* and the propagation is limited to a single direction *x*, equation 2.6 becomes (Lurton 2010):

$$\frac{\partial^2 p}{\partial x^2} = \frac{1}{c^2} \frac{\partial^2 p}{\partial t^2} \tag{2.7}$$

When this equation is solved for a sinusoidal wave of frequency f_0 it gives (Lurton 2010);

$$p(t) = p_0 \exp\left(2i\pi f_0 \left(t - \frac{x}{c} \right) \right) \tag{2.8}$$

where *p(t)* is a plane wave. The particle velocity is related to the acoustic pressure by (Lurton 2010);

$$\nabla p = -\rho \frac{\partial \underline{v}}{\partial t} \tag{2.9}$$

where ρ is the density and ∇ is the gradient operator. If the wave is only travelling in the *x*-direction then this equation becomes (Lurton 2010);

$$\frac{\partial p}{\partial x} = -\rho \frac{\partial v}{\partial t} \Rightarrow p_0 = \rho c v_0 = \rho c \omega a_0 \tag{2.10}$$

where $\omega = 2\pi f_0$ is the angular frequency.

When the propagation in all three directions is isotropic, the solution of the wave equation is a spherical wave (Lurton 2010);

$$p(t) = \frac{p_0}{R} \exp\left(2i\pi f_0\left(t - \frac{R}{c}\right)\right) \tag{2.11}$$

meaning that the decrease in the wave's amplitude is inversely proportional to the distance *R* to the source (Lurton 2010). Acoustic waves can be modelled as either plane or spherical waves. They are modelled as plane waves when the amplitude is approximately constant and the wave fronts show negligible curvature (i.e. the receiver is far from the source) and spherical when the receiver is close enough to the source that the wave fronts are curved.

2.1.4. ATTENUATION AND ABSORPTION

When acoustic waves propagate, the main cause of a decrease in intensity is geometric spreading and absorption of acoustic energy by the propagation medium, which reduces the amplitude of the signal received. The simplest case of geometric spreading is a point source radiating in all directions in a homogeneous, infinite medium where the energy transmitted is conserved but is spread over increasingly large spheres (see Figure 2.1). The decrease in acoustic intensity *I* between points 1 and 2 is inversely proportional to the ratio of the surfaces of the spheres S_1 and S_2 (Lurton 2010);

$$\frac{I_2}{I_1} = \frac{S_1}{S_2} = \left(\frac{4\pi R_1^2}{4\pi R_2{}^2}\right) = \left(\frac{R_1}{R_2}\right)^2 \tag{2.12}$$

where R_i is the radial distance from the source. The decrease in intensity is inversely proportional to R^2 and the decrease in pressure is inversely proportional to R. Sea water absorbs some energy from acoustic waves, which is dissipated through viscosity and chemical reactions. The decrease in amplitude is proportional to the amplitude itself, therefore the acoustic pressure decreases exponentially. For example, for a spherical wave (Lurton 2010);

$$p(R,t) = p_0 \exp(-\gamma R)\frac{\exp\left(2i\pi f_0\left(t-\frac{R}{c}\right)\right)}{R} \tag{2.13}$$

where γ quantifies the attenuation. Usually the attenuation in sea water is given in dB/km and the attenuation coefficient α is related to γ by (Lurton 2010):

$$\alpha = 8.686\gamma \tag{2.14}$$

Recent models of the absorption coefficient are of the form (Lurton 2010);

$$\alpha = C_1 \frac{f_1 f^2}{f_1^2 + f^2} + C_2 \frac{f_2 f^2}{f_2^2 + f^2} + C_3 f^2 \tag{2.15}$$

where the first two terms correspond to contributions from the two relaxation processes and the third term corresponds to the viscosity of pure water. The relaxation coefficients f_i and coefficients C_i depend on temperature, pressure or salinity and are determined by experiments at sea or in the laboratory. Figure 2.9 (Lurton 2010) shows the model which is currently most commonly used.

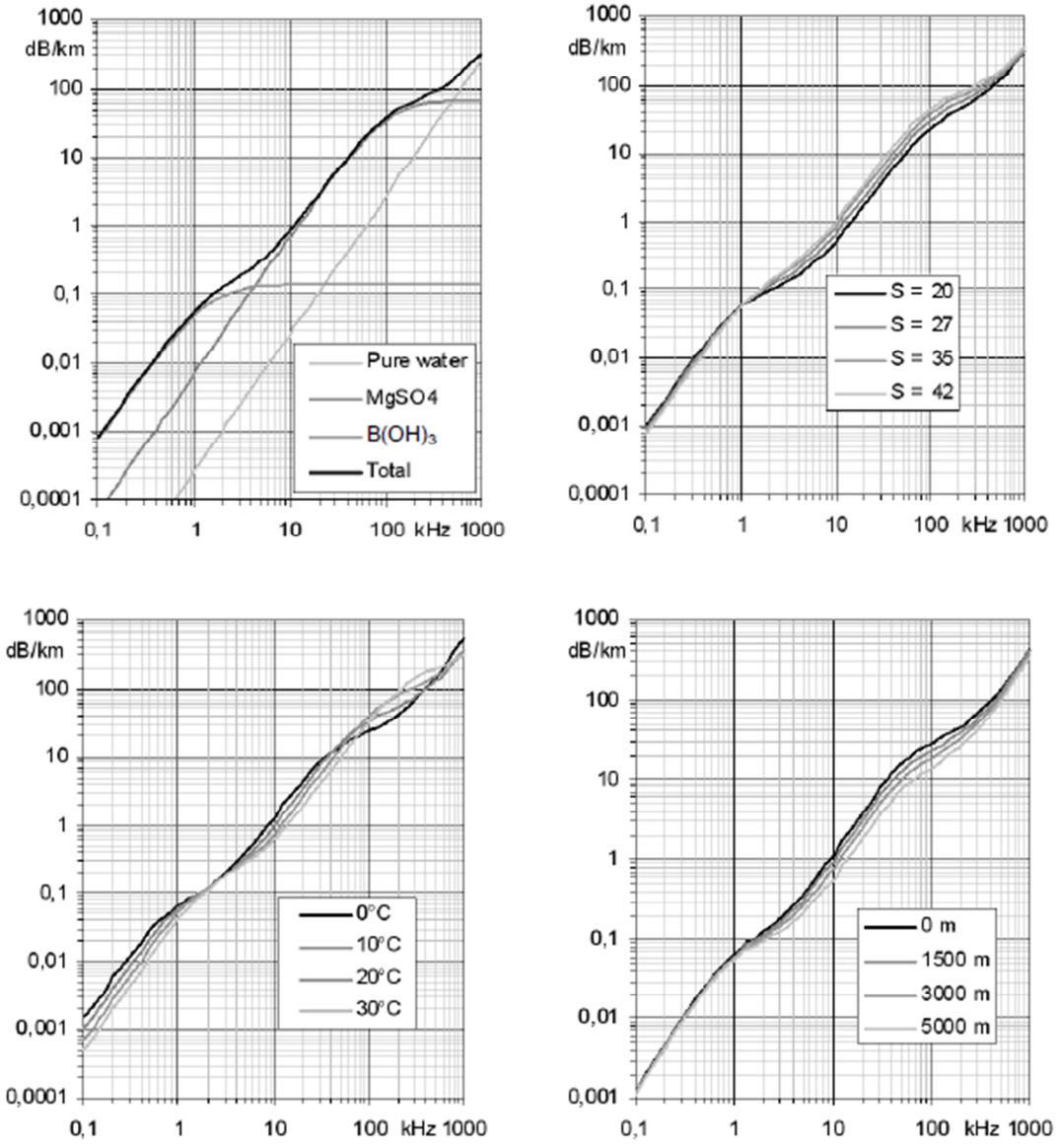

Figure 2.9: Sound absorption coefficient in sea water as a function of frequency for average conditions (T=15°C, S=35 p.s.u., z=0, top left) and showing the influence of; salinity (top right), temperature (bottom left) and depth (bottom right). From Lurton (2010)

As illustrated by Figure 2.9, attenuation increases very rapidly with frequency, with variable orders of magnitude. Below approximately 1 kHz, attenuation is of the order of hundredths of dB per km and is not considered a limiting factor. At 10 kHz, the attenuation is around 1 dB/km which limits the range to tens of kilometres. At frequencies as high at 100 kHz, the attenuation coefficient is tens of dB/km and limits the range to 1 km. For frequencies as high as MHz, the range is limited to 100 m with attenuation of hundredths of dB/km (Lurton 2010). In addition to the

attenuation decreasing the signal strength with distance from a source, attenuation decreases with depth (Lurton 2010).

At 14 kHz and in typical shallow seawater, α ~20 dB/km. When evaluating the propagation loss, spherical spreading is useful as a first approximation and the propagation loss PT (in dB) is expressed as a function of the distance travelled R (in m) and the attenuation coefficient α:

$$PT = 20\log R + \alpha\ R \tag{2.16}$$

This range-dependent variation with frequency will affect the shape of rain spectra with distance between the location of the measuring hydrophone and that of the rainfall, *especially at large distances (> 1km)*. These variations will be less important when the hydrophone is just below the rain-affected area.

Propagation losses are usually approximated by spherical spreading, which gives a transmission loss in dB of (Lurton 2004);

$$TL = 20\log R + \alpha R \tag{2.17}$$

which is illustrated in Figure 2.10 (Lurton 2010).

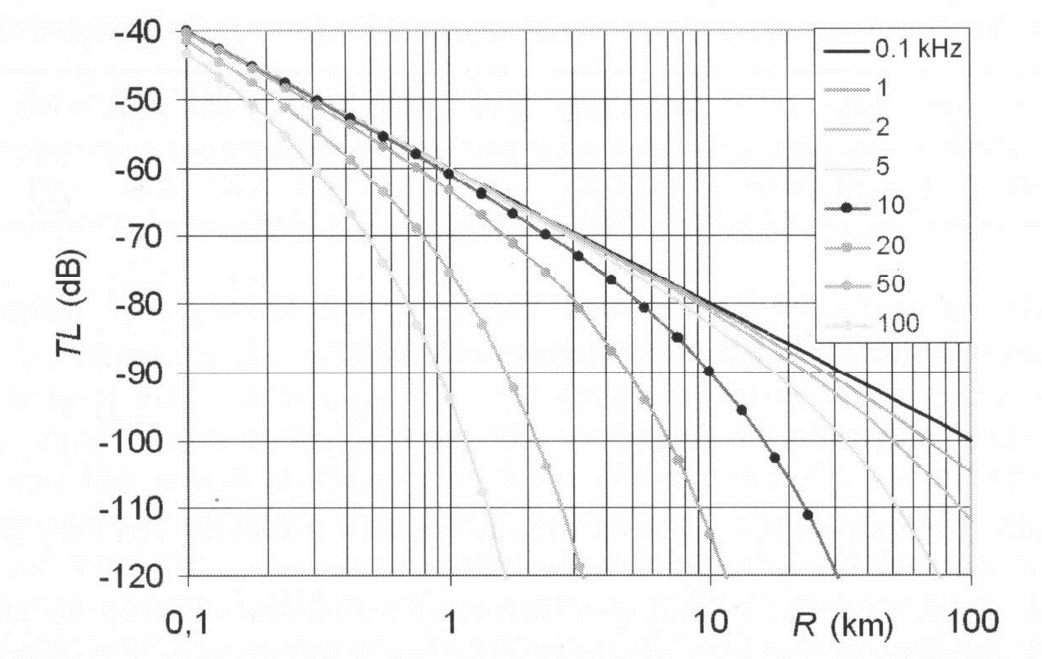

Figure 2.10: Propagation loss as a function of range for frequencies of 0.1, 1, 2, 5, 10, 20, 50 and 100 kHz, for conditions of T=10°C, S=35 p.s.u. and z=10 m. From Lurton (2010)

If a system uses an echo from a target the propagation loss will be doubled due to attenuation on the outward and return paths. R is the radius, usually expressed in metres, and α is usually expressed in dB/km (Lurton 2010).

Up to approximately 20 m below the sea surface, air bubbles caused by sea surface movements form an inhomogeneous layer which modifies the acoustic characteristics of the propagation medium, increasing the attenuation, modifying and refracting the sound velocity and leading to backscatter. Bubbles act as spherical obstacles with very high acoustic impedance contrast and scatter incident sound waves, with a maximum scattering effect around the intrinsic resonance frequency (the 'breathing frequency) of an air bubble in water (Medwin and Clay 1998)

$$f_R = \frac{3.25}{a}\sqrt{1+0.1z} \tag{2.18}$$

where f_R is the resonance frequency (in Hz), z is the depth (in m) and a is the radius of the gas sphere (in m). For higher bubble populations, the scattering processes and absorption processes add to increase the attenuation. For bubble populations which change with time and are inhomogeneous, prediction is complicated, but a simple approximation which quantifies the additional loss for a path reflecting on the surface and crossing the entire surface bubble layer is (Lurton 2010).

$$\begin{cases} TL_b = \dfrac{1.26\times10^{-3}}{\sin\beta}\upsilon_w^{1.57} f^{0.85} & \text{for } \upsilon_w \geq 6 \text{ m/s} \\ TL_b = TL_b(\upsilon_w = 6)e^{1.2(\upsilon_w - 6)} & \text{for } \upsilon_w \leq 6 \text{ m/s} \end{cases} \tag{2.19}$$

where TL_b (in dB) is the two-way transmission loss caused by the bubble, υ_w (in m/s) is the wind speed 10 m above the surface, f (in kHz) is the signal frequency and β is the grazing angle. υ_w = 6 m/s corresponds to the threshold for the existence of crashing waves that generate bubbles (Lurton 2010).

As mentioned in section 2.1, reflections from the sea surface and the seabed can lead to multiple paths. The number of paths can vary significantly, from none to several tens or hundreds over long distances. With high frequencies and signals shorter than a typical delay between arrivals, the effect of multiple paths is visible in the time domain with sequences of multiple echoes. For low-frequency, permanent signals,

the contributions add together and create a stable interference pattern with strong variations in the field amplitude (Lurton 2010).

2.1.5. INSTRUMENTATION

Transducers

Transducers used in underwater acoustics mostly use piezoelectricity. This converts acoustic energy into electric energy and vice versa. A transducer is a resonant system, therefore it has a narrow frequency band, meaning its use is specialised. An important characteristic of a transducer is its *directivity*, which controls (for example) the source level, the angular resolution and the signal to noise ratio at the reception point of the signal. The directivity is influenced by the transducer geometry. Acoustic sources are known as projectors, and a transmitter will consist of a projector and some electronics. A receiving transducer is known as a hydrophone and a receiver will consist of a hydrophone and some electronics.

Piezoelectricity uses crystals, which can be natural or synthetic (i.e. ceramics). When an electric field is applied to the crystal, the crystal undergoes deformation which is related to the electrical excitation, which causes acoustic (pressure) waves. In order to receive an acoustic wave, the piezoelectric material undergoes stress from the sound waves which generates an electric potential between its sides. Full and further details on transducers can be found in (Stansfield 1991), (Wilson 1988) and (Lurton 2010)

Hydrophones

Hydrophones (receiving transducers) are made from a variety of materials, but are usually piezoelectric. They often operate over a wide frequency band because they do not need to be tuned to one resonant frequency. The electric signal they emit can be amplified to improve efficiency, however they have internal noise from the ceramics as well as self-noise from the amplifier which means that only signals above that level can be detected. They are usually small in comparison to acoustic wavelengths and the frequency resonance is rejected beyond an upper limit of the flat part of the frequency response, so that they have low spatial selectivity.

Therefore it is possible to obtain a directivity pattern by combining several hydrophones into an array. Often, a single transducer can be used for both transmission and reception.

2.2. EXPRESSION OF WEATHER PROCESSES

Air pressure varies vertically and horizontally. Vertically, it decreases with height above the Earth's surface (barometric pressure). Horizontally, variations in pressure affect the air's horizontal and vertical movement, which in turn affects other aspects of the weather. Sea-level atmospheric pressures can be averaged for several months to determine the pattern of prevailing winds, which influence global weather patterns. An international standard for direct measurements is the Beaufort scale (Table 2.1), using both quantitative measurements of the wind speed and visual, qualitative observations of the sea state.

Force	Speed (knots)	Description	Appearance of the sea
0	0-1	**Calm**	Sea like a mirror
1	1-3	**Light air**	Ripple with the appearance of scales are formed, but without foam crests.
2	4-6	**Light Breeze**	Small wavelets, still short, but more pronounced. Crests have a glassy appearance and do not break.
3	7-10	**Gentle Breeze**	Large wavelets. Crests begin to break. Foam of glassy appearance. Perhaps scattered white horses.
4	11-16	**Moderate Breeze**	Small waves, becoming larger; fairly frequent white horses.
5	17-21	**Fresh Breeze**	Moderate waves, taking a more pronounced long form; many white horses are formed. Chance of some spray.
6	22-27	**Strong Breeze**	Large waves begin to form; the white foam crests are more extensive everywhere. Probably some spray.
7	28-33	**Near Gale**	Sea heaps up and white foam from breaking waves begins to be blown in streaks along the direction of the wind.
8	34-40	**Gale**	Moderately high waves of greater length; edges of crests begin to break into spindrift. Foam in well-marked streaks along wind.
9	41-47	**Severe Gale**	High waves. Dense streaks of foam along the wind. Crests of waves begin to topple, tumble and roll over. Spray.
10	48-55	**Storm**	Very high waves with long overhanging crests. Foam, in great patches, blown in dense white streaks along the wind. Sea surface takes on white appearance. Visibility affected.
11	56-63	**Violent Storm**	Exceptionally high waves. Sea completely covered with long white patches of foam along the wind. Edges of crests blown into froth.
12	64-71	**Hurricane**	The air is filled with foam and spray. Sea completely white with driving spray; visibility very seriously affected.

Table 2.1. The Beaufort scale is used to estimate wind speed at sea using visual observations, normalised to a reference level of 10 m above the sea surface, to avoid small-scale turbulence and transient variations. 1 knot = 1.6 km/h. From UKMO (1999).

Wind directly affects the sea state, as shown in Figure 2.11. It can cause waves, ranging in size from 1 cm to 30 m or more (e.g. Gross (1990)) and with different wavelengths. In shallow water (less than half the wavelength of the waves), they are affected by the seabed topography and their propagation speeds will vary. Conversely, in deeper water, the propagation speed will only depend on their wavelength and period. These waves will create local, small variations of the pressure in the water. Once large enough, crests and white caps will trap and entrain air bubbles, adding to the local variations of the sea surface (Figure 2.11), in particular local albedo and noise level.

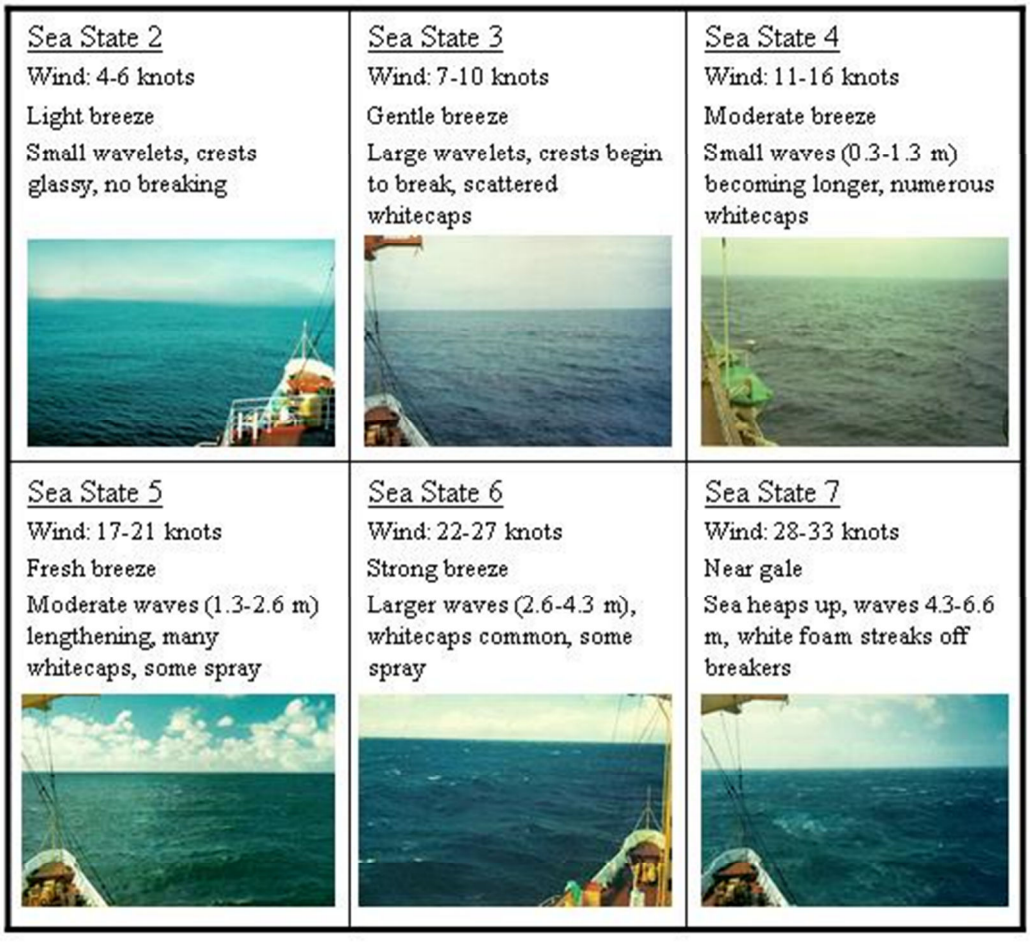

Figure 2.11. An illustration of sea states 2-7 and their physical manifestation. NOAA (2004).

All types of precipitation originate in clouds, at varying heights and with varying physical characteristics. Clouds are formed when air rises, causing small drops of

water to remain in a state of suspension due to up-currents. Moisture can condense to form a cloud if a particle, such as dust, can act as a nucleus. These droplets are very small and will not necessarily fall to the ground at this stage, but can, occasionally, collide with other droplets to increase in size. Precipitation is the term which describes all forms of weather particles falling from the atmosphere to the Earth's surface, including drizzle, snow and hail.

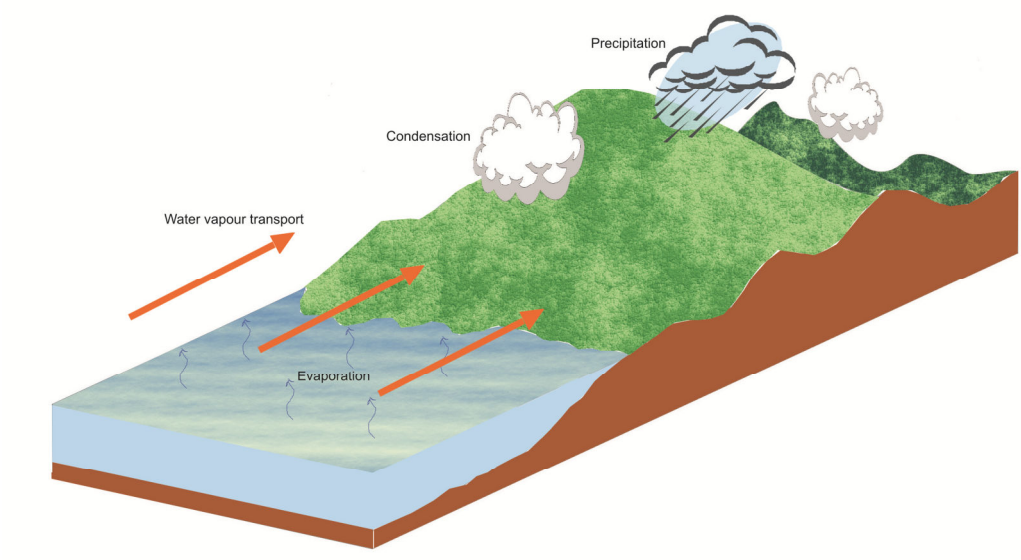

Figure 2.12. Diagram showing precipitation over water and land.

Down to temperatures as low as −30°C, ice crystals and water droplets will both exist, and sometimes the crystals will act as nuclei for the droplets, leading to the formation of snowflakes, which will grow and become heavy enough to settle at the base of the cloud. If it is warm enough, they can melt and fall as raindrops, but if the surface on which they are falling is freezing, they will not melt. The size to which a raindrop can grow before falling depends on the strength of the up-current, which means that generally larger drops will fall from cumulus clouds and smaller ones from stratus clouds.

Figure 2.13 shows a raindrop falling on water. When considering rain, it is important to remember that there are two key items to measure – the amount of rain which has fallen over a given time period, and the distribution of droplet sizes in the rain. Previous investigations (Black et al. 1997) have grouped raindrop diameters into 4 distinct ranges: minuscule (< 0.8 mm), small (0.8–1.1 mm), mid-size (1.1–2.2) mm and large (> 2.2 mm). Back-of-the-envelope calculations show that, for the August

2008 UK average rainfall of 140 mm (i.e. 140 l/m^2/month) and a medium raindrop diameter, around 25 raindrops hit a square metre every second (usually at terminal velocity).

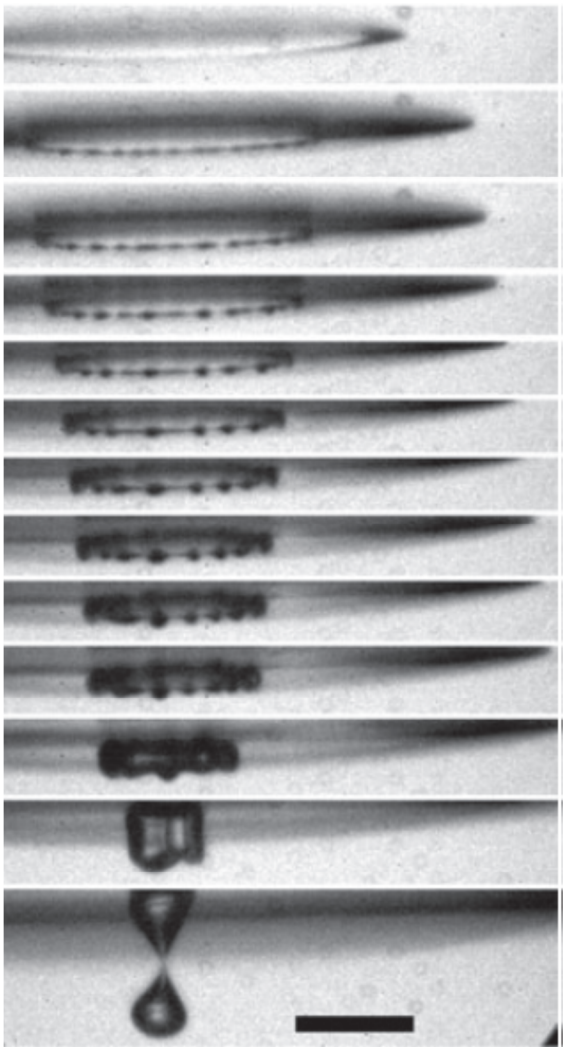

Figure 2.13. Close-up, high-speed photographs of a droplet impacting a still water surface, showing the air disc trapped below and the small instabilities at the edge of the droplet, from 10 to 750 μs after first contact. The scale bar is 0.5 mm long. From Thoroddsen et al (2003).

Down-currents also exist inside clouds, which bring small ice crystals down to gather more water droplets and be carried up again, leading to the formation of hailstones, which fall when they are heavy enough to overcome the upward thrust. Hailstones do not break up like raindrops and so their size is limited only by the

strength of the up-current. Large cumulus or cumulonimbus clouds can contain very strong vertical currents, particularly around the tropics.

Often, large differences in positive and negative electrical charge can be found in such clouds, which can be equalised by lightning, which will cause an air disturbance heard as thunder. Underneath lightning, the air converging towards the point at which lightning has occurred causes waves in concentric circles, which will appear on the sea surface as a depression, i.e. more waves at the periphery (Hulbert 1973). The sound of thunder can often be heard well below the sea surface (e.g. Godin (2006))

2.3. MONITORING WEATHER PROCESSES

Routine global measurements of the weather are standardised through the United Nations' World Meteorological Organisation (WMO). Observations may be made hourly at weather stations, or less frequently, such as once every three, six or twelve hours. (Reynolds 2006) Surface observations which might be recorded are the temperature, relative humidity, pressure and pressure gradient, cloud coverage and type, visibility, wind direction and speed, precipitation total, and historic data will be stored. Information obtained in other ways complements the surface observations, for example data collected from instruments on balloons, or from weather satellites and radar. The spatial coverage of these measurements is always a challenge, and some regions are difficult to access regularly, and obtaining measurements to a high level of accuracy can be a challenge.

Instruments able to measure the sizes of raindrops are known as disdrometers. Measuring raindrop diameter is not simple, particularly not at sea, which means that being able to make this process easier using underwater acoustics would be very useful. Precipitation is often measured using a raingauge, which collects water over one day to record the amount of precipitation which has fallen. To avoid water splashing back, measurements are commonly taken at a reference height of 30.5 cm. Although the total amount of precipitation which has fallen in one day is a useful measurement, it does not provide any information about the intensity or duration of the precipitation (Reynolds 2006). A tipping-bucket raingauge can be used to show how much rain fell in smaller time periods, highlighting periods of more intense

rainfall, but this does not give precise information about the sizes of the individual rain drops.

Surface measurements of wind speed can be made using an anemometer, usually a cup variety, which has three hemispherical cups mounted onto a vertical shaft. The wind will exert more pressure on the concave faces of the cups than on the convex faces, which will cause the vertical shaft to rotate at a rate which varies with wind speed. The measurements of wind speed derived from this rotation will be averaged over several minutes, and usually the horizontal wind speed is considered more significant than the vertical wind speed. A wind vane will be used in combination with the anemometer to show the direction from which the wind is blowing. Its movements will be recorded continuously on an anemograph (Reynolds 2006). Wind profilers can also be used which obtain the wind speed and direction for a column of air above their position.

Marine observations

The main methods of observing ocean weather are using satellites flying well above its surface, using instruments on board ships, or moored to buoys, to view the ocean at the sea surface, and using underwater acoustics to view it from below (Medwin and Clay 1998). These methods are complementary, and each has its advantages and limitations. It is beneficial to understand the capabilities of all of the methods in order to assign the methods to the best effect. If cloud coverage is significant, certain channels of satellites are limited and less able to view parts of the ocean. Weather satellites give details of the location of clouds across the globe, as well as other information such as a vertical profile of the temperature and humidity levels throughout the atmosphere. Many satellites are able to map water vapour in the atmosphere, using a radiometer, in order to find the strength of the sunshine reflected back to space. Snow and the tops of deep clouds (which are cold) will give very strong reflections, whereas areas of vegetation with no clouds above them, and ocean surfaces will give weak reflections, e.g. Figures 2.14 and 2.15.

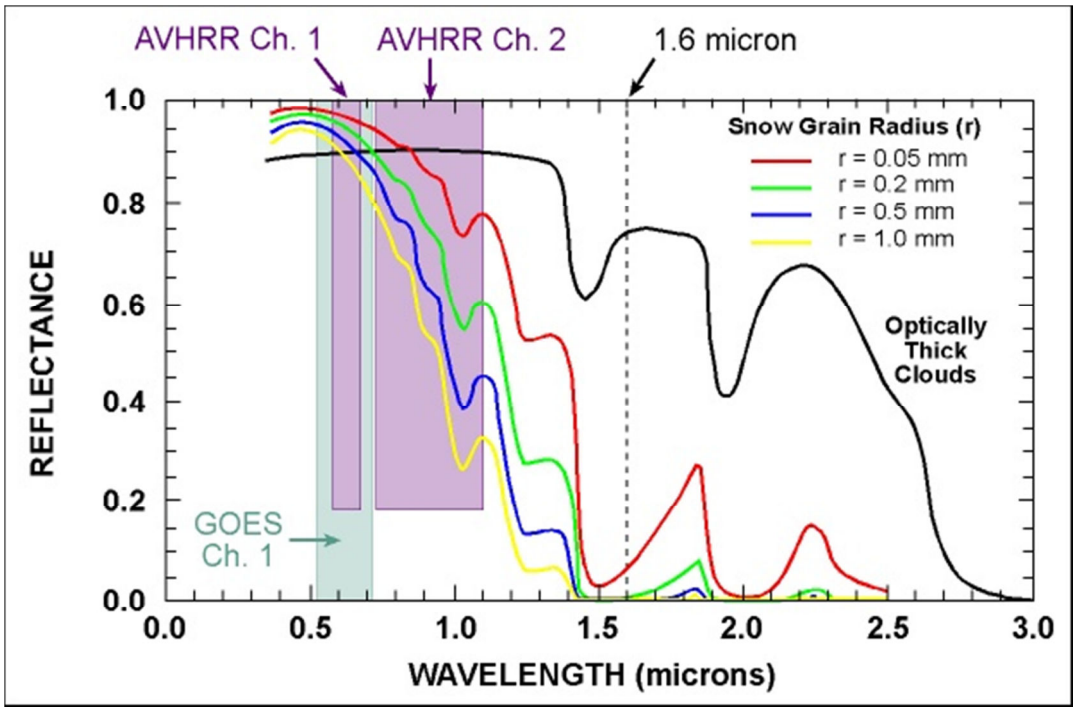

Figure 2.14: Radiometer reflection spectra from different snow grain sizes. From Fowler et al (2003).

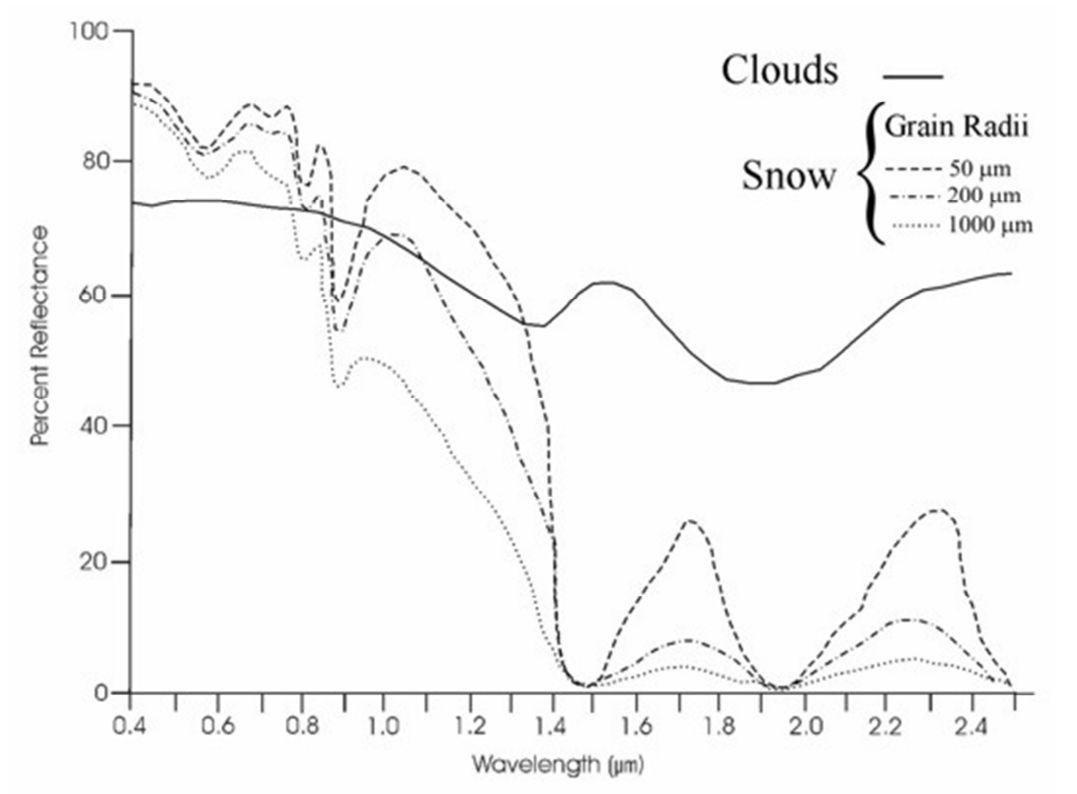

Figure 2.15. Radiometer reflectance spectra for average clouds and snow grains of radii 50, 200 and 1000 µm. (Farooq, 2011).

Images obtained in visible wavelengths are not available during the night. To overcome this, all weather satellites also use infrared to acquire images, so the strength of the signal will vary depending on the temperature of the body that emits it. Weather radars have a range of 250 km and so can be used to monitor the weather over coastal waters, but not further from land. Doppler radars can be used to measure the velocity of a target and dual polarisation radars have the potential to characterise the precipitation type (as with the present weather sensors). Radars have resolution of up to 500 m and it is possible to obtain values of the wind speed and direction by tracking the movement of the raindrops, but obviously this is limited to times when it is raining. Radar refractivity can be used to observe the humidity and this does not require it to be raining. Radiosondes on board balloons are able to record wind direction and speed, temperature and humidity up to 30 km above sea level.

In-situ marine observations of the weather are made using a network consisting of voluntary observing ships, offshore platforms and rigs, drifting and moored buoys, Argo floats and shipborne automatic weather stations. All of these different components make different types of observations – for example, sonic anemometers can be attached to ships, drifting and moored buoys, and Argo floats drift around the ocean making descents to obtain profiles of information such as the salinity. Observations from ships are usually only obtained once a day and do not cover the South Pacific region well, however some ships contain autosonde stations to give profiles of the temperature, wind and humidity above the ship's position in the ocean at a certain time.

Underwater acoustics is not particularly good at giving information about cloud coverage. However, it can cover any area where there is water present, and a hydrophone could be deployed from a marine vessel or attached to a buoy. Lower ambient noise levels are preferable, so ideally underwater acoustics should be used away from shipping lanes. Weather processes cause noise at frequencies from 5 to 50 kHz, which correspond to attenuation distances of tens of kilometres to several kilometres (Lurton 2010). A hydrophone can take continuous recordings for minutes or sample at set times over much longer periods. A large body of literature (e.g. Lurton (2010)) show that a hydrophone is able to measure (in terms of weather processes):

- rainfall intensity

- drop size distribution

- wind speed

- direction of movement of wind or rain using an array of hydrophones

- hail

- snow

- thunder

- ice cracking/movement/melting or water lapping on icebergs

- wind above icebergs.

2.4. UNDERWATER ACOUSTIC NOISE

Ambient noise underwater is the noise detected by a sonar system, of any type, and not due to a signal or self-noise. The ambient noise varies significantly with location, water depth and local conditions (including weather). The ambient noise can be either permanent – lasting for days, or intermittent – lasting several seconds, hours or days (Lurton 2010).

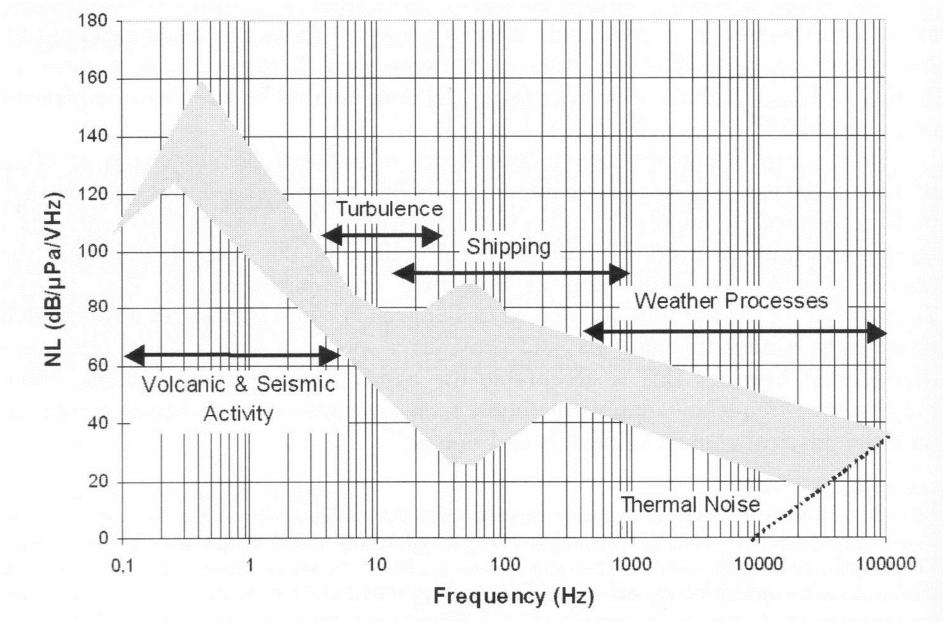

Figure 2.16: General variation of ambient noise underwater. From Lurton (2010)

Figure 2.16 (Lurton 2010) illustrates the sources of ambient noise from 0.1 Hz to 100 kHz. At very low frequencies, noise is due to seismic and volcanic activity, and non-linear interaction of surface waves. From 5 to 30 Hz, ambient noise is due to wave turbulence (Medwin and Clay 1998), where the noise is strongly correlated with wind speed. From 10 Hz to 1 kHz, the dominant source of ambient noise is shipping, along with noise from industrial activity on the shore (Lurton 2010). Other weather-related contributions will vary with frequency and weather type.

2.4.1. MODELLING PERMANENT AMBIENT NOISE

Several noise models exist, based on compilations of field observations (Wenz 1962). Some of the models describe trends and orders of magnitudes, rather than describing and predicting accurately. They state that from 10 – 100 Hz, the noise depends heavily on shipping and industrial activities, with levels typically from 60 to 90 dB re. 1μPa/√Hz[1]. From 100 – 1000 Hz, the noise is dominated by shipping contributions, but with a significant contribution from sea surface agitation caused by wind or rain. A simple empirical model derived from Urick (1986) describes the orders of magnitude of this noise:

$$\begin{aligned} NL_{ship'g} &= NL_{100} && \text{if } f \leq 100 \text{ Hz} \\ &= NL_{100} - 20\log\left(\frac{f}{100}\right) && \text{if } f > 100 \text{ Hz} \end{aligned} \qquad (2.20)$$

NL_{100} varies from 60 to 90 dB re. 1μPa/√Hz, depending on the average shipping density. From 1 kHz to 100 kHz, the main contribution is from sea surface agitation. A model proposed by Knudsen (1948) is widely used;

$$NL_{surf} = \begin{cases} NL_{1K} & \text{if } f < 1000 \text{ Hz} \\ NL_{1K} - 17\log\left(\frac{f}{1000}\right) & \text{if } f > 1000 \text{ Hz} \end{cases} \qquad (2.21)$$

[1] The spectral power density *N(f)* is the power which corresponds to a 1 Hz spectral band and can be expressed in W/Hz, or dB re 1W/Hz in logarithmic notation, but to relate it to acoustic pressure it is expressed in dB re 1μPa/√Hz. Since power is proportional to pressure squared, the latter notation is consistent with the first. (e.g. M. A. Ainslie (2010). Principles of Sonar Performance Modelling. Berlin, Springer, X. Lurton (2010). An Introduction to Underwater Acoustics. Chichester, Praxis Publishing.)

where NL_{surf} is the noise level at the sea surface, in dB re.1μPa/√Hz and NL_{1K} is a parameter depending on sea state, given in Table 2.2 (Lurton 2010).

Sea state	0	0.5	1	2	3	4	5	6
NL_{1K}	44.5	50	55	61.5	64.5	66.5	68.5	70

Table 2.2: Values of the coefficient NL_{1K} of the Knudsen model as a function of sea state. From Lurton (2010).

Above 100 kHz, noise is dominated by electronic thermal noise, and generally follows the pattern:

$$NL_{th} = -75 + 20\log f \tag{2.22}$$

2.4.2. INTERMITTENT AMBIENT NOISE

Biological noise

Biological noise is the major contributor to intermittent ambient noise, and is varied in character. Marine mammals can transmit acoustic signals for communication or echolocation, and the characteristics of the signal emitted will depend on the species. Typically, whale vocalisations range from 12 Hz to several kHz, with signals which can propagate hundreds of kilometres. The sounds produced by smaller marine mammals are modulated (such as cries and whistles) and at higher frequencies (above 1 kHz). Only certain marine mammals use echolocation, by transmitting a series of clicks, from 50 – 200 kHz. Sound levels from whale vocalisations can be as high as 190 dB re. 1μPa/√Hz at 1 m in the 100 – 200 Hz band. Echolocation clicks can be as high as 200-220 dB re. 1μPa/√Hz at 1 m (Lurton 2010).

Snapping shrimps form large colonies in warm, shallow water and are able to create cavitation bubbles using their pincers. Some types of fish also communicate using sound, or by purposefully creating bubbles. When these bubbles implode they generate intense broadband noise with a peak around 1 – 10 kHz. The levels of this sound can reach 60 – 90 dB re. 1μPa/√Hz (Lurton 2010).

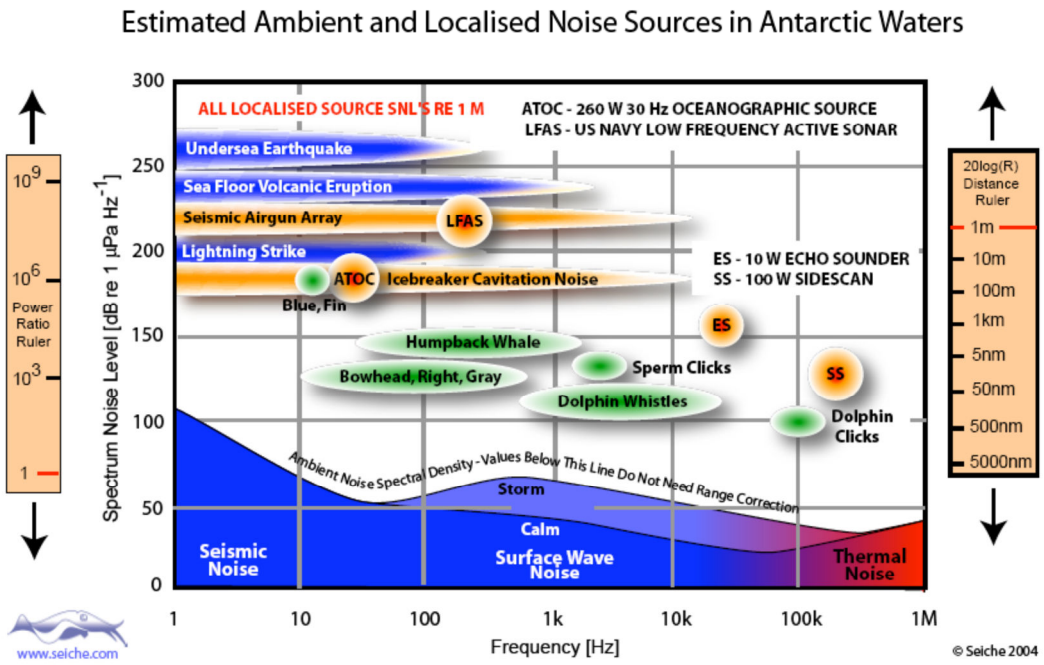

Figure 2.17: Noise sources in the marine environment in terms of levels and frequency ranges. From SCAR (2004)

Wind noise

The wind speed and sea state affect surface agitation, which generates noise from several Hz to tens of Hz. The spectra generated for the noise caused by wind of various speeds are known as Knudsen spectra. Sea state and wind speed are related by the Beaufort Scale (Table 2.1). At frequencies below approximately 10 Hz, wind causes turbulence which leads to pressure variations. Wind can also cause noise above several hundred Hz, when micro-bubbles of air dissolved in the shallow water layer undergo dilation and bursting, caused by pressure changes associated with the movements of the surface due to the wind. As the wind speed increases and the sea state worsens, the clouds of bubbles forming in the foam crests lead to increased noise levels, along with impacts of breaking waves. At frequencies below 0.5 kHz, the predominant source of noise is collective oscillations of bubble clouds with waves (Nystuen and Selsor 1997). Above 0.5 kHz, most of the noise comes from individual bubbles created within the whitecap and breakers (Farmer and Xie 1989; Tegowski 2004). When the water is shallow, waves can break on shores or reefs, increasing ambient noise levels. The sound caused by wind can propagate over

distances up to 9 km and the noise spectra spread to hundreds of kHz (Lurton 2010). Between 0.1 and 1 kHz, surf noise is scaled with the squared RMS wave height (Deane 2000).

Compared to other weather processes, wind is relatively quiet underwater, with its noise causing a relatively constant spectral slope from 0.5 kHz to 20 kHz, with higher wind speeds showing higher intensities. Numerical values of the slopes vary with regions, seasons and seabed properties (Buckingham 1987; Ramji et al. 2008) because of contributions from seabed reflections. The frequency dependence also varies with the depth of the measurements, since the sound radiated from surface bubbles is modified by inactive older bubbles beneath the surface, and attenuated by absorption (Buckingham 1997; Medwin and Clay 1998). Therefore, at frequencies above 5 kHz, the spectral levels just below the surface decrease noticeably when measured a few metres below the surface (Lemon et al. 1984). Even so, wind at the water surface can be detected at considerable depths (up to 4.9 km deep) between 50 and 500 Hz (Gaul et al. 2007). Since noise caused underwater by wind has been studied so extensively through laboratory and field experiments, it is possible to investigate more extreme weather processes such as typhoons (Iwase 2008), tropical storms (Knobles et al. 2008) and hurricanes (Wilson and Makris 2008).

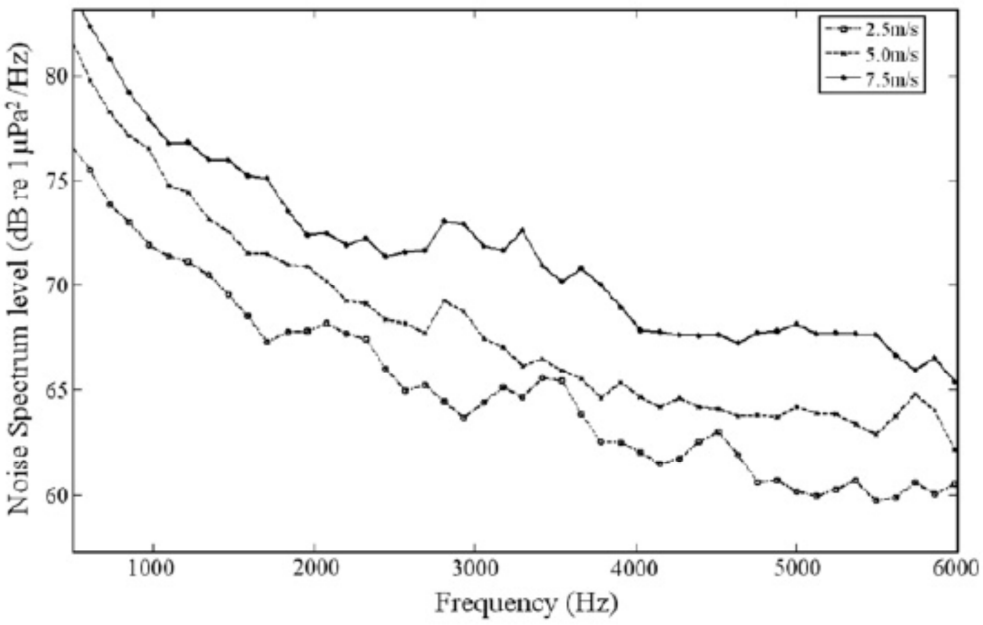

Figure 2.18. Noise spectrum at different wind speeds. (Ramji et al. 2008).

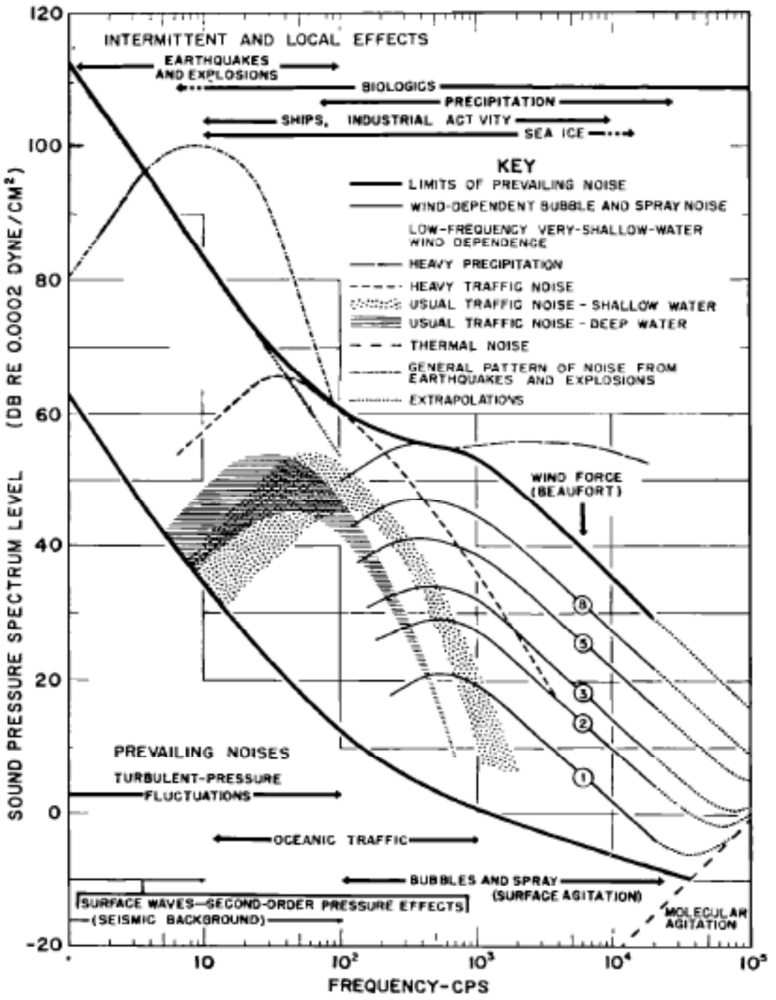

Figure 2.19. A composite graph of ambient noise spectra showing probable sources and mechanisms of the ambient noise from 1 – 100 kHz (cps – 1 cps = 1 cycle per second = 1Hz). The horizontal arrows indicate the approximate frequency bands. From (Wenz 1962)

Rain noise

When a raindrop falls on water, the sound from the impact lasts several microseconds and is usually followed by sound from a bubble created by the impact, which lasts several milliseconds and is usually much more energetic than the impact sound. The frequency of the bubble radiation is related to the drop size and to the bubble size (e.g. Leighton (1994), which means that using passive underwater acoustics to listen to raindrops can provide comprehensive information about the drop size distribution within the rainfall. The shape of the underwater sound spectrum can be used to determine the type of cloud from which the rain has fallen.

If no rain is falling, sound from 500 Hz to 20 kHz is usually caused by microbubbles generated by breaking waves, which may be caused by wind. (Leighton 1994)

Rain makes noise underwater from 1 – 100 kHz, in a similar way to sea surface noise, since the underlying processes are similar. However, the spectra of rain-induced noise do not decrease regularly with frequency. Numerous studies (Nystuen 1986; Scrimger et al. 1987; Pumphrey et al. 1989; Leighton 1994) noted that the frequency spectrum from acoustic emission of rain on water has a characteristic shape (Figure 2.20). Its peak is at ~14 kHz, with generally a sharp fall-off to lower frequencies (<10 kHz) and in some cases, a smaller rise below ~3 kHz.

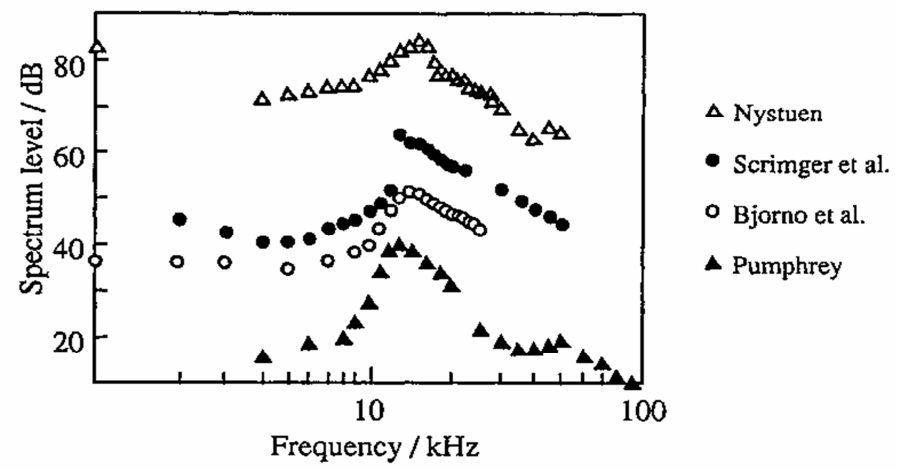

Figure 2.20: Sound spectra of various rain measurements : (Δ) heavy rain in a lake; (•) light rain in a lake ; (o) and (▲) light rain in a land-based water tank. The overall level decreases with rainfall rate, and the shape of each spectrum varies with local conditions. (Leighton 1994).

The physical processes associated to rainfall at sea are well documented but there is no consensus on the influence of each process on the acoustic frequency content (Nystuen and Farmer 1987; Laville et al. 1991; Oguz and Prosperetti 1991; Leighton 1994). Figure 2.21 illustrates a raindrop falling on a liquid, along with the observed acoustic pressure underwater and the associated frequency. Figure 2.21a shows how the resonating bubble is formed – the initial impact from a raindrop, which in natural rain would fall at terminal velocity, causes the formation of a water column, from which a resonating bubble detaches. Acoustic pressure shows an initial spike associated to the impact, followed by an exponentially decaying sinusoid associated

with the resonating bubble (Figure 2.21b). The corresponding spectra are similar in shape to those of Figure 2.20, but authors disagree over the relationship between the different parts of the bubble-forming sequence and their associated frequencies. Figure 2.21c shows that for Nystuen (Nystuen 1986; Nystuen and Farmer 1987; Pumphrey et al. 1989) the initial impact is responsible for the 13-15 kHz peak and the resonating bubble for the presence of higher and lower frequencies, whereas for (Pumphrey et al. 1989), the peak is caused by the resonating bubble and the initial impact causes noise at all other frequencies. These effects have been independently studied in several experiments, at sea and in land-based tanks, as presented in chapters 4 and 5.

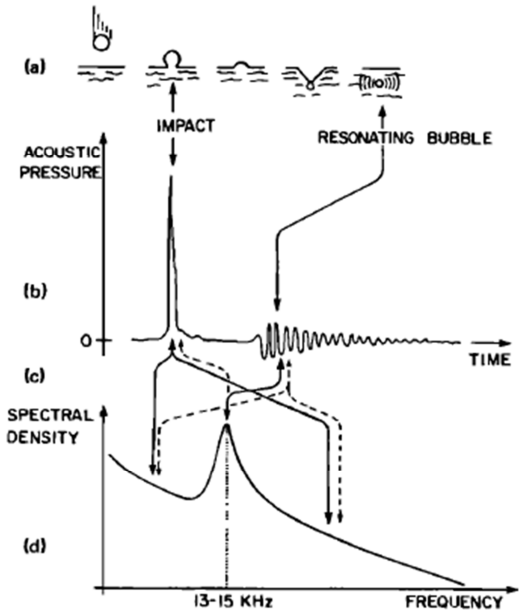

Figure 2.21: Schematic of underwater sound generation by rainfall. (a) raindrop fall; (b) acoustic signals in the time domain; (c) relationship between time and frequency plots:- - - Nystuen model (Nystuen 1986; Nystuen and Farmer 1987), − Pumphrey et al. model (1989); (d) resulting rain noise spectrum. From Laville et al (1991).

When a solid sphere impacts a liquid surface above a certain speed, bubbles are always entrained. However, when a liquid drop impacts a liquid surface, bubbles are only entrained for certain impact velocities and drop sizes (Leighton 1994). The two different sources of noise from rain impacting on water have been studied, and based on measurements (Figure 2.25), Oğuz and Prosperetti (1991) dismiss the initial

impact as incapable of explaining the underwater sound of rain impacting a liquid body, by developing models of the noise caused by both the initial impact and the entrained bubbles, then comparing both models with field data obtained in varying weather conditions.

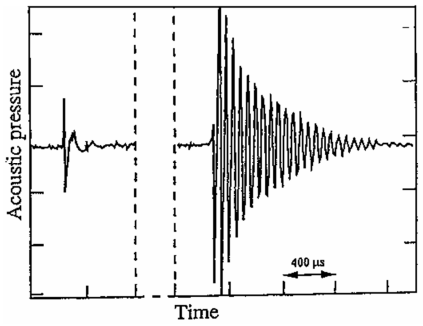

Figure 2.22: Pressure field from rain impacting on water. There is a characteristic bubble-generated exponentially-decaying sinusoid emitted some time after the pressure signal. (Leighton 1994)

Laboratory experiments (Pumphrey 1989; Pumphrey et al. 1989) have suggested that the pressure amplitude associated with the impact pulse is proportional to $v^{2.5\text{-}3}$, where v is the drop velocity. The initial sharp pulse is of the order of tens of microseconds and falls off as r^{-1} (where r is the distance from the centre of the drop). This is a far-field pressure fluctuation; the near-field pressure fluctuations falling off as r^{-2} (Pumphrey 1991). The time between the initial impact and bubble emission has been shown to be around 20 ms (Pumphrey et al. 1989; Medwin et al. 1990). The impact is short and therefore has a broadband frequency spectrum. But as it is larger in amplitude, lasts longer and is repeated for each successive raindrop, the noise created by the bubbles is likely to be the most important contributor to acoustic noise.

The sound produced by objects (liquid or solid) falling onto liquids is well-documented in Franz (1959). This paper explains that the most common example of sound being radiated by a splash from a gas-to-liquid entry of an object is the sound produced by splashes of water droplets on a surface. It documents work by Minnaert (1933) which related to the generation of underwater sound by bubbles, and suggested that the sounds of running water were associated with bubble resonance. A significant result of Minnaert's paper was the determination of the resonant frequency of a pulsating bubble:

$$f_M = \frac{1}{2\pi R_0}\sqrt{\frac{3\gamma p_0}{\rho}} \quad (2.23)$$

where ρ is the density of the water, p_0 is the hydrostatic liquid pressure outside the bubble, and γ is the ratio of the heat capacity of a gas (air, in this case) at constant pressure to that at constant volume.

Franz (1959) sums up the direct sources for the underwater sound of raindrops as:

- The transient introduction of the object into the water
- The vibrations of the body, the secondary splashes of water droplets thrown up by the entry
- The oscillations of air bubbles and of cavities which are open to the atmosphere
- The secondary slaps of the afterbody against the side of the cavity behind the object.

For a single water droplet impacting a liquid surface, the initial droplet entry always produces a characteristic peaked pulse of sound, shown in Figure 2.22. Under some conditions, an air bubble can be entrained in the water by the later development of a splash, which usually leads to the radiation of a damped sine wave. Figure 2.23 (Franz 1959) illustrates a water droplet of radius 0.24 cm impacting a water surface at 3.5 m/s. The impact sound (consistent and reproducible) was shown to be produced between frames 1 and 2, and the bubble sound was shown to be produced between frames 13 and 15. The bubble sound varies in amplitude and frequency and sometimes does not exist at all.

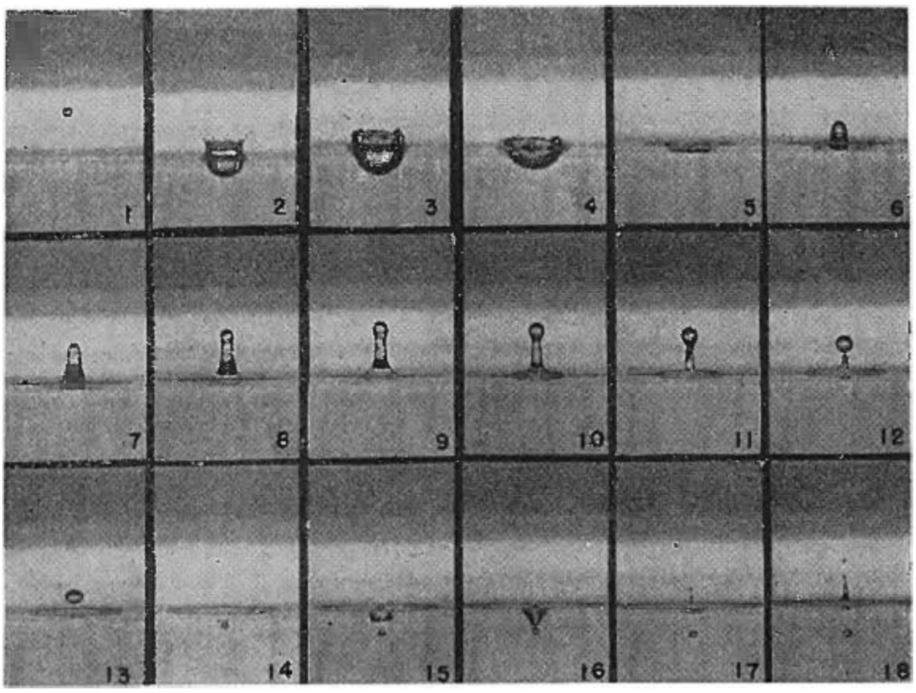

Figure 2.23: Photographs of the splash of a 0.24 cm radius water droplet with vertical impact velocity of 3.5 m/s. The frames are spaced at 13 ms intervals. (Franz 1959)

Figure 2.24 (Franz 1959) also shows water droplets of radius 0.24 cm falling on a water surface, at speeds of between 5 and 9 m/s.

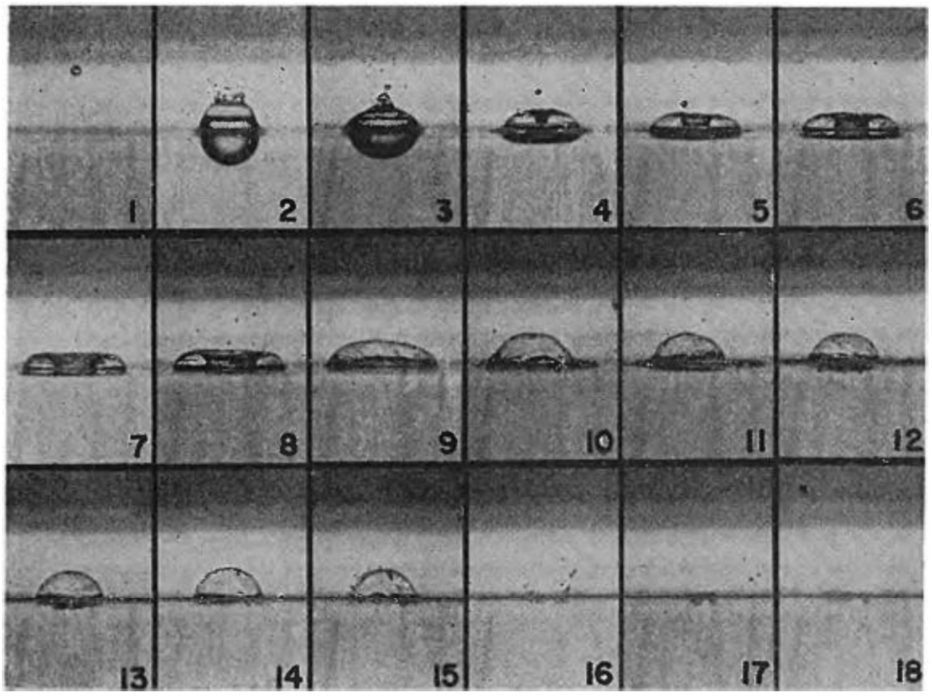

Figure 2.24: Photographs of the splash of a droplet of radius 0.24 cm, with vertical impact velocity 5.5 m/s. The frames are spaced at 20 ms intervals.

The splash produced by the droplet shown in Figure 2.24 is a typical splash produced by a large droplet. Bubbles are not produced due to the closing of a canopy – comparison of Figures 2.23 and 2.24 shows the lack of bubbles formed in Figure 2.24. The only time that appreciable underwater sound was produced in Figure 2.24 was between frames 1 and 2. Figure 2.25 (Franz 1959) shows the splash produced by a large water droplet followed by three smaller water droplets – the smaller droplets are produced behind the large droplets after the large droplet has fallen from the dropper.

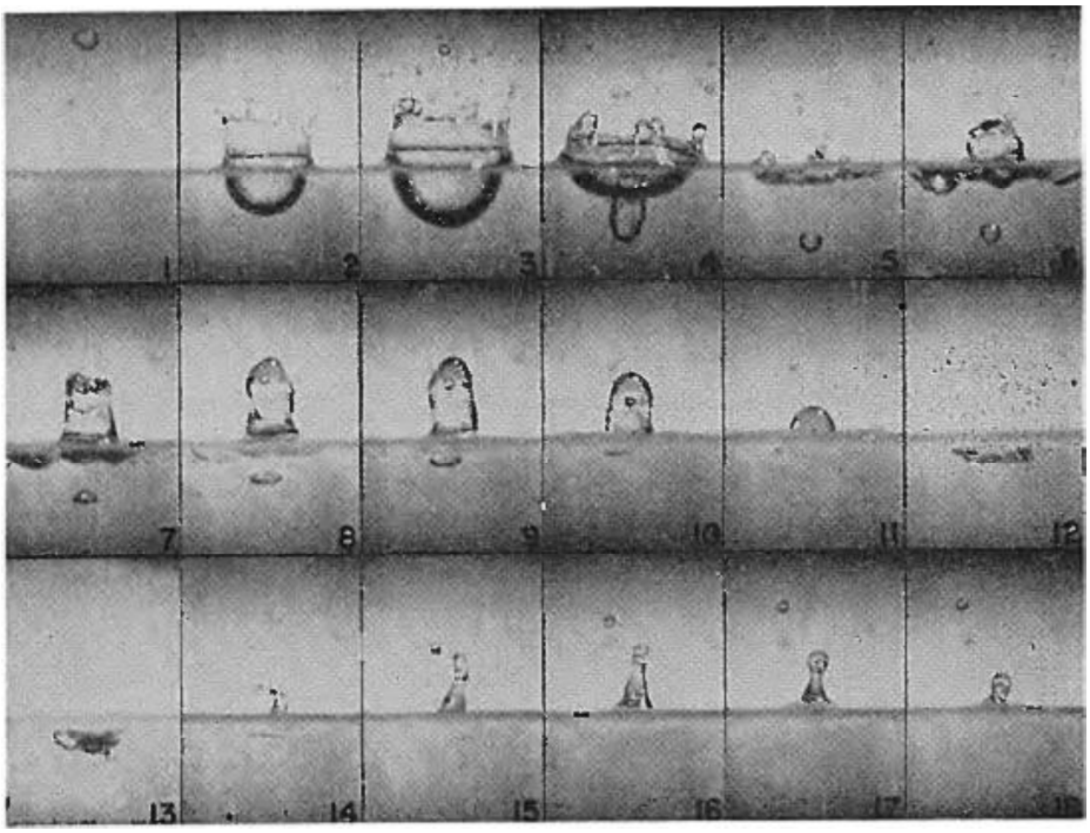

Figure 2.25: Photographs of the splash of a 0.35 cm radius (mass 182 mg) water droplet, with vertical impact velocity of 4 m/s and with three smaller droplets with total mass of 50 mg. The frames are spaced at 21 ms intervals.

In a situation such as Figure 2.25, large bubbles can be entrained if the small following droplets hit in the bottom of the hemispherical cavity made by the impact of the large droplet. The impact sounds of all three small droplets appear just before the bubble sounds (Franz 1959).

The frequency spectrum and the amplitude of the sound radiated into water by splashing droplets can depend on many variables, (Franz 1959) particularly the size, shape and velocity of the droplet and the density and acoustic properties of water. Other influences come from the surface tension and viscosity of water, and the density, compressibility, pressure and viscosity of the air above the water. Figure 2.26 (Franz 1959) shows the typical shape of a sound pressure pulse from the impact of a water droplet on water.

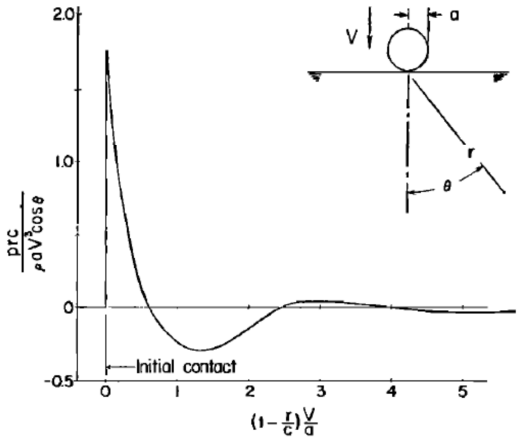

Figure 2.26: The typical shape of the sound pressure pulse radiated into the water by the vertical impact of a water droplet (Franz 1959).

It is possible to obtain separate spectra for the impact and bubble sounds due to the time delay between the two. Figure 2.27 (Franz 1959), which shows the half-octave frequency spectra for the impact part of the sound caused by splashes from single water droplets.

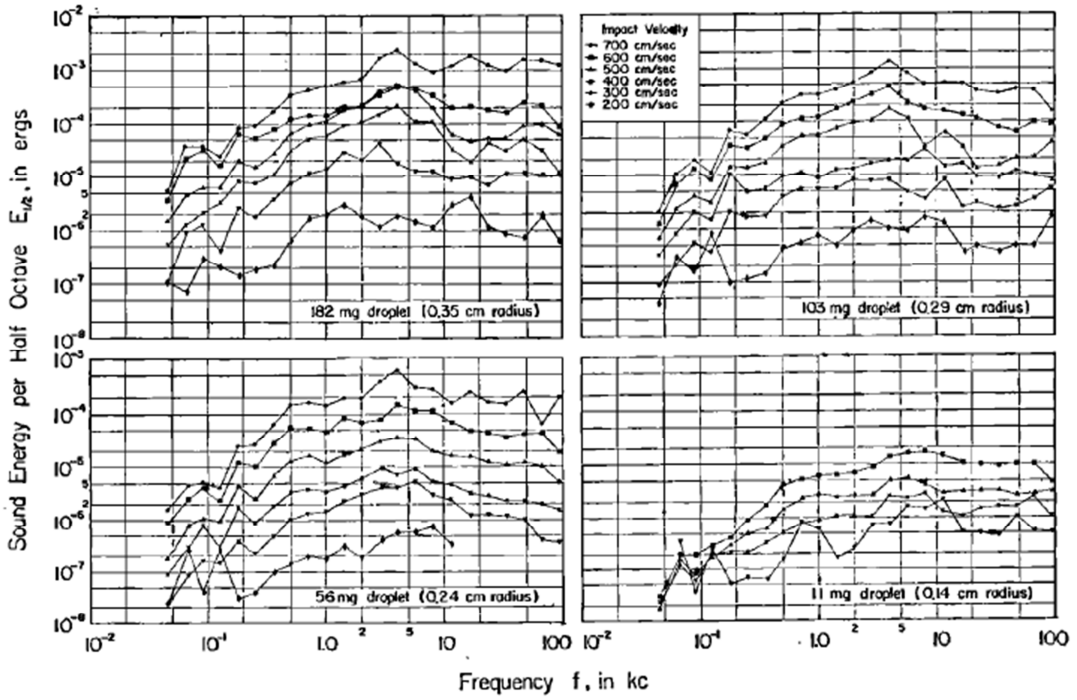

Figure 2.27: The half-octave frequency spectra of the impact part of the sound energy radiated into the water by the splashes of single water droplets (Franz 1959).

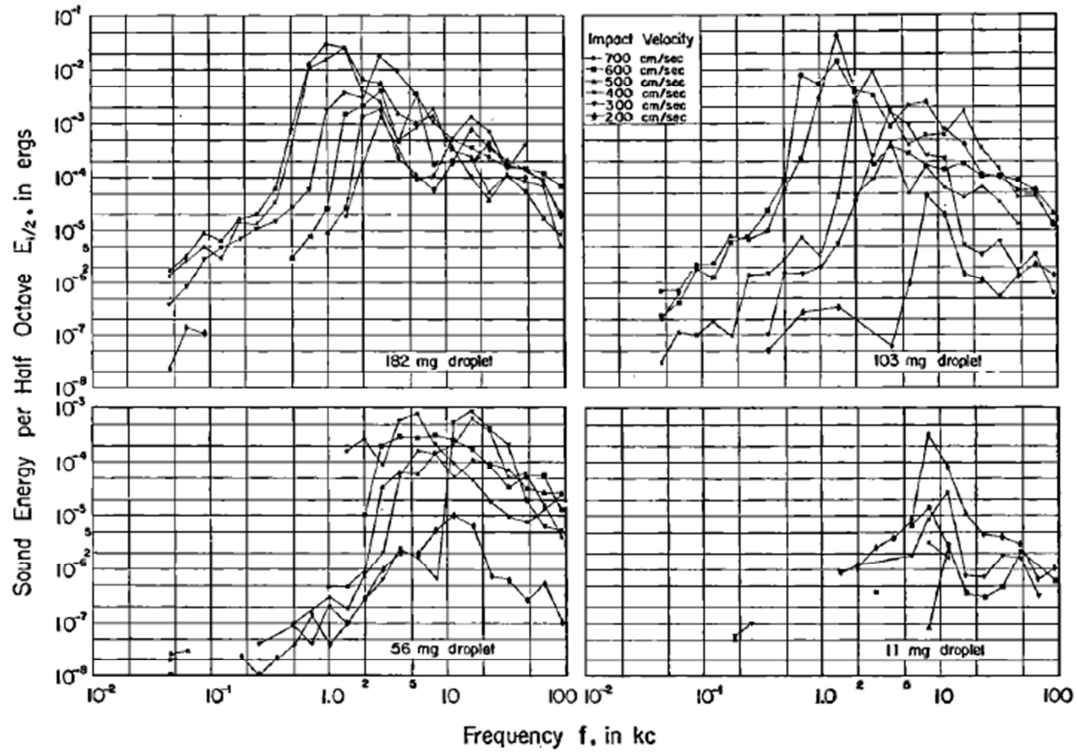

Figure 2.28: The half-octave frequency spectra of the bubble part of the sound energy radiated into the water by the splashes of single water droplets (Franz 1959).

The frequency spectra in Figure 2.28 show that the sound energy radiated into the water by the initial entry of a droplet increases systematically with increasing droplet size and velocity. Figure 2.28 (Franz 1959) is similar to Figure 2.27 but illustrates clearly the effect of variation in droplet size and velocity.

Figure 2.28 shows that certain ranges of droplet size and velocity are more conducive to bubble production than others. Therefore droplets at intermediate velocities produce more bubble sound than droplets at high or low velocities, and small droplets trap small bubbles which oscillate at higher frequencies. The bubble sound from large drops is more repeatable and depends less on the impact velocity (Franz 1959).

The total sound energy radiated by an individual bubble can be greater than the sound energy radiated by the impact of the water droplet, and the sound energy in the half-octave band in which the bubble was radiating most of its energy was shown by Franz (1959) to usually be much greater than the sound energy in the same band due to the impact. However, since the frequency varied and bubbles were not always formed, the sound energy per half-octave averaged over many droplets is approximately the same for the bubble and impact components of the sound, over the frequency range in which the bubble sound is appreciable. Since the bubble sound energy decreases with increasing impact velocity, whereas the impact sound energy is proportional to the fifth power of impact velocity, the impact sound is more dominant at higher velocities.

Bubbles are not systematically entrained underwater (Leighton 1994). In *regular entrainment*, single bubbles are regularly captured by the formation of impact craters. In *irregular entrainment*, bubbles are produced through complex processes associated with the splash, and it is not possible to predict with certainty whether entrainment will occur. *Large bubble entrainment* confines most of the volume of the crater within the bubble, and could be influenced by surface oscillations on the falling drop, yet it does not occur often. *Mesler entrainment* occurs for drops at low velocities and is unpredictable, occurring when many small bubbles are trapped in the initial stages of impact. It does not produce significant acoustic emission. Each process is related to different frequencies (Leighton 1994).

Pumphrey and Walton (1988) showed that the exponentially decaying sinusoid characteristic of bubbles occurred at the resonance frequency of a bubble of the same size as the entrained one. This means that bubbles cause that part of the signal, however, to show that bubble entrainment contributes significantly to the sound spectrum of natural rain, it must be shown that there are enough drops in natural rainfall (Pumphrey et al. 1989). Figure 2.29 relates regular entrainment to the speed of drops of different sizes (at normal incidence). It shows that, for regular entrainment to occur, rain must include drops of diameter 0.8 – 1.1 mm (Leighton 1994).

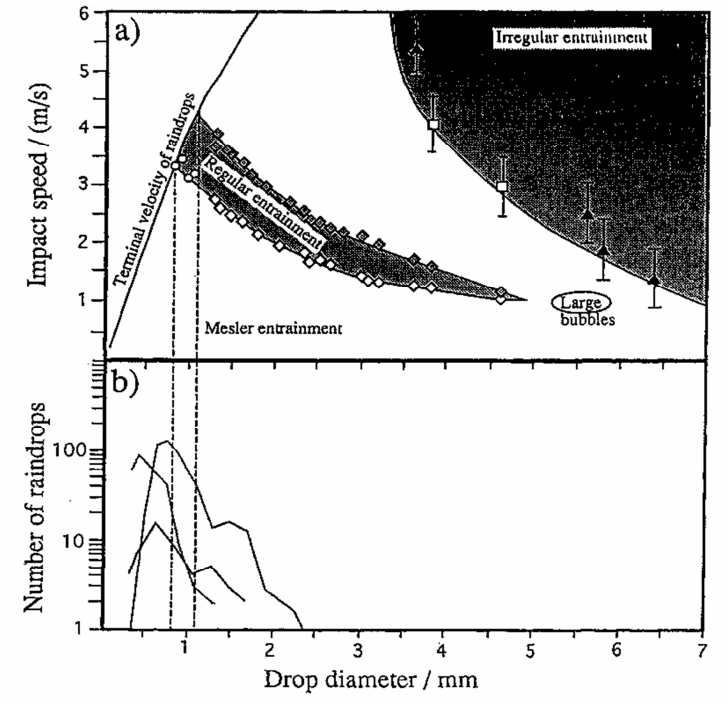

Figure 2.29: (a) Different types of entrainment for combinations of drop diameter and speed at normal impact, showing the terminal velocity line. Real rain falls at this speed and the graph shows that raindrops sized between 0.8–1.1 mm diameter at normal incidence and terminal velocity will lead to regular entrainment. This size range is shown by two lines, connecting to plot (b), showing drop size distributions from three rain showers, (Scrimger et al. 1987; Leighton 1994).

Since the signal generated by a bubble is an exponentially-decaying sinusoid, it contains a range of frequencies, around the resonance frequency f_0. This means that there will be contributions to the sound spectrum of rain from sources other than just

the bubble pulsation resonances (e.g. irregular entrainment of bubbles), concentrated in a specific interval of frequencies.

This can be extended to other source mechanisms than raindrops. In general, oscillations of gas bubbles in liquids are caused by an initial displacement, in this case the drop impacting on the water surface and leading to bubble formation. When the bubble is spherical, the restoring force is the elasticity of the gas and the oscillation approximates to simple harmonic motion at the natural frequency of the bubble (Minnaert 1933). The motion of the bubble wall is described by

$$R = -R_0 e^{2\pi i f_0 t} \tag{2.24}$$

about a mean radius R_0, with f_0 being the resonance frequency. R is the displacement of the bubble radius from the equilibrium. Minnaert (1933) derived an expression for the resonance frequency in the adiabatic form and assuming negligible surface tension for mm-sized air bubbles in water (equation 2.23), and it is realistic to assume that bubbles produced by rain on water will oscillate at this frequency.

The oscillations in bubble volume can be excited by changes in the environmental pressure or when the bubbles are formed. When the bubble is formed within one wavelength of a bubble diameter of the free surface, most of the radiated sound is cancelled by a negative image source in the free surface, which means that the bubble source and its negative image constitute a dipole source of sound. To find the dipole sound pressure, the sound pressure expected from the bubble itself in the free field is multiplied by a factor equal to (Medwin and Clay 1998) $\frac{2\pi f d \cos\theta}{c}$ where d is the distance from the source to the image. The frequency of the dipole sound is approximately the same as for the bubble in the free field, except for when the bubble is within a few bubble diameters.

Air bubbles from various sources form an inhomogeneous layer close to the surface. The mixing of water and gas caused by the bubble layer affects the acoustic characteristics of the propagation medium, in terms of velocity and attenuation. As depth increases this process becomes less significant, due to increasing hydrostatic pressure – and at depths greater than 20 m the effect of bubbles can be ignored (Lurton 2010).

Surface bubbles can also affect the reflection of waves from the sea surface. Theoretical and experimental work has shown that each bubble acts as a spherical obstacle with a very high acoustic impedance contrast, thus scattering the incident sound wave. The scattering effect is greatest around the intrinsic resonance frequency of the bubble (Medwin and Clay 1998), already given as equation 2.18;

$$f_R = \frac{3.25}{a}\sqrt{1+0.1z} \qquad (2.18)$$

where f_R is the resonance frequency, z is the depth and a is the radius of the gas sphere. The behaviour of bubbles with simple statistical distributions is well understood (Lurton 2010). However, predicting the effects of evolving, inhomogeneous bubble populations is more complicated.

2.5. OTHER NOISE SOURCES

Other potential sources of ambient noise underwater include:

- hail, which without rain or winds will show peaks around 2 – 5 kHz (Scrimger et al. 1987)
- snow, which shows noise levels which increase linearly with frequency, showing peaks around 35 kHz (Scrimger et al. 1987; McConnell et al. 1992; Alsarayreh and Zedel 2009)
- sediment transport (usually gravel, clay or fine sand in water shallower than 10 m) which exhibits noise above 10 kHz with peaks at several tens of kHz (Thorne 1985; Thorne 1993)
- noise from far above the sea surface, such as thunder or aircraft, detectable below 10 kHz (Urick 1972; Buckingham 2005)
- diving birds, which cause sound detectable around 1 – 4 kHz in calm waters (Szczucka 2009)

All these sources will potentially include the range of sound-generating mechanisms described by Franz (1959).

2.6. ACOUSTICS OF ICE-RELATED PROCESSES

Sea ice and icebergs are documented in numerous textbooks (Harvey 1982; Barry and Chorley 1998) and the main reference of Wadhams (2000). Sea ice can be caused by the freezing of sea water, or from being moved by glaciers or partially frozen rivers.

When sea water first begins to freeze, only water molecules will form ice, since salt lowers the freezing point of water. The leftover salt will increase the salinity of the surrounding water. When the ice is thicker than 5 cm, it is called young ice, and when thicker than 20 cm but still less than a year old, it is called winter ice. Once it is older, it is called polar ice and will have a lower salinity because salt leaches out and is reduced by precipitation. Sea ice is broken up by wind and waves and becomes piled up – in the Arctic this makes an uneven surface but in Antarctic the surface is more even.

Glacier ice builds up from the net balance of snow accumulation and summer melt. In small glaciers, the ice can persist for tens to hundreds of years, but in ice caps and ice sheets it can stay for 10^3 to 10^6 years. Ice brought to the sea by glaciers forms icebergs, and icebergs found in the Northern hemisphere are very different to those found in the Southern hemisphere (see Wadhams (2000), for details). Arctic icebergs are small and dense with irregular shapes, whereas Antarctic icebergs have larger surface areas and are less tall, with a higher air content which makes them less dense. Their size means that icebergs are more influenced by ocean currents than by the wind. Individual bodies of glacier ice and sea ice are easily recognised on satellite and airborne imagery (Figure 2.30), at least in the absence of cloud cover (e.g., Wadhams (2000)). Their movements through the water, and their melting, will also be noticeable acoustically (e.g. Urick (1975)).

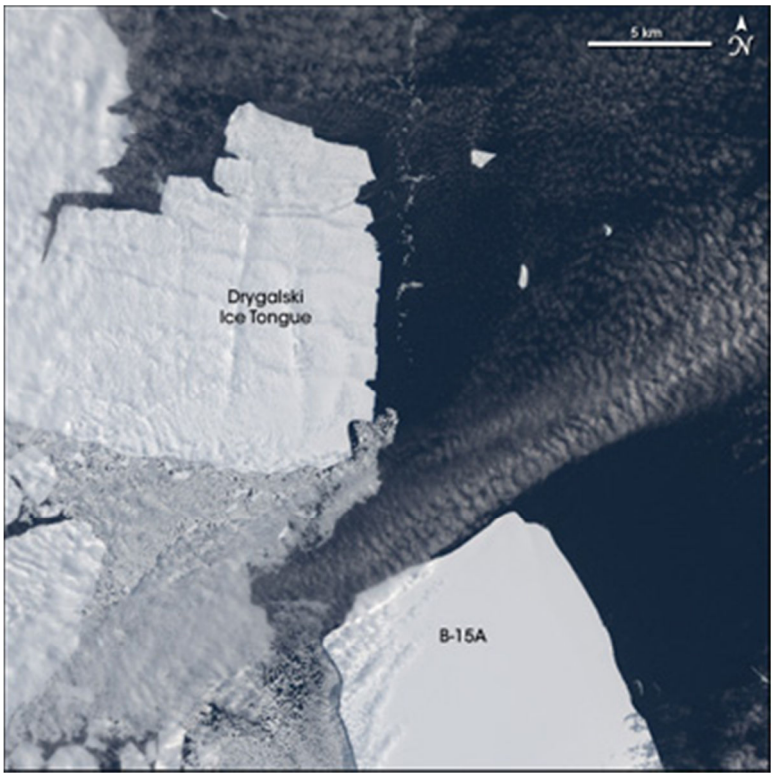

Figure 2.30. Landsat satellite image from a calving glacier in the Antarctic, taken in visible wavelengths (Wadhams 2000).

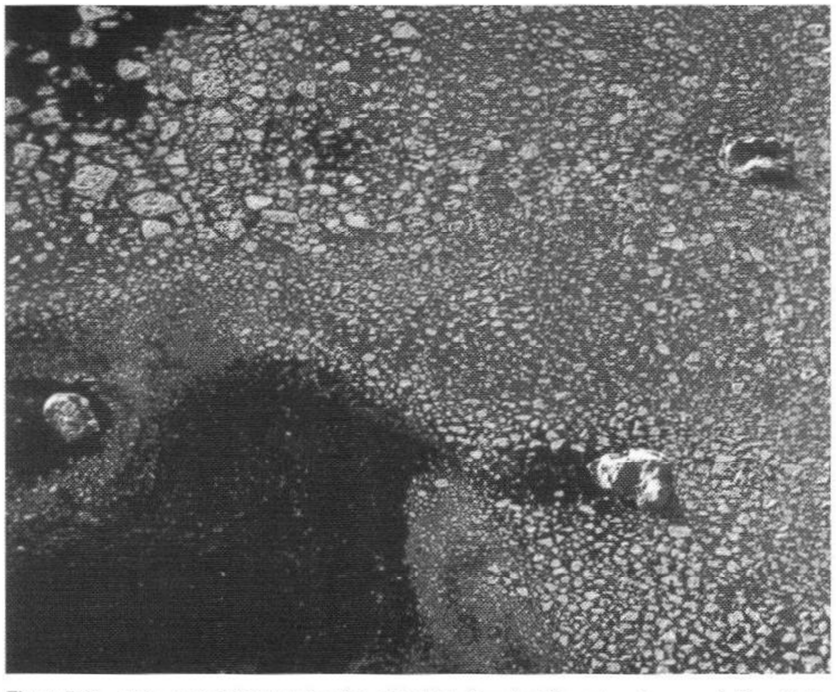

Figure 2.31. A photograph of three small icebergs near Fram Strait, from Wadhams (2000).

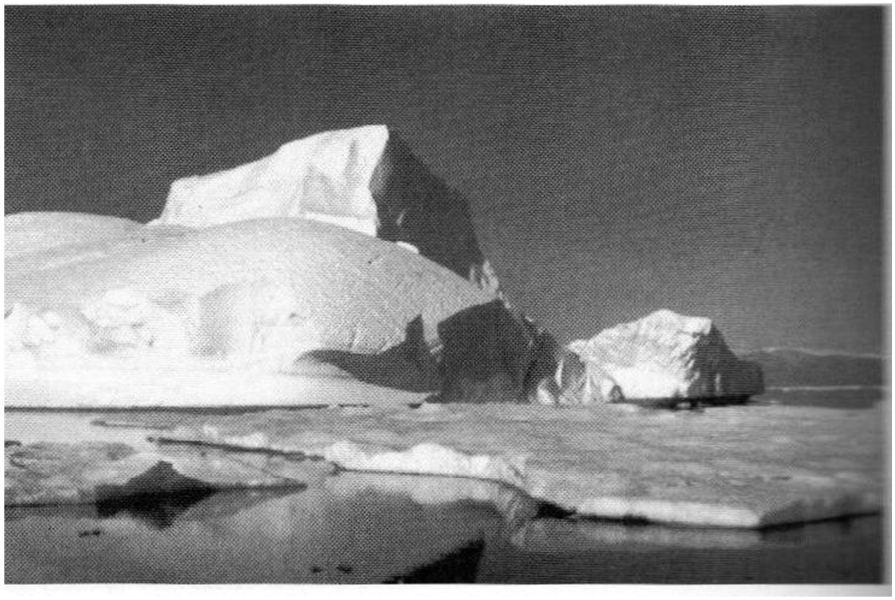

Figure 2.32. A photograph of a capsized iceberg in East Greenland, from Wadhams (2000).

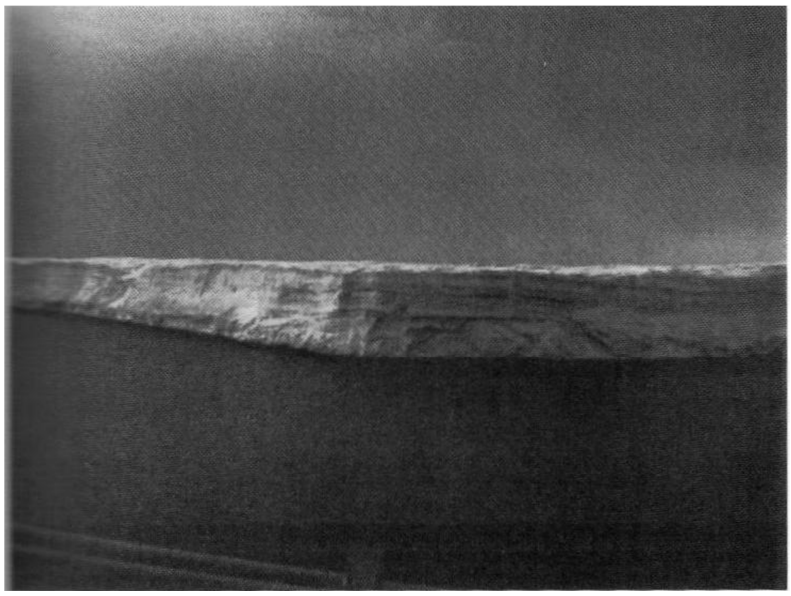

Figure 2.33. Photograph of an ice island (a type of iceberg) off NE Greenland. From Wadhams (2000).

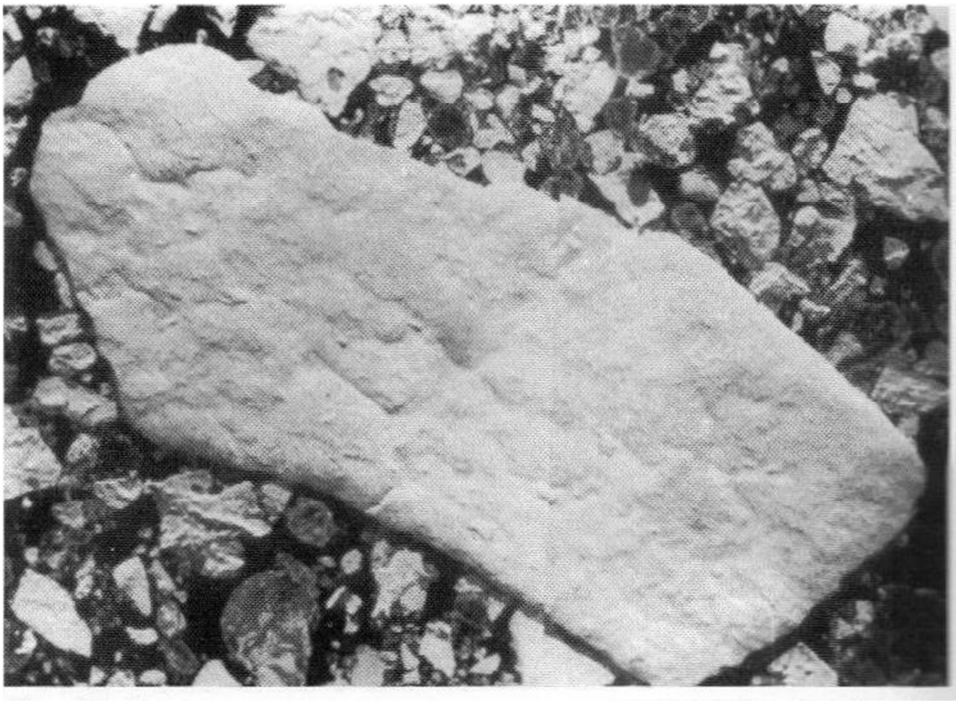

Figure 2.34. A photograph of a 400-m long ice island, 35-m thick, in East Greenland. From Wadhams (2000).

If ice is present on the water, for example as icebergs or pack ice, the noise measurements will be more complex, with some processes (such as wind, rain or snow) being damped, and other processes combining. Furthermore, the acoustic signature of the ice cover will vary with its composition, for example the presence of salt, sediment or embedded rocks, as well as its age and state. The noise caused by ice, observed in polar regions, has several origins.

Figure 2.35. The edge of part of a capsized iceberg showing where the iceberg dragged along the seafloor, acquiring large blocks (marked by red arrows). The vertical dimension is between 5 and 10 m high. Taken by Philippe Blondel during the ARCFAC 2007 expedition.

a) Ice cracking. In shore-fast spring and winter ice, short bursts of noise can be observed which originate in tensile cracks in the ice. These cracks occur near the surface of the ice and are caused by radiative cooling as the air temperature decreases. Surface cracking only occurs when the ice near the surface is brittle and exposed to the air with little or no snow cover. Bursts of cracking sound have been observed to reach a maximum near midnight, when air temperatures in the Arctic are at their lowest. Each burst of cracking resembles a decaying sinusoid which lasts for several milliseconds, and the spectrum of the sound from ice cracking has a maximum from 0.1-1 kHz (Urick 1986).

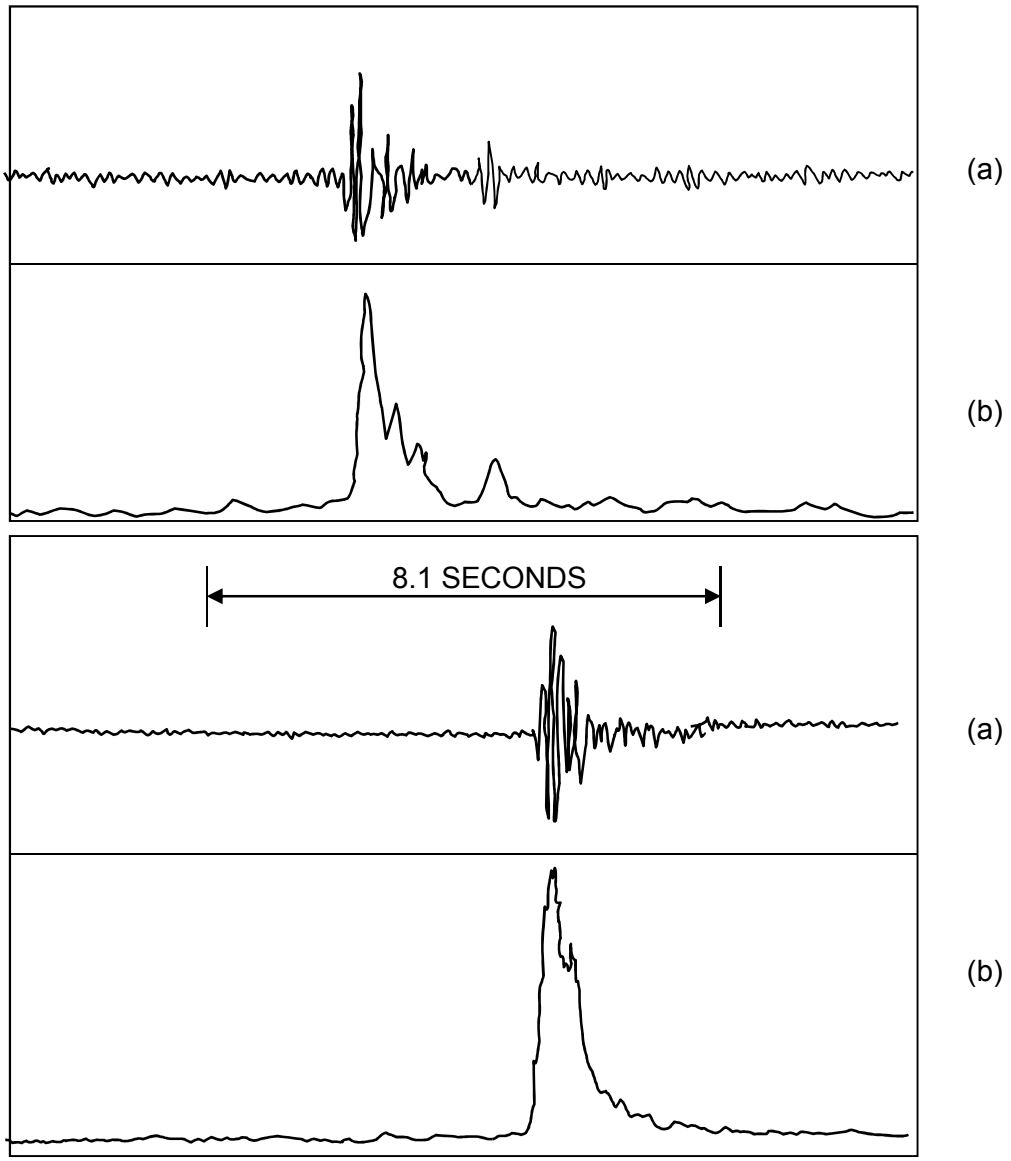

Figure 2.36, adapted from (Milne 1967): Ice cracking pulses (a) and their envelopes (b), frequency band 200 to 600 Hz.

The cracks should only occur in low salinity, very cold sea ice where ice responds elastically to thermal stresses – internal stress built up by thermal tension and the effects of wind and current. For individual cracks the sounds will have 'spiky' amplitudes and non-Gaussian shapes, but with increasing depth below the ice, noise spikes become more numerous and their amplitudes become quasi-Gaussian. The effects of the response of the ice to stress can be seen as cracks, pressure ridges, buckling and fragmentation (Farmer and Xie 1989).

Farmer and Xie (1989) expected that an understanding of the physical processes of sound generation would help studies of ice behaviour and properties. They therefore

carried out an experiment to study the sound of ice cracks beneath landfast ice, extending measurements to 20 kHz. They applied a theory of earthquake mechanics to the case of a floating ice sheet with some success. The first of the four events examined contained a short pulse followed by a longer and louder pulse, 30 ms later, with a dominant frequency of 500 Hz. The other three events showed different properties, they contained a pulse of frequency 150 – 200 Hz, modulated by a much higher frequency. Farmer and Xie (1989) concluded that the lower-frequency components were from longitudinal waves, and that the source of noise moved along with the crack, leading to a Doppler shift of each frequency component in the signal. They also concluded that the ice cover is an efficient waveguide and therefore little energy leaks into the water, and that the direct acoustic path is very important to the ocean sound field. However, they noted that leaked longitudinal waves could still be detected, although being very small contribution to the signal intensity. Their model of the noise source means that a significant fraction of the energy in the signal is contained within one lobe, which has a frequency determined by the propagation speed and the coherent length of a crack segment. The fine structure has a frequency determined by the roughness elements in the mechanical failure. They suggested that the lack of low-frequency sources was due to a lack of macroscopic ice motions at the site of their investigations, and implied a need for similar experiments investigating the crack orientation.

The work published by Farmer and Xie (1989) was followed by Xie and Farmer (Xie and Farmer 1991), which looked at the sound radiated by shallow surface cracks in ice caused by thermal stress. The thermal stresses were simulated using hammer blows and small explosive charges. As with their previous study they concluded that most of the energy radiated by ice into water is from near field radiation, and that the far field contribution could be ignored. They stated that a broadband ice-cracking sound would appear as a narrow-band signal of low frequency, probably below 200 Hz, because the ice cover would act as a waveguide. However, their observations did not agree with this theory, and so they felt that the vibration of ice at the source was a predominant mechanism for sound radiation from sea ice into the ocean. They observed that a weak P (compression) wave of around 140 Hz arrived at the hydrophone first, followed by the acoustic wave, with a frequency of 516 Hz, at almost the same time as a low-frequency pulse of frequencies ranging from 30 to 60

Hz. This was an SV (vertical shear) wave. The final sound wave to be observed was the reflected acoustical wave. There was also a shift in frequency between direct and reflected signals.

They made several conclusions, for example that cracks from first-year ice are acoustically different from those which originate in multiyear ice. They did not know the reason for this, and suggested that further research into ice physics using higher-frequency signals could be helpful.

b) Moving ice masses. Where ice cover is not continuous but consists of summer ice floes, noise is produced by slow jostling of ice blocks. Milne (1967) noted that the level of this noise was surprisingly low. However, rafting and cracking causes isolated noise bursts of extreme amplitudes. For example, near Nova Scotia, the noise in 120 metres of water showed wide variations over timescales of several minutes, due to ice floes along the shore. Also, short bursts of noise occurred due to shear stresses set up by the movement of the ice floes.

Dwyer (1981) suspended a hydrophone in saltwater pack ice to a depth of 91 m, and detected non-Gaussian noise containing bursts of duration 0.1 – 0.3 s, caused by the rubbing and bumping of ice masses. These bursts were very different from the transient sounds produced by the cracking of non-moving shore-fast ice, a fact which was noted by Greene and Buck (1964). Another kind of transient noise is produced by ice ridging, which occurs in heavy ice conditions, when ice floes are fractured and crushes and ice blocks pile up into ridges. A study was performed over winters from 1961-1964 (Macpherson 1962; Payne 1964; Payne 1967), where background noise was seen to decrease steadily from January to April as the ice cover increased from zero to several metres. The experiments mentioned covered frequencies from 3 – 3200 Hz, with the smallest range being 25 – 1000 Hz (Greene and Buck 1964). The slope of the sound spectrum also decreased and the noise level became less dependent on wind speed as the ice cover became continuous – an observation which disagrees with data at higher frequencies and further north, where there was a strong variation of noise with wind speed. Therefore, the interaction of ice with air depends not only on its roughness and snow cover but also on the temperature of the ice and the air.

Xie and Farmer (1991) researched the sound of cracking in landfast ice, and focused on one particular event where ice broke up and consequently interacted with other ice. The signal was analysed and started with two impulse type sounds, 6 seconds apart, followed by many broadband pulses for about 8 seconds, after which it was postulated that the ice floe gained freedom to move with respect to its adjacent floe. During these processes, wind and current were applying stress causing adjacent ice floes to move against each other, leading to a sound which lasted around 25 seconds, with a frequency centred around 778 Hz. It was hypothesised that the ice breaking event in question started with ice breaking at positions where stress was greater or the ice was weaker, due to strong winds or currents. This led to further failure related cracks and the ice breaking, leading to a sound field composed of many sound pulses, continuing until the ice was separated into several floes, where the ambient sound level sharply decreased. Then, the wind and current caused the ice floes to gain momentum and due to their proximity to each other they would be unable to achieve rapid motion normal to each other, so crushing events would be rare, although they would be able to move along the new fault, leading to a pure-tone signal. This was modelled as a boundary value problem and subsequently the authors derived a model to investigate the generation mechanism of the pure-tone sound, which led them to believe that the dry friction between adjacent floes excited an SH (horizontal shear) wave in the ice, which radiated sound with a frequency close to the fundamental frequency predicted by theory.

c) Ice melting. Urick (1971) noted a lack of attention to the noise made by melting icebergs during their southward drift as a source of underwater sound. When a cube of ice is placed in a glass of water, two kinds of noise are observed, a loud impulsive noise caused by cracking under thermally induced stresses due to the temperature difference between ice and water, and a crackling sound that only occurs with cloudy ice and not with ice free of air bubbles. Urick (1971) postulated that this crackling noise is caused by the expansion of the entrapped bubbles as they burst out of the ice during melting, or that alternatively, it is caused by the implosion of air cavities by inrushing water as the cavity walls are broached. It is possible to observe air bubbles bursting out from their walls by looking at melting refrigerator ice under a microscope. Glacier ice is noticeably different from refrigerator ice, due to the presence in glacier ice of worm-like air tubes which could be caused by the shear

flow of the moving glacier in which they were formed (Urick 1971). Figure 2.36 (Urick 1971) shows the escape of air from both a spherical and tubular cavity.

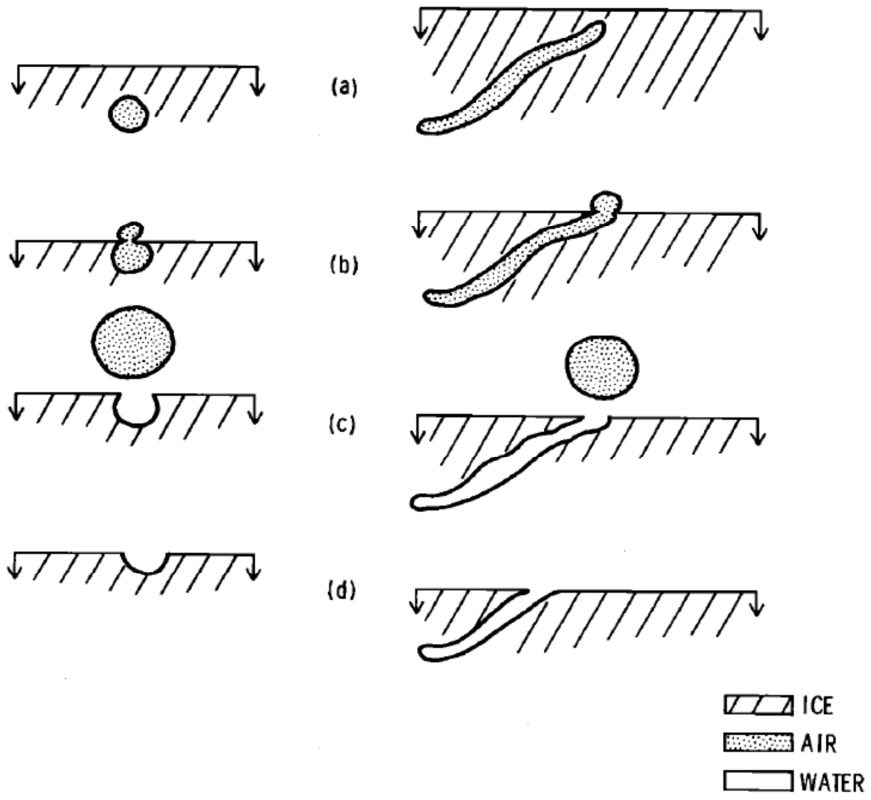

Figure 2.37: Air escaping from a spherical (left) and tubular (right) cavity. In Figure 2.37(a) the melting wall (moving downward) has not reached the bubble, Figures 2.37(b) and 2.37(c) show the beginning and end of the escape process, where a pulse of sound is generated.

The results presented by Urick (1971) show no significant difference at low frequencies between noise levels at different distances from an iceberg. However, above 1 kHz, the noise levels increase with decreasing distance from the iceberg, although this rate of decline is lower than from a point source in the free field. It was therefore concluded that the high-frequency noise originates from the iceberg. The radiated noise power was found to be 0.1 W and 0.01 W for two different icebergs, in the band 0.1-10 kHz (note, though, that Urick's experiments were limited to <10 kHz).

d) Noise at the edge of ice bodies. Noise can be observed at the edge of ice bodies (such as ice sheets), caused by the impact of waves on ice floes on or near the edge

of the ice. Close to the boundary, the levels of noise would be expected to be higher than those in open water or well under the ice. A maximum of noise at the ice edge was observed by Diachok and Winokur (1974). Figure 2.38 (Diachok and Winokur 1974) illustrates the variation of noise with distance from the ice edge.

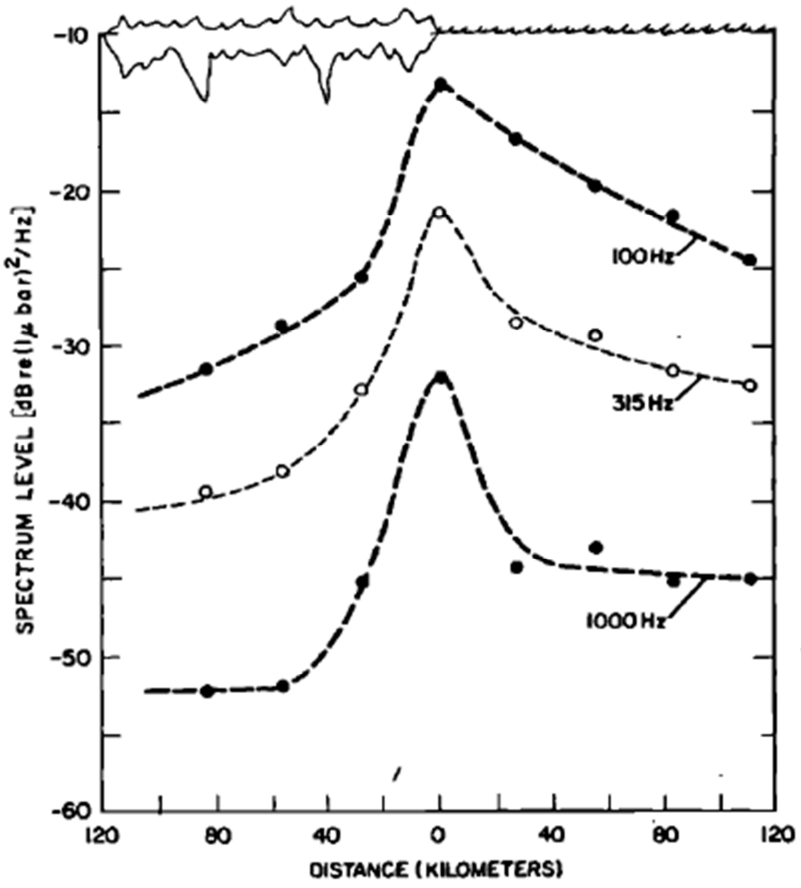

Figure 2.38, from (Diachok and Winokur 1974): Noise level beside a sharp ice edge. Sea state 2. A more diffuse ice edge leads to less pronounced peaks on the curves.

The noise maximum at the edge was around 12 dB higher than the levels in open water. With a diffuse ice edge, the measured levels were 4 and 10 dB higher at the edge than in open water and far under the ice, respectively, which implies that the ice edge acts as a long-line noise source, which produces a higher level in open water than under ice at the same distance, due to the poorer sound propagation under ice. Peters (1979) found similar results. Urick (1971) found that icebergs make noise when melting, and that the noise appeared to be caused by the escape of air contained under pressure in minute vacuoles in the ice, due to the melting ice wall. The observed sound showed a flat spectrum extending to frequencies above 10 kHz,

and dominates wind as a high-frequency source of noise in locations where actively melting icebergs are prevalent.

e) Ice bobbing. Low frequency noises such as flexural gravity waves have been postulated (Urick 1986) to occur on individual ice floes, therefore generating pressures unattenuated with depth at twice the frequency of the standing wave in the water below. Low frequency noises are also produced by the buoyant bobbing of sea ice, where the frequency of the noise depends on the thickness and density of the ice. This theory was verified by Milne (1967). Underwater earthquakes have been observed in the ice-covered Arctic, often originating along the mid-Arctic ridge, and are able to last up to 72 seconds and have a broad spectrum with a peak around 5 Hz. The resulting sound waves travel through the earth's mantle like most earthquakes but in the Arctic they are received more strongly as 'T-Waves' (Transverse Waves), where they are scattered by the ice around the earthquake and travel as waterborne sound under the Arctic ice cover.

f) Wind above the ice. In the Arctic, under solid ice in the absence of cracking noises, the wind produces noise by its flow over the rough ice surface and through the impact of blowing snow. This leads to a flat spectrum above 1 kHz, in contrast to the spectrum of wind noise on an ice-free sea surface, which has a spectral slope of around 5 dB per octave (Urick 1986). The increase of noise with wind speed from 3.2 – 6.4 kHz is faster over ice than over open water, which suggests that the scale of the turbulences which cause the noise is different in the two cases. For example Milne (1967) suggested that wind generates noise as it moves over the ice by the collapse of tiny eddies forming in the lee of tiny snow and ice crystals.

2.7. CONCLUSION

Over the past century underwater acoustics has been used increasingly, for detection of submarines and fish shoals, for imaging of the seabed, for data transmission and for monitoring of the ocean temperature. An acoustic wave can be described by its amplitude, the velocity of the vibrating particles and the resulting acoustic pressure. Acoustic signals are characterised by their frequency, which typically ranges from 10 Hz to 1 MHz in underwater acoustics. Acoustic waves are attenuated underwater due to geometric spreading and absorption of energy by the medium. Underwater

acoustic monitoring can be active or passive, and usually measurements of the noise related to weather are taken using passive acoustics, using a single hydrophone or an array of several hydrophones. Attenuation of sound waves underwater increases very rapidly with frequency.

The frequency range applicable to monitoring of ocean weather patterns is approximately 1 kHz – 50 kHz. At 10 kHz, the attenuation is around 1 dB/km, limiting the audible range to tens of kilometres. At 100 kHz, the attenuation is tens of dB/km, limiting the audible range to 1 km. Sound waves can also be scattered by a layer of bubbles caused by sea surface movements up to 20 m below the surface. The scattering from this inhomogeneous layer is at a maximum around the resonance frequency (f_R) of the bubbles, which is related to the depth (z) and radius (α) of the bubble by equation 2.25. Prediction of the path of an acoustic wave around bubble populations which change with time is complicated but can be approximated.

A variety of weather processes can be monitored using underwater acoustics, namely wind and precipitation, as well as the noise produced by icebergs. Wind directly affects the sea state, causing waves ranging in size from 1 cm to over 30 m. In shallow water these waves are affected by the topography of the seabed leading to variations in their propagation speeds, but deeper than half a wavelength (of the surface wave) the propagation speed depends only on the wavelength and period of the surface waves. These waves cause small localised variations of the pressure in the water, as well as causing crests and whitecaps when large enough, which in turn trap and entrain air bubbles, which affect the noise levels.

Rain is quantified by the amount which has fallen over a given time period as well as the distribution of droplet sizes which have fallen. Droplet sizes range from under 0.8 mm to over 2.2 mm at speeds up to the terminal velocity (Montero Martínez et al. 2009). Typically surface observations include the temperature, relative humidity, wind direction and speed and precipitation total. Radiosondes, weather satellites and radar provide extra data to be used with the surface observations. Although instruments exist which can determine the drop size distribution in rainfall, it is a difficult parameter to observe, particularly at sea. Due to the complex interactions between different processes, there have been reported cases of discrepancies between the noise measured underwater (similar to heavy rain) and the weather observed *in*

situ (no rain at all) (e.g. Quartly et al., 2001). Observations of the ocean are mostly made using satellites, instruments on board ships or moored to buoys and underwater acoustics. Satellite observations are limited by cloud coverage and the field of view of the satellite. Radar can detect precipitation 250 km away from an antenna but gives little coverage of the oceans beyond 250 km from land.

Ambient noise underwater is also affected by a variety of other sources, detailed in Appendix A.3: seismic and volcanic activity and interaction of surface waves below 5 kHz, wave turbulence at 5 kHz and shipping from 10 Hz to 1 kHz. Intermittent ambient noise is largely caused by biological sources, such as whale vocalisations ranging from 12 Hz to several kHz and propagating hundreds of kilometres. Snapping shrimp create bubbles which have a peak at around 1 – 10 kHz. The underwater noise caused by wind varies with the wind speed. Noise from wind ranges from below 10 Hz to 5 kHz, with the lower frequency components able to propagate up to 4.9 km deep. Rain makes noise underwater from 1 – 100 kHz, with a particular peak at 13 – 15 kHz related to resonating bubbles caused by the individual droplets. As icebergs crack, the noise can be observed underwater at around 500 Hz and below. Ice masses jostling against each other cause noise centred around 778 Hz. Wind blowing above an iceberg can alter the ambient noise spectrum at frequencies above 1 kHz, and variations in noise relating to increasing wind speed happen more rapidly over ice than over open water, possibly due to eddies forming behind snow and ice crystals.

In conclusion, the extensive body of literature on acoustic noise underwater is based on theory as well as laboratory-based tank experiments and field measurements in a variety of conditions and locations. The basic physical mechanisms for rain, wind, wave and shipping noise are well understood, even if the exact frequency ranges and amplitudes vary significantly. Biological sources of ambient noise are increasingly better constrained (e.g. deRuiter, in Lurton et al., 2010). Conversely, noise caused by ice has been studied mostly at lower (< 1 kHz) frequencies, concentrating on pack ice. The combination of these processes has been poorly studied, especially in complex regions such as the Arctic shores.

CHAPTER 3 - ARCTIC FIELD EXPERIMENTS

3.1. INTRODUCTION

A dataset was acquired during a field trip to the Arctic in the summer of 2007. The study aimed to investigate the response of Arctic ecosystems to climate change. The main objective of the survey was to provide an acoustic tool for the evaluation of benthic habitats and the survey included systematic, co-registered, single-beam and multibeam echosounder measurements (Kruss et al. 2008). The measurements were taken in a fjord on the west coast of Spitsbergen, by Dr Philippe Blondel of the University of Bath and several scientists from the Institute of Oceanology Polish Academy of Sciences, and the field trip was carried out as part of investigations funded by the European Centre for Arctic Environmental Research (ARCFAC). Towards the end of the field trip, recordings were taken of the ambient noise at six different locations along the fjord. Although the time limitations meant that these recordings were only carried out over one day and for periods of less than ten minutes, the dataset was considered to be large enough to be meaningful when used with further laboratory experiments. The setup in the field experiments was intentionally easily accessible and affordable so that it could be used in similar studies, even by non-specialists (such as environmental groups e.g. Earthwatch in other settings). It was not as sophisticated as instruments used in other research settings but used commercial off-the-shelf hardware to make it easier to replicate and be used in a wider variety of settings and by other research groups. These recordings were intended to be used to compare to the results obtained by previous authors (Nystuen 2001; Quartly 2001) and to try to investigate a more rigorous method of selecting frequency bands best suited to classification of different weather events, as suggested by previous authors. It was hoped that this would lead to the development of tools which could improve the accuracy of the monitoring of weather conditions

at the sea surface, which in turn would lead to improvements in the understanding of climate change.

The recordings of ambient noise taken in the Arctic fjord varied in duration from just under a minute to five minutes. The duration was chosen to be long enough to ensure that the processes were not moving. In some locations, repeat recordings were taken to minimise the possibility of short-lived transient sources of noise affecting the data. Weather in the Arctic changes frequently and rapidly, therefore the recordings encompassed a wide variety of conditions. The measurements covered the combination of varying levels of rain (from none to light rain), wind (from none to 11 km/h), ice (from none to growlers and bergy bits), shipping (from none to a large cruise ship) and animal activity (including whales and diving seabirds). The set of ambient noise recordings was the first set to be carried out in this kind of environment.

The field measurements were later supplemented by several sets of tank experiments carried out at the University of Bath. These results are discussed further in chapters 5 and 6.

3.2. THE ARCTIC DATASET

3.2.1. GENERAL SETTING

In August 2007, measurements were taken along the fjord of Kongsfjord, which is an inlet on the west coast of Spitsbergen, an island forming part of the Svalbard archipelago in the Arctic Ocean. The Arctic Ocean is a nearly closed basin, with just one deep passage (Fram Strait, reaching depths greater than 5km (Schenke 2011)) between Svalbard and Greenland where water exchanges with the rest of the Global Ocean. There are other links, for example the Nares Strait, a narrower and shallower (several hundred metres) passage, connects to Baffin Bay, and there are many shallow links with the Atlantic and Pacific (Wadhams 2000).

Figure 3.1: Map showing the topography and bathymetry of the Arctic.
http://maps.grida.no/go/graphic/arctic-topography-and-bathymetry-topographic-map

Salinity and temperature profiles of the Arctic Ocean show that it is generally split into three layers. The uppermost layer (polar surface water) is up to 200 m thick and is close to the freezing point, with very low salinity, due to the influx of fresh water from river systems (Wadhams 2000). The depth at which the temperature rapidly decreases (the thermocline) is not necessarily the same as the depth where the salinity rapidly increases (the halocline). The next layer down is the warmer (3°C) and more saline Atlantic water layer, which partly enters the Arctic through the Fram Strait where the warm North Atlantic Current runs up the west side of Spitsbergen

and sinks as it meets the less dense polar surface water (Wadhams 2000). Deeper than 900 m, the water temperature is below 0°C and decreases with increasing depth – this is the Arctic Ocean deep water and moves slowly around the basin (Wadhams 2000).

In the long term, ice and surface water move in the same way. The surface current system in the Arctic Ocean is mostly clockwise in the Canada Basin (the Beaufort Gyre, where ice takes 7 – 10 years for a complete circuit) and translatory in the Eurasian Basin – the Trans Polar Drift Stream, which transports ice and water across the Pole and down towards the Fram Strait, taking about three years. Most of the ice leaving the Arctic Basin follows this path, so most water and heat exchange between the Arctic and the rest of the world ocean occurs through Fram Strait, where heat is mostly exchanged as latent heat, transported northward as ice moves southward (Wadhams 2000).

The numerous studies of weather and oceanography carried out in the Arctic have led to its recognition as an area of interest to investigate the effects of climate change. For example, recent studies (Serreze 2006) have demonstrated that an increased concentration of greenhouse gases in the atmosphere will cause warming to occur first in the Arctic, where it will be most pronounced. Arctic fjords are considered to be more extreme than other fjords because they experience greater seasonality, high levels of freshwater input, sea ice formation and melt, and strong, persistent orographic winds (Cottier et al. 2005).

The western coast of Svalbard is mainly influenced by the West Spitsbergen Current (WSC) and Arctic Coastal Water. The upper 600 m of the WSC are dominated by warmer, more saline waters of Atlantic Water (AW), which leads to the low levels of ice in western Svalbard. The water which originates from the Atlantic and mixes with Arctic Coastal Water has lower salinity and temperature, and is mostly confined to the intermediate waters whilst the deeper waters of the fjord basins are colder (temperatures typically below 1°). Even colder and higher salinity waters (-1.4°C) can be found in the deepest basins, and are caused by winter cooling and sea ice formation. Surface water (occupying the top few metres of the water column) has

lower salinity, 28-30 psu and can therefore be heated quickly by the sun and can reach temperatures of up to 4°C.

Figure 3.2: Map of Spitsbergen and surrounding areas (Makarov 2002). Ny-Alesund (79°N, 12°E) was the research base during the ARCFAC-2007 expedition.

Kongsfjord is 20 km long and ranges in width from 4 to 10 km (Howe et al. 2003). The seasonal hydrography of Kongsfjord and the West Spitsbergen Shelf is dominated by the balance between Atlantic Water, Arctic waters and glacial melt (Cottier et al. 2005). These waters converge, mix and are exchanged, and as the balance between the three sources changes with the seasons, shelf waters and adjacent fjords switch within one annual cycle from being predominantly Arctic (i.e. cold and fresh) to Atlantic (warm and saline) and back again (Cottier et al. 2005).

The mixing of the different types of water leads to significant changes in temperature and salinity, so that the fjord mixes boreal and Arctic ecosystems (Hop et al. 2002).

Kongsfjord is an important feeding ground for marine mammals and seabirds, with marine mammals making up the largest top-predator biomass but seabirds consuming the most energy and exporting nutrients and energy out of the marine environment (Hop et al. 2002). Since Kongsfjord is situated on a border between the Atlantic and the Arctic, the biodiversity and animal populations are structured due to the different physical factors affecting the fjord from both ends (Hop et al. 2002). Kongsfjord is inhabited by a wide variety of fish species as well as many communities of marine mammals (pinnipeds, cetaceans and polar bears) and seabirds. Some species are resident to Kongsfjord but many are migratory, leading to a seasonal peak from May to August. Food availability varies seasonally, largely due to the retreat of the ice edge leading to a phytoplankton bloom in the spring meaning that organisms which consume the phytoplankton are concentrated in the upper water layers, attracting marine mammals and birds. Furthermore, freshwater discharge from the bottom of the glacier leads to increased populations of zooplankton, which makes the area important feeding ground for marine mammals and birds in late summer and early autumn (Hop et al. 2002). The peak biomass consumed in Kongsfjord is approximately 110 tonnes in May (Hop et al. 2002). The most commonly sighted cetacean in Kongsfjord is the white whale, and minke whales are commonly seen through late spring and summer. Fin whales can occasionally be seen but not usually inside the fjord. Polar bears are occasionally present. An estimated 15,000 pairs of nine species of sea birds breed in significant numbers (over 50 pairs in each group) in Kongsfjord, with almost all of the birds being migratory (Hop et al. 2002).

The fjord is characterised by a variable acoustic character (Howe et al. 2003). It consists of an inner fjord with water up to 100 m deep, and a deeper central and outer fjord basin – the deepest point being -394 m in the outer fjord basin. Its total area is estimated to be 29.4 km^3 and several tidewater glaciers drain into it (Howe et al. 2003). At the surface, meltwater from the glaciers provides freshwater, and at deeper levels, freshwater comes from calving and melting icebergs. As fast ice freezes and melts in the inner fjords, freshwater is removed from the surface layers and the water stratification is homogenised (Howe et al. 2003). On the more gentle slopes of

Kongsfjord, the sediment package is thin, yielding relatively high acoustic impedance. However, the most common acoustic character in the fjord is a continuous, highly reflective seabed, with a thin or non-existent sediment cover. This is most common in water depths of less than 100 m (Howe et al. 2003). Its latitude and width mean that Kongsfjord is strongly affected by rotational dynamics (Cottier et al. 2005). The sources of noise present in Kongsfjord are the complex weather patterns, which can vary over short time periods, icebergs causing noise as they move, capsize and melt. Ice masses calving from glaciers also contribute to the ambient noise in the fjord, as well as the abundant marine life previously mentioned. These noise sources all vary seasonally as well as over short time periods, meaning that the noise present in the fjord is complex and variable. The propagation of this sound is difficult to predict due to the variations in the acoustic character throughout the fjord, coupled with high levels of sound reverberation from the highly reflective seabed.

3.2.2. LOCATION OF RECORDINGS

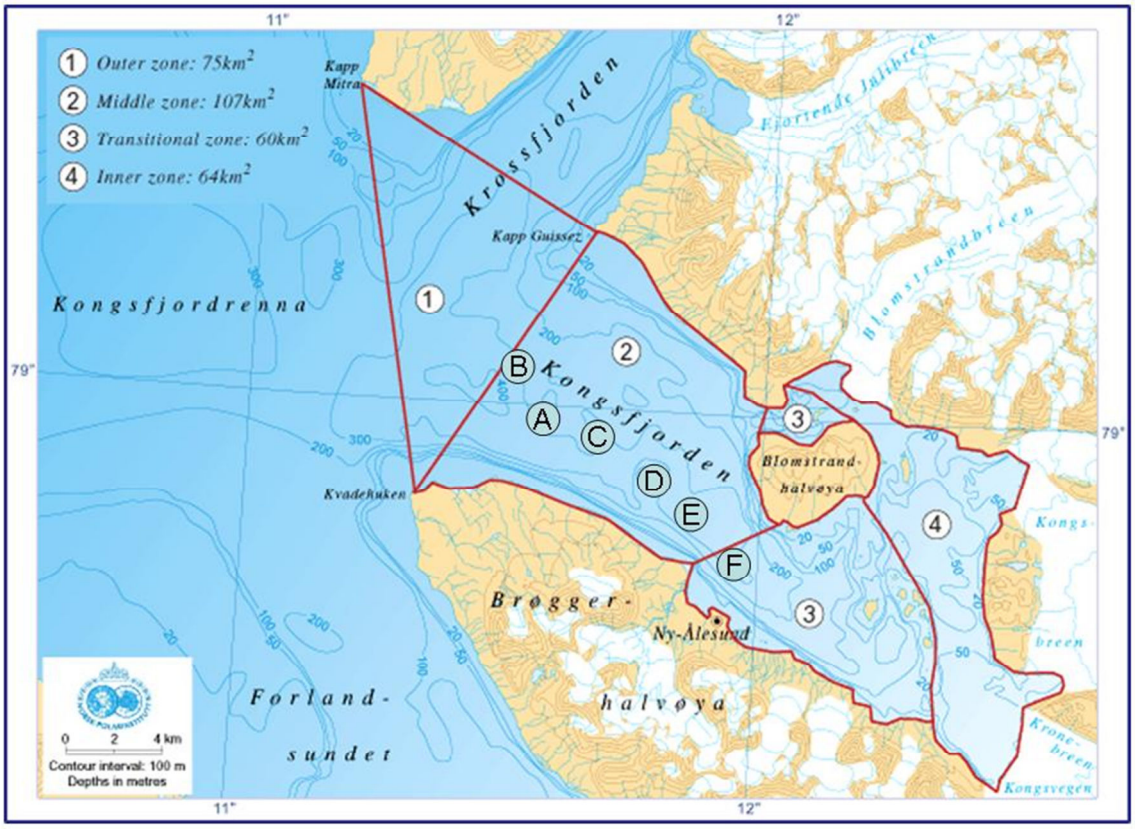

Figure 3.3: Map of Kongsfjord with positions of recording stations A-F. Basemap from Norwegian Polar Institute (http://miljo.npolar.no/temakart).

Measurements were taken at the six recording stations labelled A-F in Figure 3.3. In each case, the ambient noise was measured using a single SQ26-07 broadband hydrophone, with an operational frequency band from 10 Hz to 50 kHz, placed 9.5 m deep, always in water deeper than 200 m. The environments at the six locations all differed from each other – from the junction of Kongsfjord with the neighbouring Krossfjorden, through the middle zone, to close to the harbour. The nearby research base of Ny-Ålesund has a meteorological station and since the measurements were taken over a short period of time, the wind speed was measured at Ny-Ålesund as 11 km/h (Sea State 2). The wind speed at Ny-Ålesund is usually a little lower than in the fjord, which matches the visual observations at the time of the experiments. The wind chill temperatures, which would have affected the ice melting rate, were always sub-freezing.

Position A – 78°59’45.7”N ; 11°34’47.4”E – File A (5’00”) Light rain. Small waves. No ice. Depth ~ 300 m – Closest shore ~ 3 km away. Whale less than 50 m away + ship far away (~ 5 km)
Position B – 79°00’53.6”N ; 11°30’00.4”E – Files B_1(1’20”), B_2 (2’01”), B_3 (3’01”) Light rain. Very small waves. No ice. Depth ~ 300 m – Closest shore ~ 4 km away. Whale visible at the surface + ship at horizon (~ 5 km)
Position C – 78°59’30.9”N ; 11°40’41.8”E – Files C_1 (0’46”), C_2 (3’01”), C_3 (3’01”) Light rain, increasing. No waves. No ice. Depth ~ 300 m – Closest shore ~ 3 km away.
Position D – 78°58’47.4”N ; 11°46’53.4”E – Files D_1 (3’00”), D_2 (1’31”) No rain. No waves. No ice. Depth ~ 300 m – Closest shore ~ 2 km away.
Position E – 78°58’01.0”N ; 11°52’26.9”E – File E (2’01”) Very light rain. Very small swell. Small icebergs (growlers and bergy bits) ~20 m away. Depth ~ 250 m – Closest shore ~ 1.9 km
Position F – 78°57’0.9.4”N ; 11°57’42.2”E – File F (2’00”) No rain. No waves. No ice. Depth ~ 200 m – Closest shore ~ 1.9 km away In front of Ny-Ålesund harbour, with cruise ship at berth.

Table 3.1: Details of measurements at each recording station, with duration.

At positions B, C and D, several recordings were taken in order to measure ambient noise stationarity. This is illustrated in Table 3.1, which also shows that the recording times ranged from approximately 1 - 5 minutes, and encompassed light rain, light winds, calm conditions, whales, ships and icebergs.

Point A Point B

Point C Point E

Figure 3.4: Photographs of environmental conditions at some of the recording points. A surfacing whale was spotted in the top two photos (tentatively identified as a minke or fin whale). The melting icebergs at point E are identified as bergy bits (this picture) and growlers.

3.2.3. INSTRUMENTATION

The single hydrophone used in the Arctic experiments was an SQ26-07, manufactured by Cetacean Research Technology, Seattle (USA). Earlier tank experiments conducted at the University of Bath confirmed that this hydrophone was omnidirectional across the entire frequency range considered. The operational frequency band ranges from 10 Hz to 50 kHz, with slight variations in sensitivity throughout; it is nearly constant at -168 dB re. 1V/µPa from 100 Hz to 30 kHz, decreases linearly to -174 dB re. 1V/µPa at 35 kHz and increases linearly again to -168 dB re. 1V/µPa above 40 kHz. The preamplifier gain was set at 25 dB.

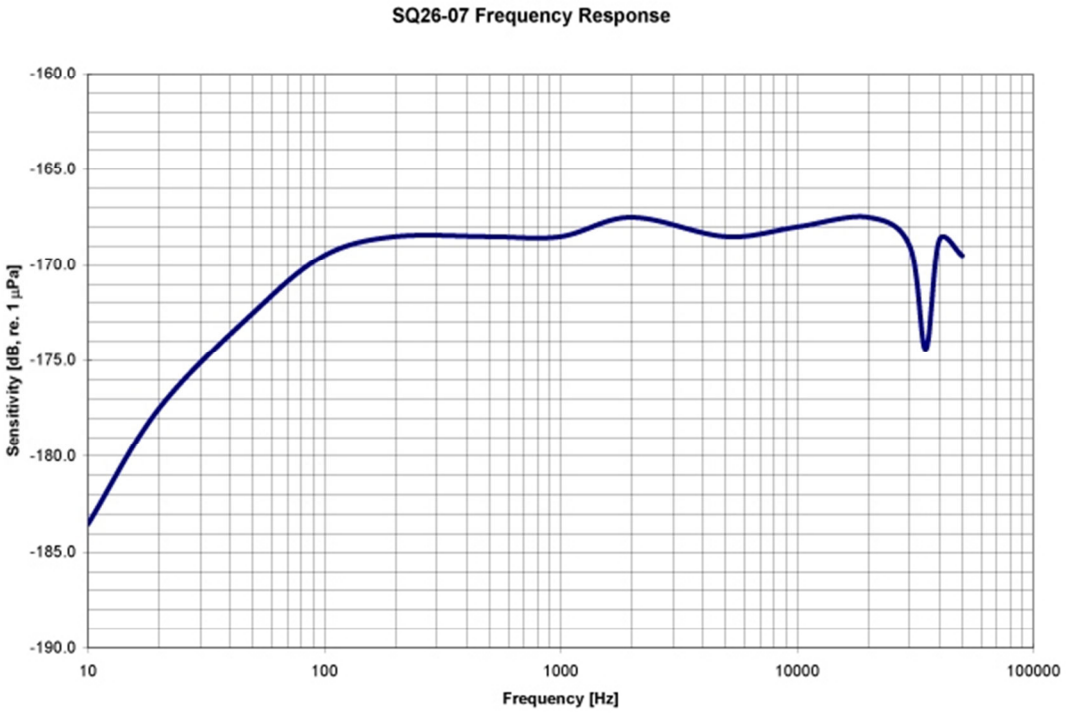

Figure 3.5: Frequency response for the SQ26-07 hydrophone used in the Arctic experiments.

The shielded cable on the hydrophone was 10 m long, so when combined with the low gunwhale of the supporting vessel (a Buster-L boat with an aluminium hull), it was possible to deploy the hydrophone 9.5 m deep each time. The data obtained were fed into a digital recorder (M-Audio Microtrack 24/96), sampling at a frequency of 96 kHz, therefore the measurements covered an effective broadband frequency range of 10 Hz to 48 kHz.

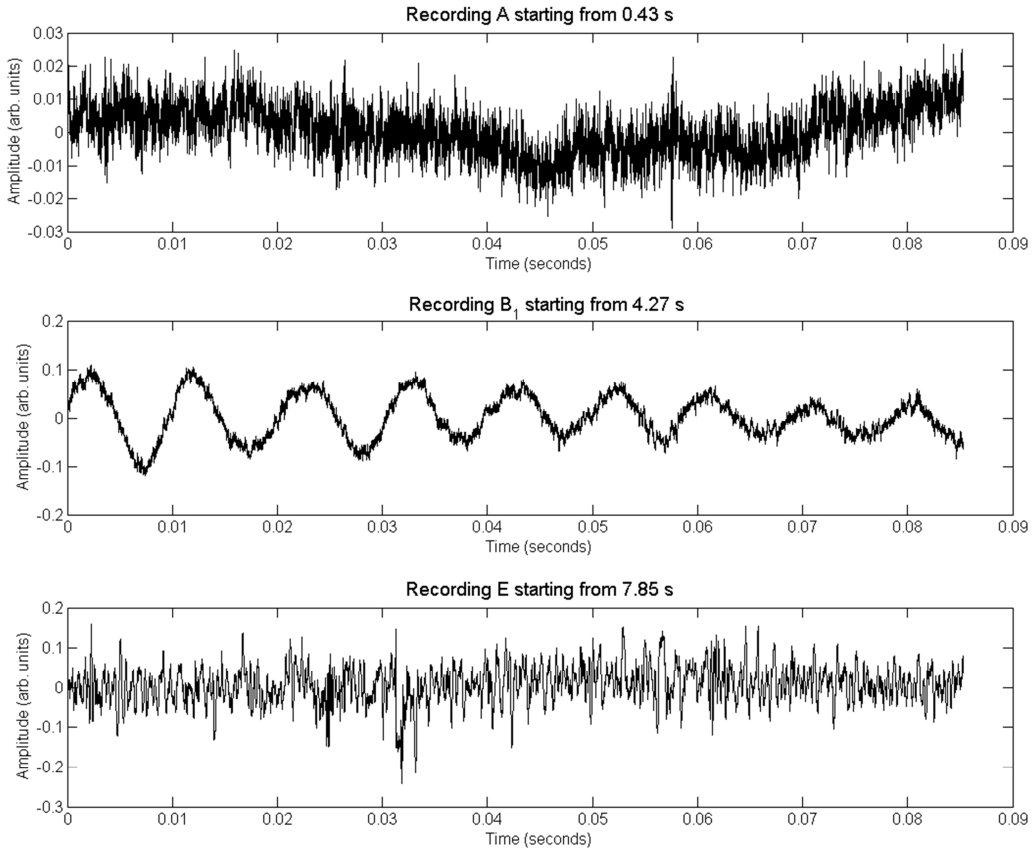

Figure 3.6: Examples of raw files in time-domain (segments of recordings A, B_1 and E). Amplitude (y-axis) varies from one recording to another.

The different measurements were recorded in 24-bit .WAV format, which permitted full access to the normalised waveform[2]. WAV files contain uncompressed audio data, giving maximum audio quality and making it easy to edit and manipulate. Examples of the raw data for locations A, B_1 and E are shown in Figure 3.6.

3.3. CONCLUSION

The Arctic regions have been identified as one of the key regions where the effects of climate change can be identified and measured. Observations of the weather conditions there are considered particularly important. A collection of recordings of ambient noise were obtained with a single hydrophone in the summer of 2007 in the Arctic fjord of Kongsfjord, an important feeding ground for marine mammals and

[2] WAV is a standard Microsoft format, based on the wider RIFF format used in the music community. More details are available on http://en.wikipedia.org/wiki/WAV_file.

sea birds due to the wide variety of resident fish species, and the peak in their populations between May and August. Taken at 6 locations evenly spaced along the 20-km length of the fjord, from its opening to the sea to the glaciers at its termination, these measurements cover the combination of varying levels of rain (from none to light rain), wind (from none to 11 km/h), ice (from none to growlers and bergy bits), shipping (from none to a large cruise ship) and animal activity (including whales and diving seabirds). The recordings covered frequencies from 100 Hz to 48 kHz and lasted for between one and five minutes each. They were taken 9.5 m deep each time. The maximum depth of the fjord is 394 m. The highly reflective nature of the bottom of the fjord can make it complicated to predict the propagation of sound through its waters, although the large ranges involved mean attenuation would be important.

Weather-focused analyses of ambient noise data by other teams had used the comparison of noise levels at pairs of frequencies (or frequency bands) in order to separate the different weather types present, in a similar method to the rainfall classifications performed by disdrometers. Although these techniques usually successfully separated different rainfall intensities and wind noise graphically, there was little mention of the method of selection of the frequencies used and its physical justification.

The high amount of frequency bands available, the potential high correlation between neighbouring bands, and the large amount of data available all hint that techniques such as Principal-Component Analyses could be useful. Principal Components Analysis on the Arctic data should identify in a more repeatable manner three combinations of frequencies (rather than single frequencies) to separate the noise sources present in the recordings. This method could then potentially be applied to other datasets, in different environments and with different sources of noise.

CHAPTER 4 – FIELD DATA ANALYSIS

4.1. FREQUENCY ANALYSES

4.1.1. FOURIER ANALYSIS - BASICS

The images of the raw data shown in Figure 3.6 illustrate the issues encountered with analysing acoustic recordings of the weather. Due to the levels of background noise it is not practical to look at the amplitude over time. Therefore, it is more common to consider instead the variation of amplitude with frequency. To determine the variation with frequency of a function which varies with time, the Fourier transform of the function should be found. The Fourier transform of a function *f(t)* is given by;

$$F(\omega) = \int_{-\infty}^{\infty} f(t) e^{-i\omega t} dt \tag{4.1}$$

where ω is the frequency which arises from repeating a non-periodic function.

4.1.2. FREQUENCY SPECTRA

As mentioned in chapter 2, different types of weather can be associated with amplitude peaks at certain frequencies, for example rain shows a peak at about 15 kHz and wind shows a peak around 5 kHz.

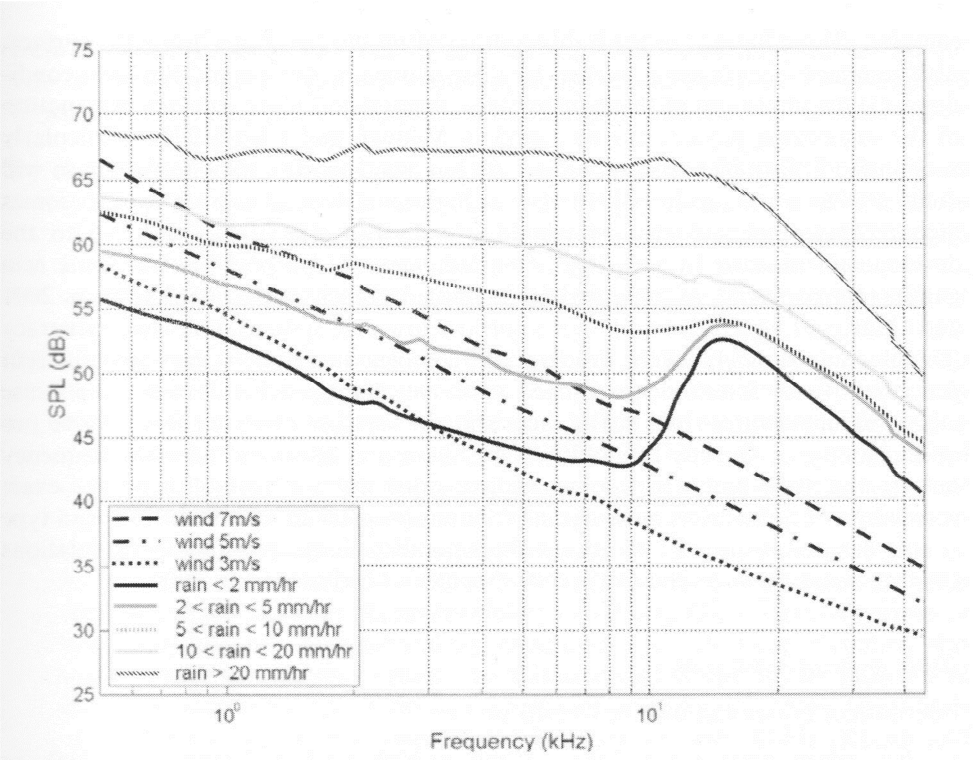

Figure 4.1: Generic spectra of acoustic noise induced by rainfall and wind. From Ma et al (2005) and Nystuen and Howe (2005)

Matlab's FFT functions were used on the Arctic data to obtain frequency spectra for the 11 recordings and some examples are illustrated in Figure 4.2.

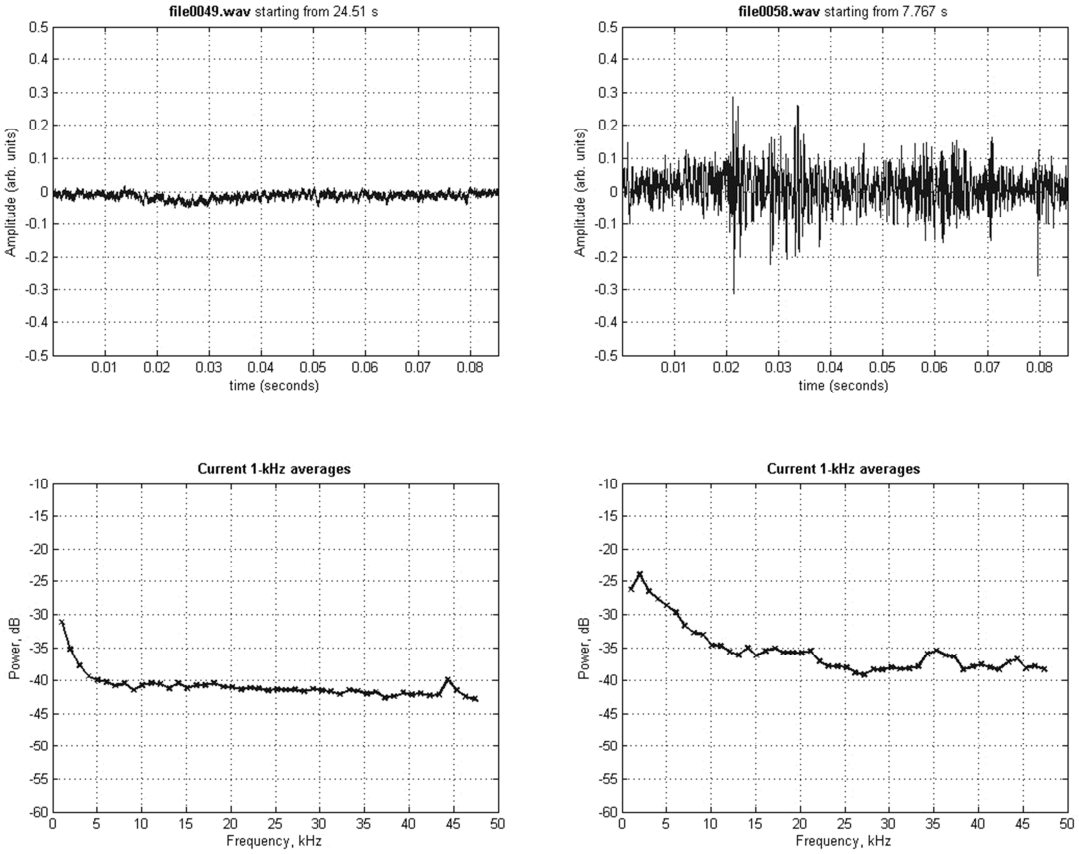

Figure 4.2: Plots of the raw data (top) for two files (at location A, left and E, right) and their frequency spectra (bottom) for frequencies from 1 – 48 kHz.

4.1.3. ACOUSTIC DISCRIMINANTS

Various authors have used the spectral peaks of certain weather types to try to identify the weather patterns present in ambient noise recordings. For example, Nystuen and Selsor (1997) plotted the average amplitudes at 25 kHz against the amplitudes at 5 kHz for a dataset including drizzle, heavy rain and noise from ships and high seas. These two frequencies enabled separation of the different sources of noise present in the dataset.

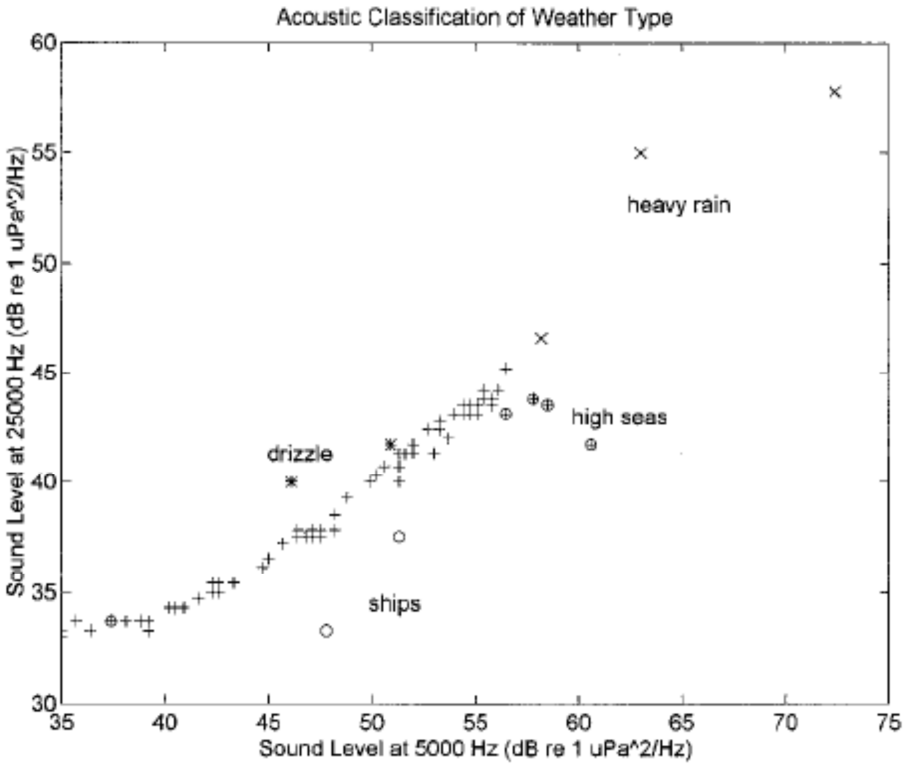

Figure 4.3: Comparison of sound intensity at 5 and 25 kHz, showing separation of shipping, high seas, drizzle, rain and wind. (Nystuen and Selsor 1997)

Following that, Quartly (2001) used the same frequency combination (25 kHz and 5 kHz) on a dataset also including heavy rain, drizzle, and noise from ships and high seas, which again enabled separation of the different processes as well as separation from just wind.

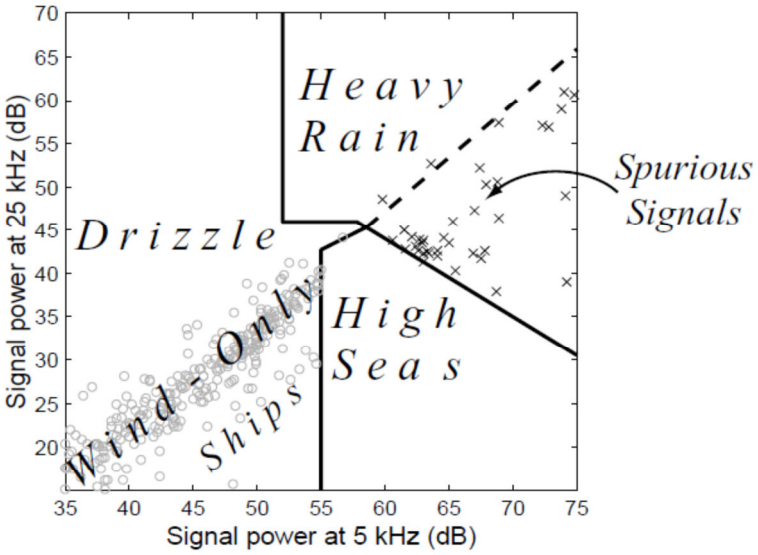

Figure 4.4: Comparison of sound intensities at 5 and 25 kHz, showing separation of wind, high seas, drizzle and heavy rain. (Quartly 2001)

Nystuen (2001) then used frequency bands instead of single frequencies to separate rain of different intensities. By plotting the sound level at 4 – 10 kHz against the sound level at 10 – 30 kHz, it was possible to separate three different types of rainfall.

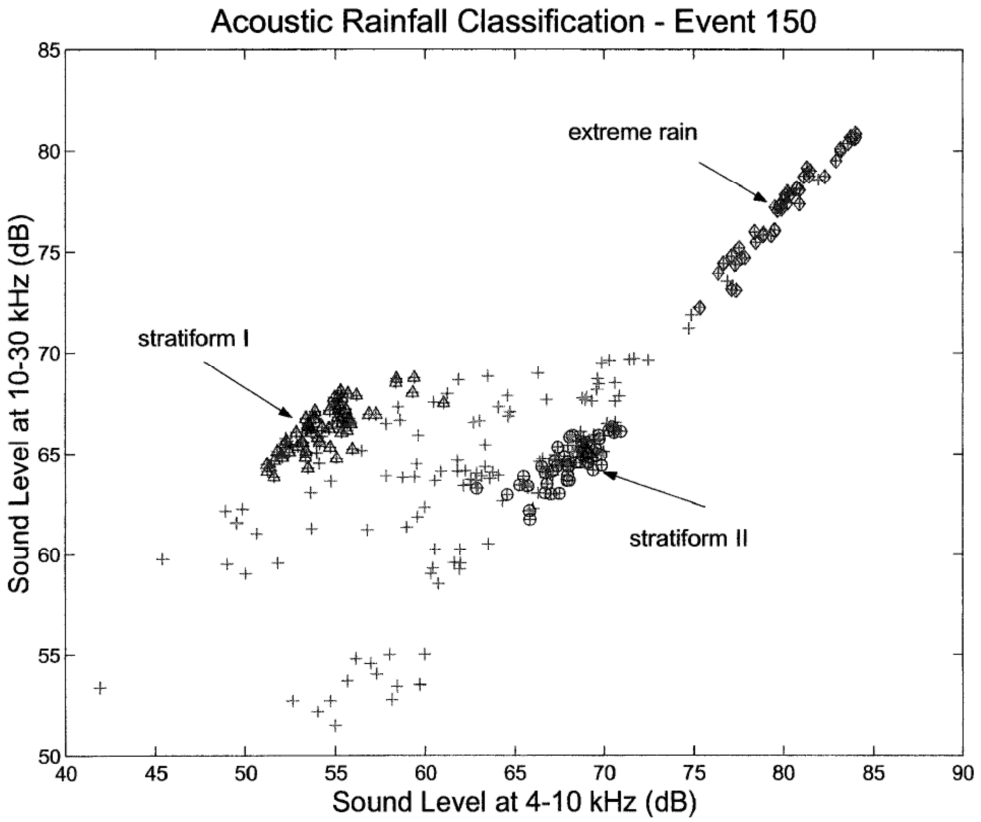

Figure 4.5: Acoustic classification of rainfall using sound levels at 4-10 kHz and 10-30 kHz (Nystuen 2001).

Despite the fact that authors agreed that using the sound levels at pairs of frequencies, or frequency bands, was an effective method of distinguishing the sources of noise present in a recording, there was little agreement between authors about the most appropriate choice of frequencies, and little mention of how the frequencies had been chosen. Some of the choices were openly based on the hardware available at the time, as much as on the acoustic levels expected at specific frequencies. Quartly (2001) showed for example that using the method of another group to detect rain created spurious results in their own, validated measurements, when no rain was present (Figure 4.4). In general, all publications allude to a need for a more rigorous method of selecting the frequency combinations which would be most effective at distinguishing the sources of noise present. The high amount of frequency bands available, the potential high correlation between neighbouring bands, and the large amount of data available all hint that techniques such as Principal-Component Analyses could be useful.

4.2. PRINCIPAL COMPONENTS ANALYSIS

4.2.1. PRINCIPLES

Principal Components Analysis is a statistical technique used to reduce the dimensionality of a dataset. It reduces a large set of correlated variables ($x_1,\ldots,x_p$) into a smaller set of uncorrelated variables ($y_1,\ldots y_p$) (Figure 4.6), which makes the dataset easier to understand, but retains all of the information contained in the original set of variables (Bartholomew et al. 2008). The first principal component (y_1) explains the maximum amount possible of the total variance; the second principal component (y_2) explains the maximum amount possible of the remaining variance, etc. If the initial dataset contains p variables then the full set of p principal components will fully explain the total variance – there will always be as many principal components as there are variables in the initial dataset. However, if the first few (e.g. three) components are able to explain a significant part of the total variance, then all of the others can be discarded without losing too much information. Usually the x-variables are standardised before carrying out a principal components analysis, so each variable makes the same contribution to the total variance.

$$X = \begin{pmatrix} x_{11} & x_{12} & \cdots & x_{1p} \\ \vdots & & & \vdots \\ x_{n1} & x_{n2} & \cdots & x_{np} \end{pmatrix} \text{PCA} \rightarrow Y = \begin{pmatrix} y_{11} & y_{12} & \cdots & y_{1p} \\ \vdots & & & \vdots \\ y_{n1} & y_{n2} & \cdots & y_{np} \end{pmatrix}$$

Figure 4.6: Illustration of Principal Components Analysis on an n x p matrix of data. Although the amount of data will remain the same, it will have been rearranged so that the first few columns in the matrix are able to represent the majority of the dataset.

Principal Components Analysis aims to interpret the underlying structure of the data using the most important components – often, the first principal component is positively correlated with each variable x_n and can be interpreted as a measure of something that all of the variables have in common. Components are ordered not only by their importance but also by how much of the variance they explain (Bartholomew et al. 2008).

For n observations on variables x_i, the sample mean is;

$$\bar{x}_i = \frac{1}{n}\sum_{t=1}^{n} x_{ti} \tag{4.2}$$

and the sample variance is:

$$s_i^2 = \frac{1}{(n-1)}\sum_{t=1}^{n}\left(x_{ti} - \bar{x}_i\right)^2 \tag{4.3}$$

The standard deviations are the square roots of the variance. The covariance between x_i and x_k is:

$$\operatorname{cov}(x_i, x_k) = \frac{1}{(n-1)}\sum_{t=1}^{n}\left(x_{ti} - \bar{x}_i\right)\left(x_{tk} - \bar{x}_k\right) \tag{4.4}.$$

The correlation between x_i and x_k is (Bartholomew et al. 2008)

$$corr(x_i, x_k) = \frac{\operatorname{cov}(x_i, x_k)}{s_i s_k} \tag{4.5}$$

If variables have high correlation, they will vary similarly and convey very similar information. The components that emerge from a principal components analysis will be linear combinations of the x-values and can be written as:

$$\begin{cases} y_1 = a_{11}x_1 + a_{21}x_2 + \ldots + a_{p1}x_p \\ y_2 = a_{12}x_2 + a_{22}x_2 + \ldots + a_{p2}x_p \\ \vdots \\ y_p = a_{1p}x_1 + a_{2p}x_2 + \ldots + a_{pp}x_p \end{cases}$$

Each component is a weighted sum of the x values with a_{ij} as the weight (or coefficient). If a_{ij} was significantly large, the variance of the corresponding y could be very large, therefore it is necessary to place constraints on the possible values of a_{ij}. In order to maintain the relative positions of the points (recalling the example where x_1 was plotted against x_2) it is necessary that:

$$\sum_{i=1}^{p} a_{ij}^2 = 1 \qquad (j = 1,2,\ldots,p) \tag{4.6}$$

$$\text{and} \qquad \sum_{i=1}^{p} a_{ij} a_{ik} = 0 \quad \left(j \neq k; j = 1,..., p; k = 1,..., p\right) \tag{4.7}$$

Therefore the total variance of the *y*-values is equal to the total variance of the *x*-values; the variance does not change but is redistributed among the variables. No data is lost in using this method, instead it is viewed in a new, and hopefully more meaningful way.

The components (*y*-values) are derived in order of decreasing importance – y_1 has the maximum variance and therefore accounts for the largest proportion of the total variance; the second component will have the second largest variance (and will be uncorrelated with y_1), and subsequent components will be derived in decreasing order of variance, each one being uncorrelated with previous components.

The weightings a_{ij} are determined by finding the eigenvalues and eigenvectors of either the covariance or the correlation matrix. The variances of the principal components are usually denoted by ($\lambda_1, \lambda_2, ..., \lambda_p$) and are listed in descending size order.

Although the number of principal components derived will equal the number of *x*-values, usually only some are chosen so that the dataset is reduced in size as far as possible whilst still representing the original data well. Several criteria can be used to decide how many components to use:

(a) Retain the first *k* components which explain a 'large' proportion of the total variation, e.g. 70-80%.

(b) If the correlation matrix was analysed, retain only the components with eigenvalues larger than 1, because they will explain the same amount of variation as the original *x*-values.

(c) Consider whether each component has a physically sensible and useful interpretation. The relative sizes of the weightings (a_{ij}) represent the relative contributions made by each variable to the component, therefore to interpret a component, its pattern in a_{ij} values should be used.

Often a plot is also made with bars for each component, for however many components contribute to the first 95% of the variance, showing their individual contribution to the variance, along with a line showing the cumulative variance

explained. This is known as a Pareto plot and demonstrates clearly which how significant the contribution from the first few components are, and after which points further components stop adding useful information.

4.2.2. EXAMPLE – MULTISPECTRAL SATELLITE IMAGERY

When analysing multispectral image data from satellites, it is common to encounter issues with interband correlation. For example, Figures 4.7(a-b) (Lillesand et al. 2004) show multispectral images of a town. Figure 4.7(a) shows band 1 (green) and Figure 4.7b) shows band 2 (red)

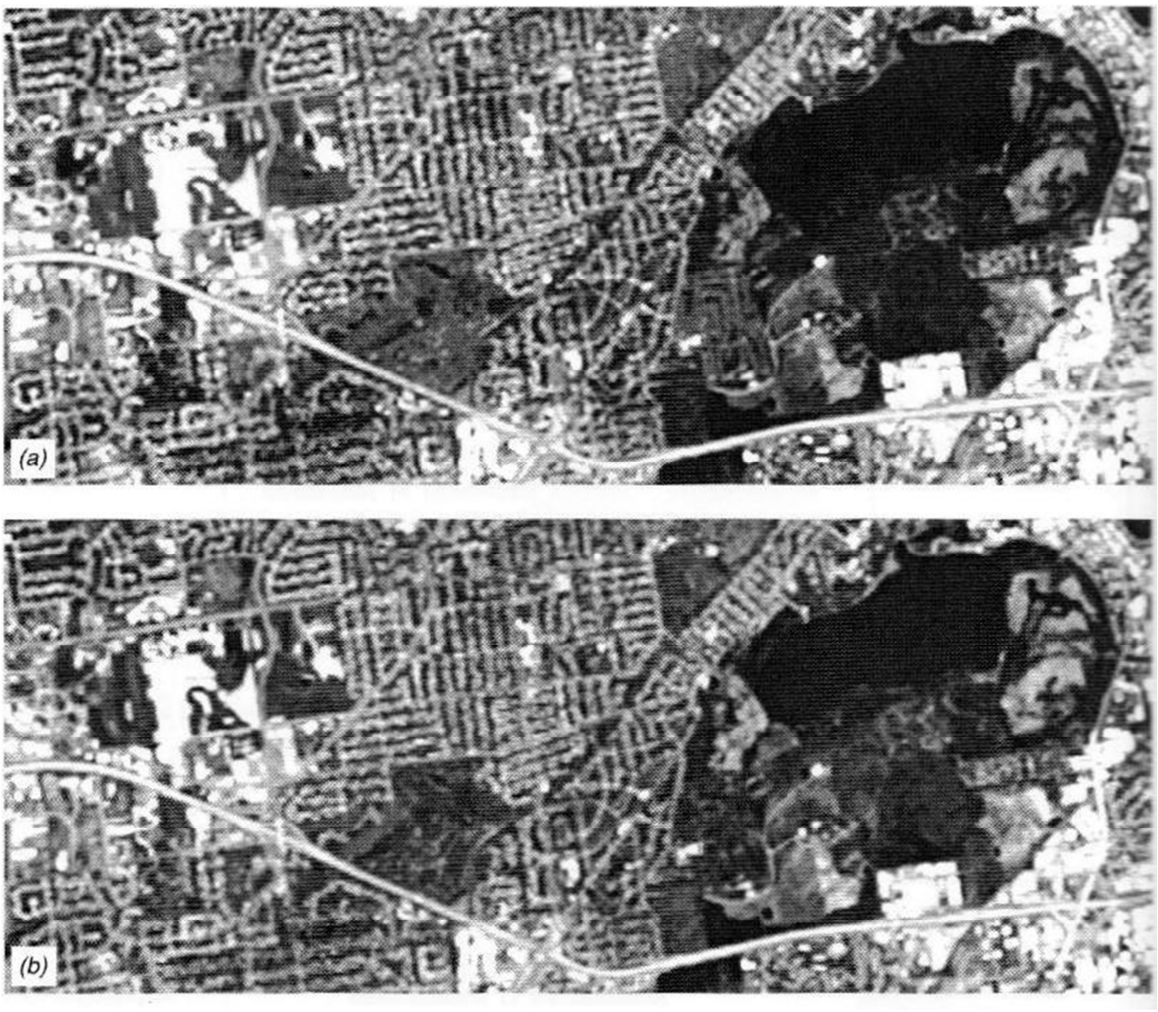

Figure 4.7: SPOT HRV multispectral images of a town (resolution 20 m): (a) band 1 (green – 0.5 – 0.59 μm); (b) band 2 (red – 0.61 – 0.68 μm). From (Lillesand et al. 2004).

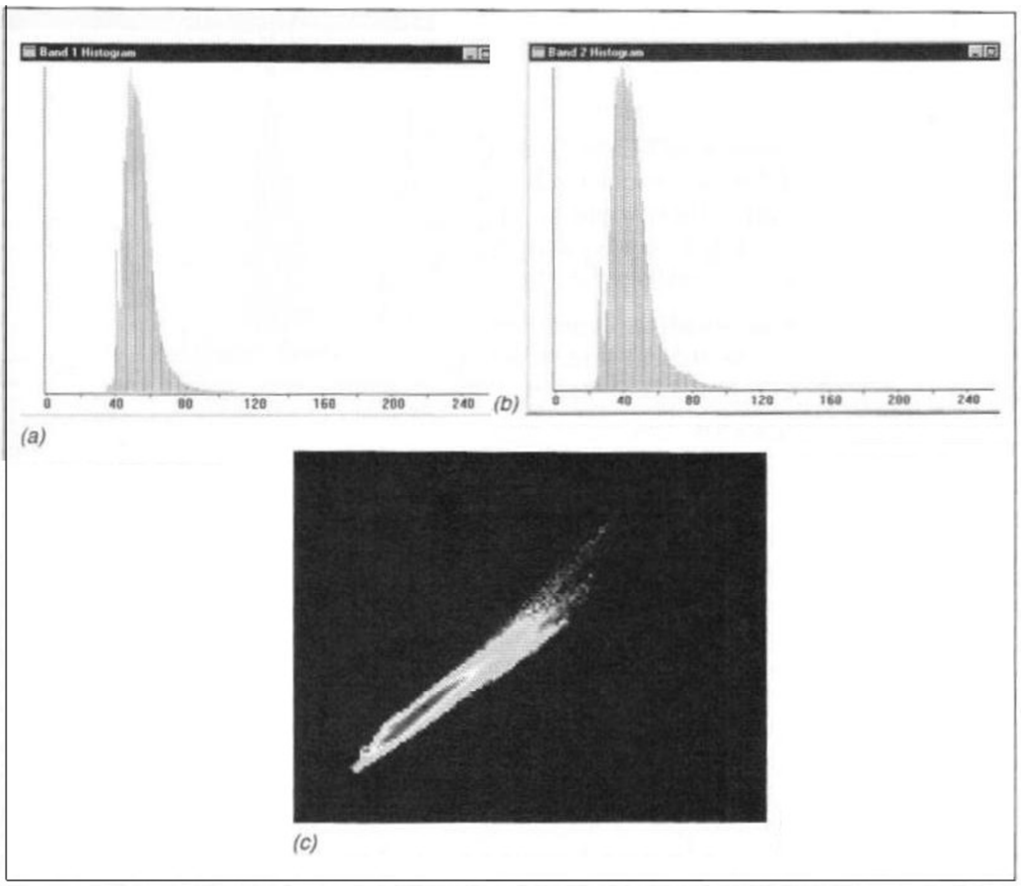

Figure 4.8: Histograms and two-dimensional scatter diagram for the images shown in Figures 4.7*a* and *b*: (*a*) band 1 (green – 0.5 – 0.59 μm) histogram; (*b*) band 2 (red – 0.61 – 0.68 μm) histogram; (*c*) scatter diagram plotting band 1 (vertical axis) against band 2 (horizontal axis)

Figure 4.8(a-c) shows the histograms and 2D scatter diagrams for the multispectral images. 4.8(a) is the band 1 (green) histogram, 4.8(b) is the band 2 (red) histogram and 4.8(c) is the scatter diagram plotting band 1 (vertical axis) against band 2 (horizontal axis). The high level of correlation between the two visible bands demonstrated the problem, which means that it is difficult to differentiate between data in band 1 and data in band 2 (Lillesand et al. 2004).

Principal Components Analysis can be used to reduce the amount of data which is redundant due to this correlation, which arises due to the fact that many of the data points are ‘red’ and many are ‘green’, so that one ‘green’ point is highly correlated with another ‘green’ one. It could be used before visual interpretation of the data or as a pre-processing procedure before automated classification of the data.

A further example (Figure 4.9 – a set of Landsat MSS images) shoes how Principal Components Analysis can be used to reduce the number of significant variables, highlighting specific features or processes at the same time.

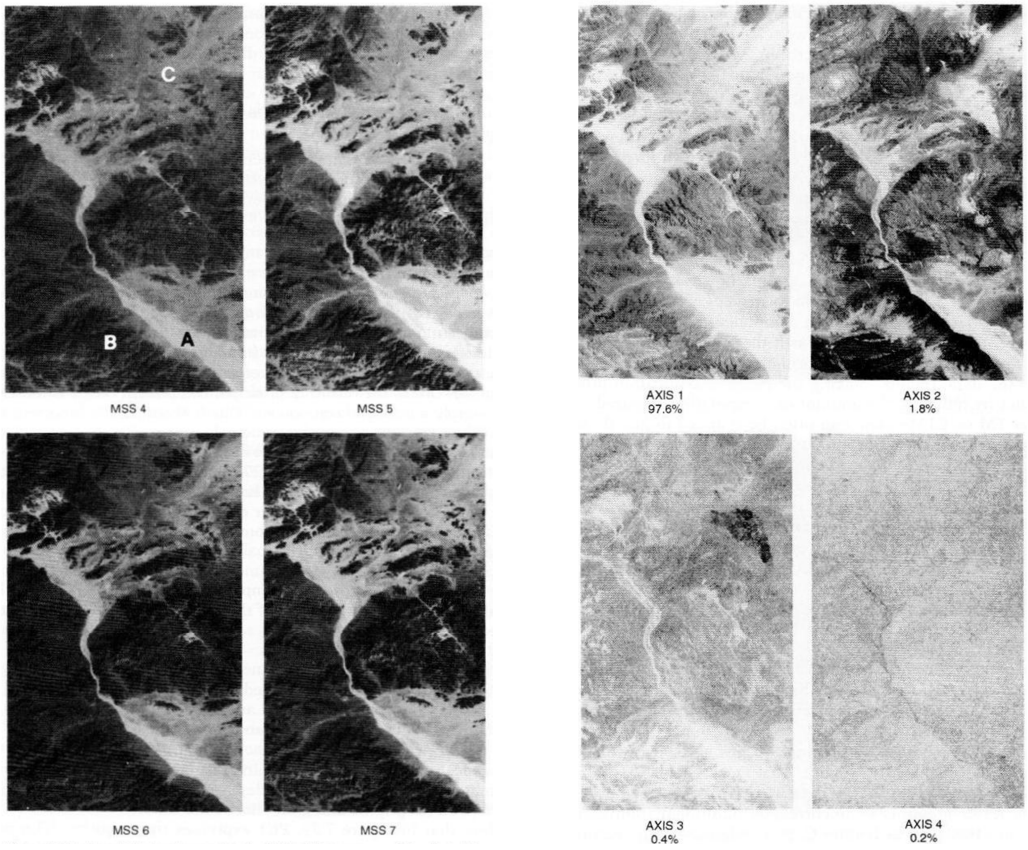

Figure 4.9: (left) original Landsat Multi-Spectral Scanner (MSS) bands covering an area of desert in Saudi Arabia (MSS bands 4: 0.5 – 0.6 μm, MSS 5: 0.6 – 0.7 μm, MSS 6: 0.7 – 0.8 μm, MSS 7: 0.8 – 1.1 μm). Ground resolution is 79 m. Labels correspond to: (A) alluvial material in a dry stream valley, (B) flat-lying quaternary and tertiary basalts, (C) granite and granodiorite intrusions. Right: Principal-Component Analysis transforms these data to highlight the areas with most variance From Lillesand et al. (2004).

Figures 4.8 and 4.9 show how principal components analysis can be used on a satellite image. The first two components explain almost all of the variance in the scene (99.4%) and the fourth principal component contains so little information that the image shows mostly system noise. However, the second and third components are able to illustrate certain features which are obscured by the dominant patterns in the first principal component, such as the feature labelled C. In this example the

images are shown in black and white, but images from three components can be combined to form a colour image (Lillesand et al. 2004).

4.3. ARCFAC 2007 DATA ANALYSIS

4.3.1. FREQUENCY ANALYSIS

As mentioned earlier, the raw data obtained in the Arctic was difficult to interpret due to the high levels of background noise at the higher frequencies (particularly above 10 kHz). When analysing ambient noise data, it is commonplace to consider the variation of the amplitude with frequency instead of with time, since it is difficult to spot patterns in noisy time-domain data. Initially Matlab's FFT (Fast Fourier Transform) functions were used to obtain plots of the frequency variations for the entire ARCFAC-2007 dataset, as shown in Figure 4.10.

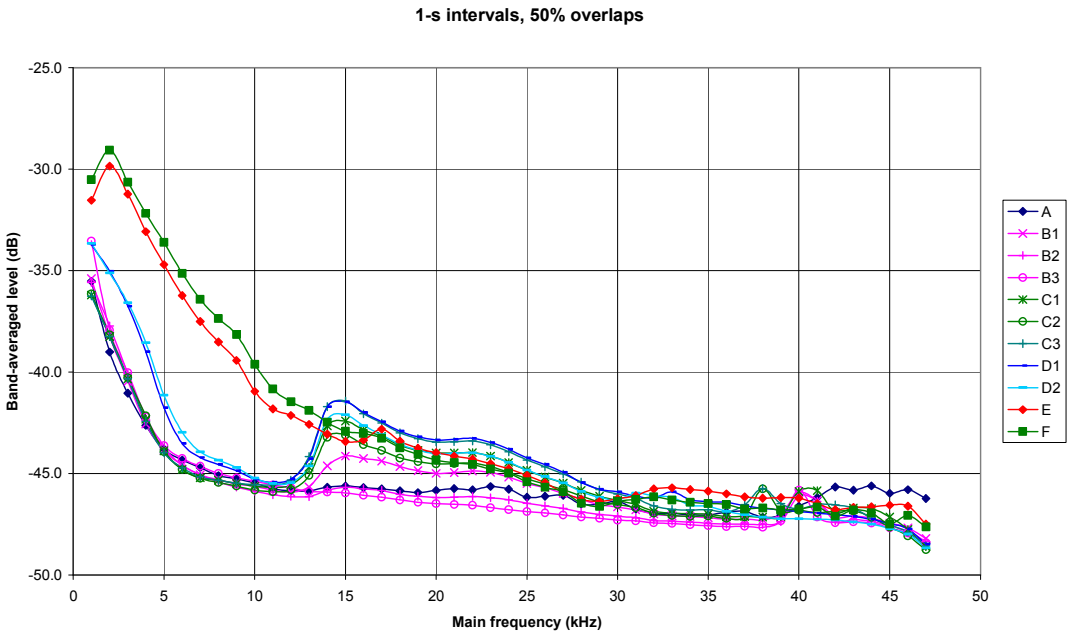

Figure 4.10. Values for the ARCFAC-2007 dataset, averaged over the entire sets each time.

The plots of the frequency spectra for the entire dataset show systematic differences between locations, particularly for locations E and F as well as within the recordings at location B. These variations could be attributed to variations in weather conditions between the different locations; however, it is important to note that averaging over

durations of (typically) 5 minutes can lead to the data being represented inaccurately. The power levels in dB were averaged over 1-kHz bands. In one single recording the power levels for one of these bands did vary by up to 10 dB in a few seconds (for marine mammal vocalisations). Furthermore, the rain rate could vary within the 5-minute recordings. And the recording vessel would sometimes drift slightly. Therefore a basic analysis of the average power levels at the different frequency bands is insufficient to obtain an accurate representation of the dataset and any analysis should look at the temporal variation of the events observed along with the duration of recordings and consider this when selecting appropriate segments of time over which to average.

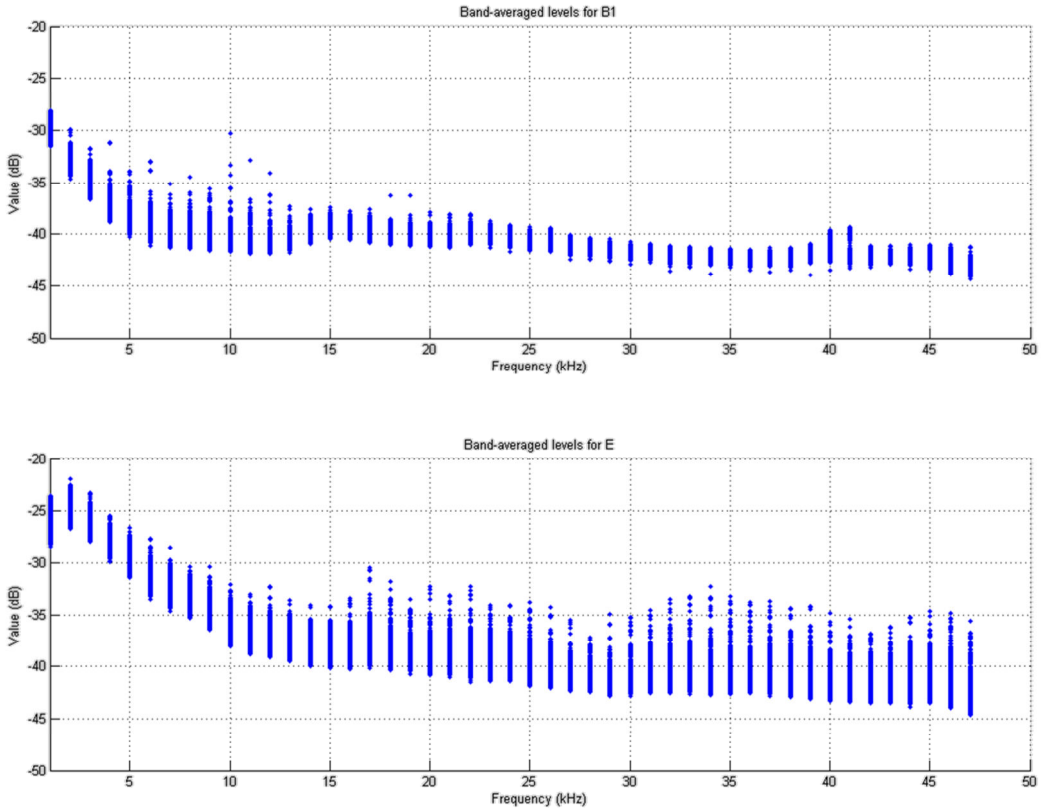

Figure 4.11. Variations of values for recordings B1 and E in the ARCFAC-2007 dataset.

Figure 4.11 shows the results of averaging over 1-kHz bands for two different recordings, demonstrating the difference in the spread of amplitude values between one recording and another. A broader spread of amplitudes is visible in recording E, at all frequencies. Recording B_1 was 1'20" long and included rain and wind but no ice, with a whale and ship within view. Recording E was 2'01" long and included very light rain and wind as well as some small icebergs (Table 3.1).

Chapter 4.1.3 discussed the use of ratios of spectral bands to identify specific weather processes in ambient noise data, similarly to methods used in satellite remote sensing. Black et al. (1997) plotted band-averaged levels from 4 – 10 kHz against those from 10 – 30 kHz to successfully identify differences in rainfall. However, other studies (Nystuen and Selsor 1997; Nystuen 2001; Quartly 2001) use different ratios (5 vs 25 kHz), and there seemed to be no rigorous method of selecting the most appropriate groupings of frequencies to identify weather events. To identify a more rigorous method using the Arctic data, it was important to begin by determining:

- The optimal bandwidth on which frequencies should be averaged.
- The optimal segment length for those band averages.
- The optimal overlap between segments.

Bandwidth

To determine the optimal bandwidth over which frequencies should be averaged, 1-kHz averages were compared to 0.5-kHz averages for all of the ARCFAC files and the two different averages were found to give the same values. Other bandwidths still gave very similar values and the same overall representation. Therefore 1 kHz was deemed to be a sufficient level of resolution.

Segment length

A segment length means the time interval over which the frequencies were calculated. The literature contained a variety of segment lengths. These variations could be due to the hardware used to acquire the data limiting the storage, or different sampling frequencies, or differences in application (e.g. monsoon rain compared to light drizzle).

Initially in the present case the choice of segment length was made by considering the sources of noise – weather-related events last for several seconds, while those caused by marine life typically last tens of milliseconds. Therefore, segment lengths of 1 second, 100 milliseconds and 10 milliseconds were selected and 1-kHz band-averaged levels were calculated for each file. Statistical analyses showed systematic

variations of 5 dB between calculations over 1-s and 100-ms intervals, and 5 dB between 100-ms and 10-ms intervals (and therefore 10 dB variations between 1-s and 10-ms intervals). Although these differences in sound levels are shown in band-averaged levels at 4-10 kHz and 10-30 kHz, for ratios the difference was less than 1%, with the only significant differences (4-7%) occurring with the last file, where there was no rain present but some potential ship noise. The difference can be explained by the size of the computation window, since decreasing it means that variations within the window become less important, for example the 1-kHz averages will vary less overall.

Further comparisons were made using sound files from various other sources which corresponded to more clear-cut cases (where there was just one source of noise instead of several acting in combination); marine mammal vocalisations, ship noise, different rain rates and different wind speeds. They were acquired at a variety of sampling rates (all below 96 kHz). The files did not come with any explanation of the processing (if any). For example, files from the Glacier Bay National Park website (2011) were sampled at 44 kHz but all showed a consistent and unexplained sharp drop above 15 kHz. The results are shown in Figures 4.12 and 4.13.

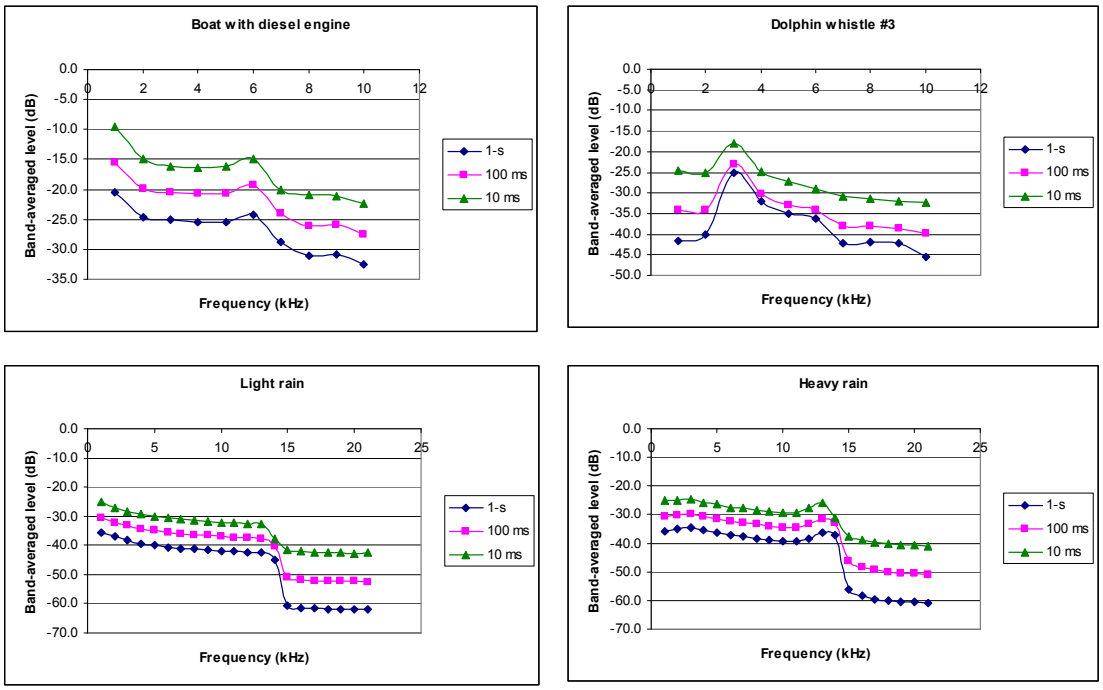

Figure 4.12. Examples for selected files from other sources. Note the systematic and unexpected high-frequency drops in the two bottom files, from the same source; Glacier Bay National Park web site (2011).

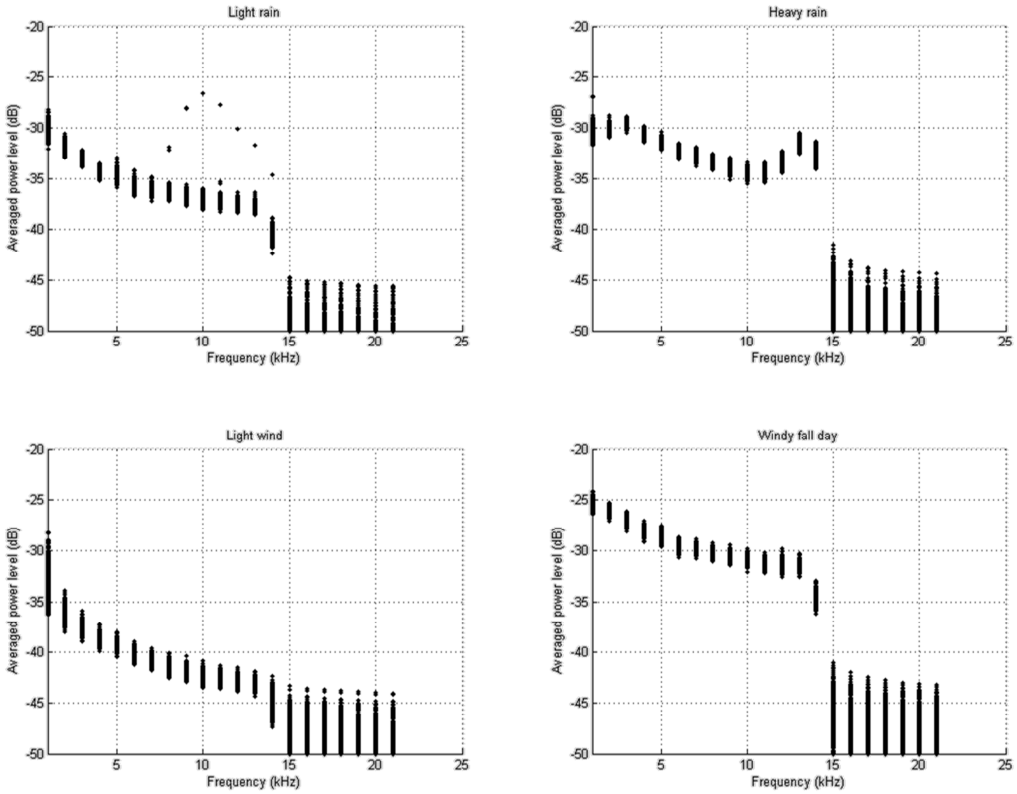

Figure 4.13. (top) distribution of band-averaged levels for light and heavy rain; (bottom) the same for light and higher wind. These examples are taken from the Glacier Bay files. Note again the systematic drop for frequencies above 15 kHz.

FFT algorithms need computational windows whose size is a power of 2 (Press 1999) and the chosen value needed to be large enough for the segment to contain enough meaningful data. After examining the time-domain signals, it seemed that a value close to 100 ms would be suitable. At the sampling rate of 96 kHz, this means that there would be 8,192 points in each segment, corresponding to 85.33 ms, a close approximation. The difference between a segment length of 100 ms and 85.33 ms is illustrated in Figure 4.14.

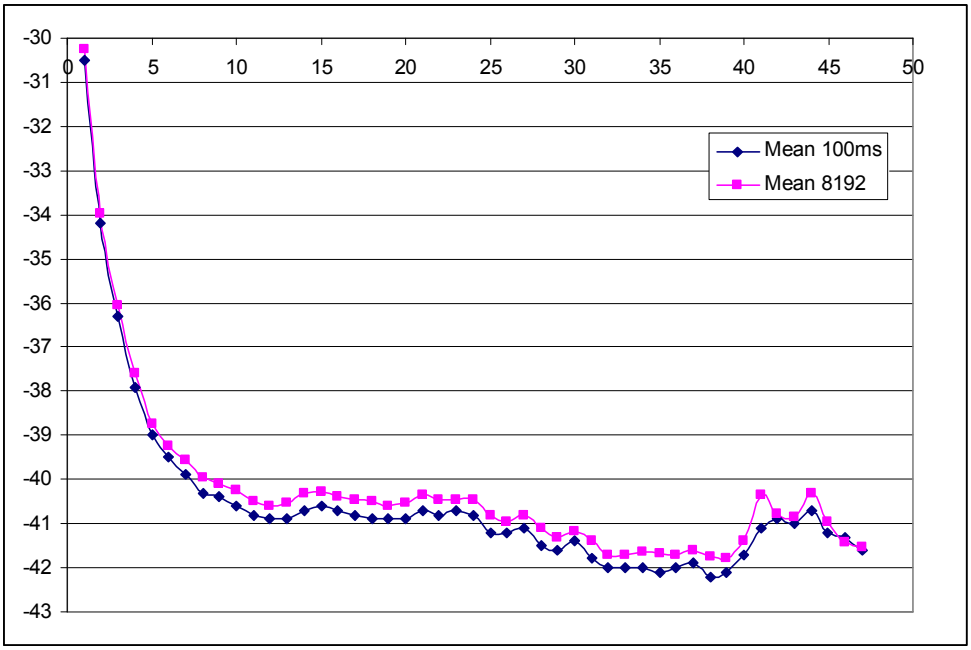

Figure 4.14. Averages of the band-averaged levels for file A. 100-ms segments are best approximated with segments of 85.33 ms (i.e. 8192 points at 96 kHz). The offsets on the average levels are negligible, but small-scale variations seem better revealed using a segment length of 85.33 ms.

Segment overlap

Physical processes may not always begin and end within the segment of interest. A 10% overlap is therefore used between segments, to optimise event coverage without using too much computer time. In this case, 50% overlaps were compared to 10% overlaps on the 8,192-point segments (Figure 4.15) and the difference was less than 0.001 dB. Therefore a 10% overlap was considered sufficient.

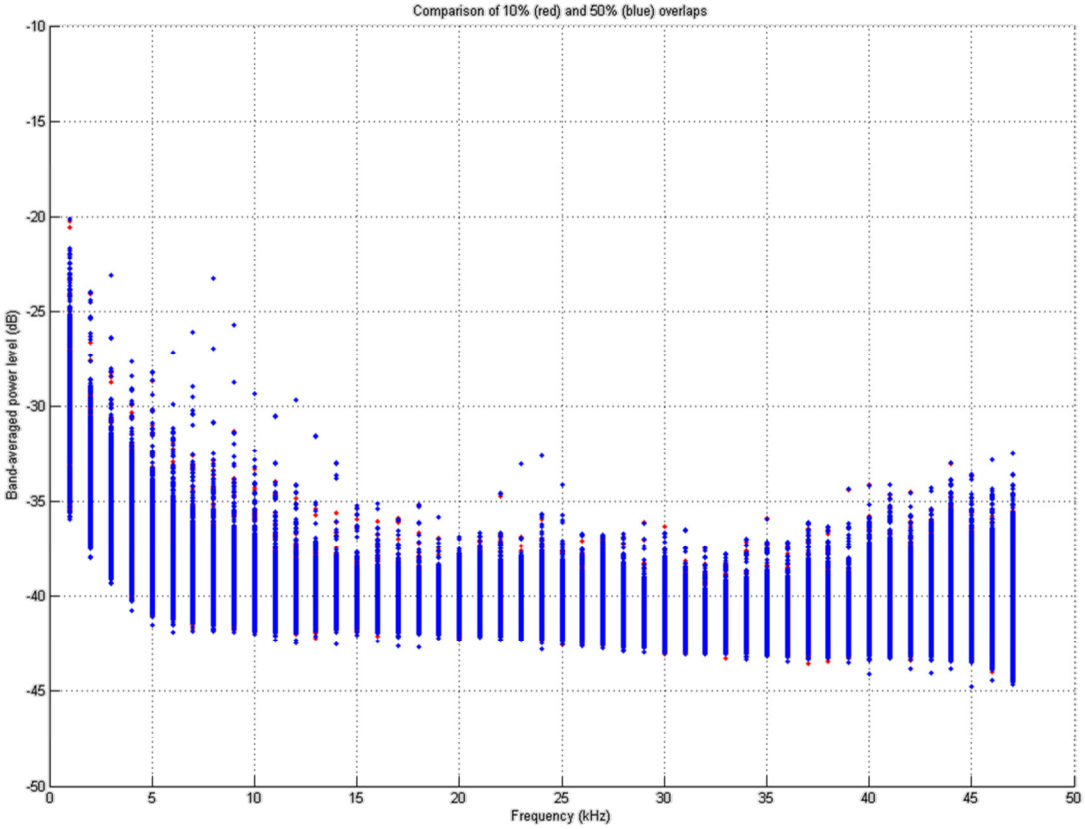

Figure 4.15. Spread of band-averaged levels for file A, processed with different overlaps (illustrated by red and blue points), generally at very similar values and thus indistinguishable.

4.3.2. PRINCIPAL COMPONENTS ANALYSIS

Once the Arctic data had been split into short segments, which had then been Fourier-transformed using Matlab, each segment showed 8,192 values of frequency over the 85.33 ms time period. To reduce the size of the dataset, the power spectra were averaged over 1-kHz frequency bands, between 1 and 48 kHz. Although other studies showed successful use of frequency pairings to separate different weather processes, there was little agreement between authors about the most appropriate combinations to use, and no mention of the method of selection. It seemed that possibly the frequency pairings were being chosen after inspecting the frequency spectrum for the ambient noise, which, although successful, was inadequately rigorous to be used on any kind of automated system. So, to produce a more thorough method of selecting frequency combinations to represent the large dataset, a principal components analysis was performed. In this situation, the reduced dataset consisted of 48 values for each 85.33-ms segment (one for each 1 – kHz band from 1

– 48 kHz). The analysis was performed using Matlab and the resulting output is shown in Figure 4.16.

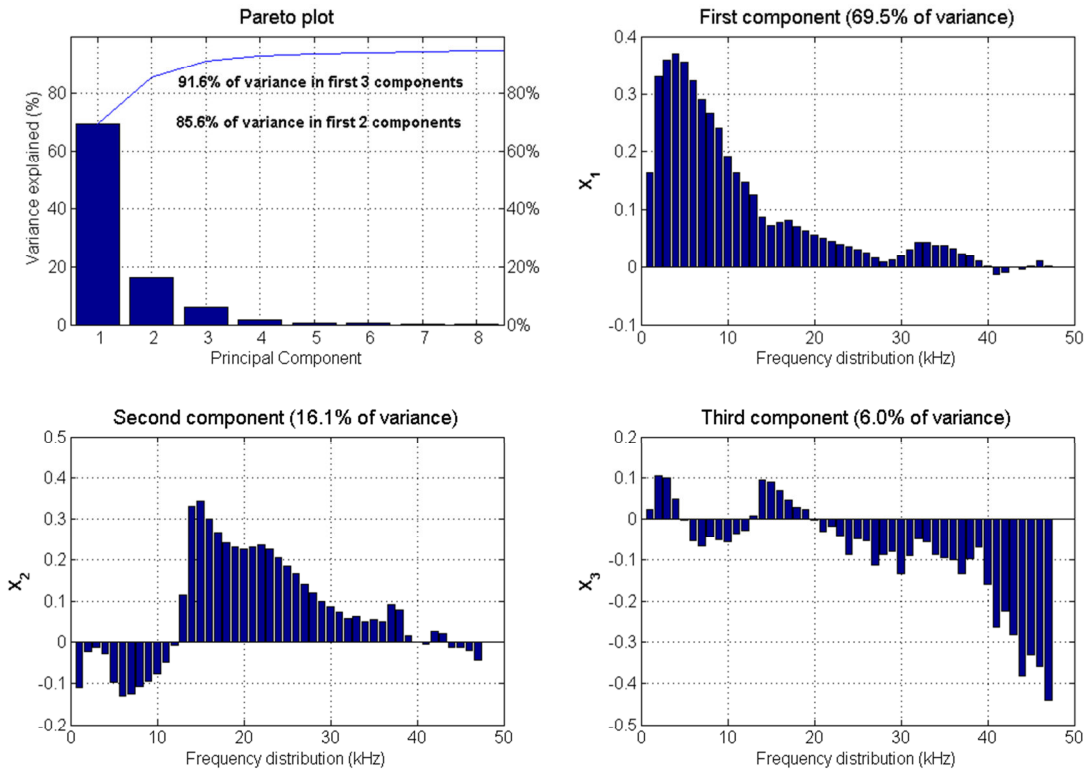

Figure 4.16: PCA output showing the first three components, noted X_1, X_2 and X_3.

91.6% of the variance was explained by the first three components, X_1, X_2 and X_3, as shown in the top left hand plot. Since this percentage was above 90%, the first three components alone give a good representation of the 48-component dataset. The resulting output also shows the frequency values which contributed to each component. X_1 shows a peak at approximately 5 kHz and X_2 has a peak at around 15 kHz. X_3 has a distribution which shows less clearly-defined peaks, with some smaller ones at frequencies up to 20 kHz and a larger one around 40 – 45 kHz. X_3 had a smaller contribution to the total variance, just 6%.

The physical observations from the Arctic measurements and tank experiments (by ourselves and others) as well as the theoretical explanations (Leighton 1994) show that wind-related processes usually create noise at about 5 kHz and that rain-related processes exhibit noise at about 15 kHz. These values correspond with the frequencies at the peaks in X_1 and X_2, as well as with the weather types observed

when the measurements were obtained. The frequency distribution of X_3 was less simple to explain, and to probe its physical cause, the relevant measurements were plotted using the three components.

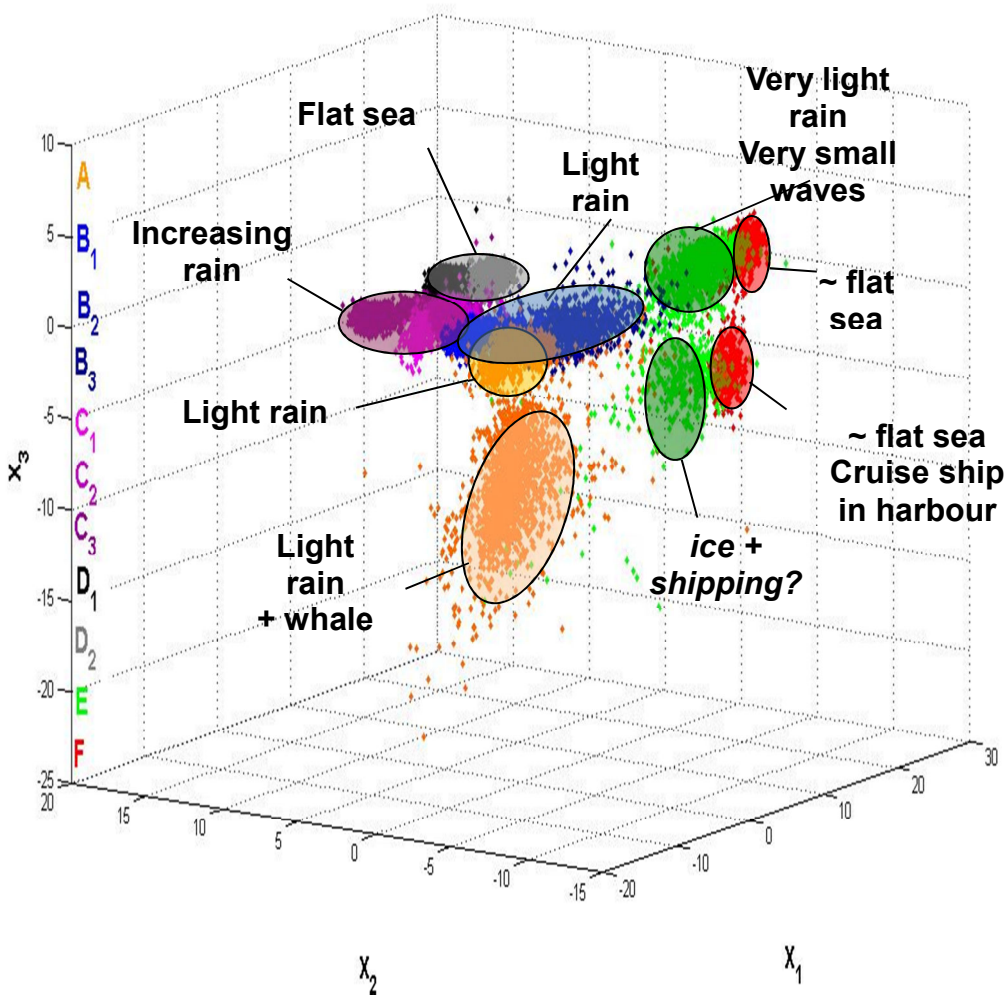

Figure 4.17: Plot of Arctic data using three frequency bands identified using principal components analysis.

The points at the different recording locations are clustered, showing that the three principal components are able to separate the different recordings. Furthermore, recordings which had been repeated at one site were still close together on the plot, indicating that the three components could separate the sources of noise as well as just differences in acoustical character of the location.

Looking at the variations in X_1 and X_2 for each of the clusters and comparing to Table 3.1 showing the weather conditions present, X_1 indeed seems associated to wind noise and X_2 to rain. The sites where it was raining (A, B, C and E) exhibit lower values of X_1 (Figures 4.18 and 4.19), whilst the recording stations where it was windy (A, B and E) show lower (more negative) values of X_2 (Figure 4.19).

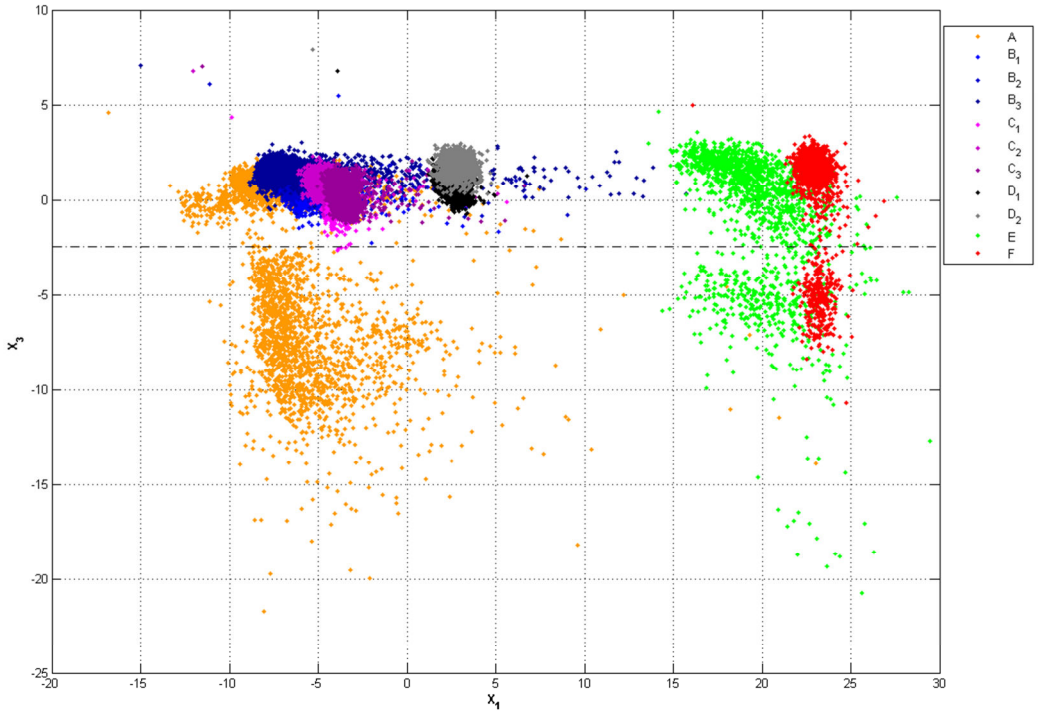

Figure 4.18. Plot of Arctic data using the first and third frequencies identified using principal components analysis.

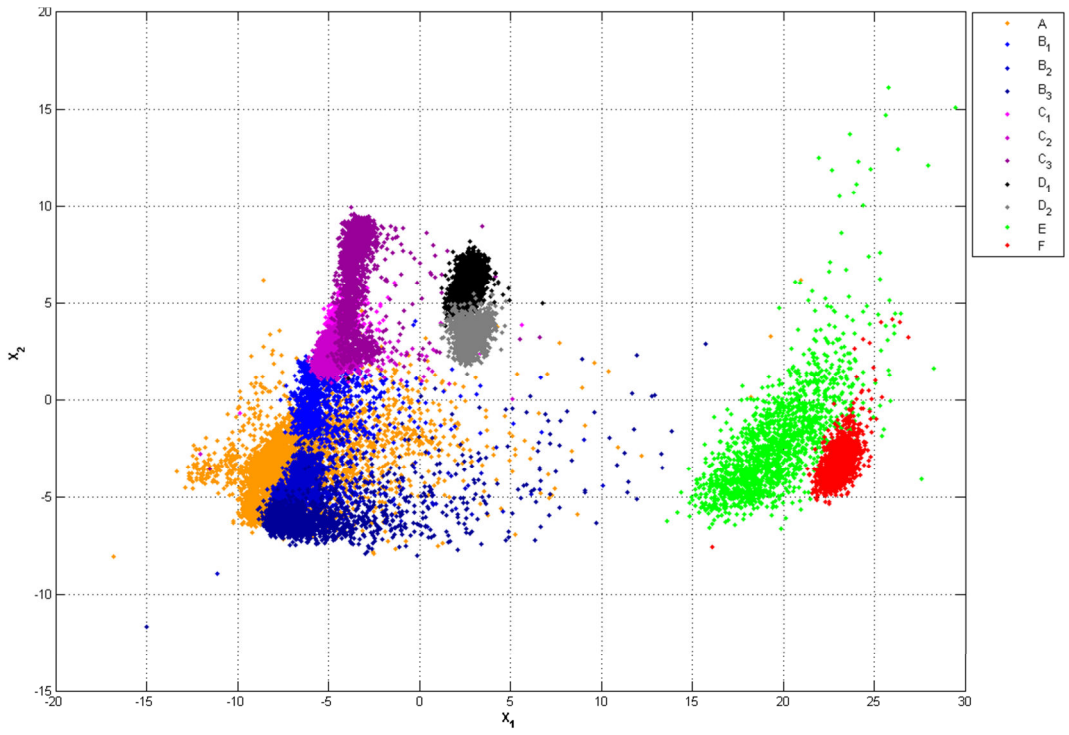

Figure 4.19. Plot of Arctic data using the first and second frequencies identified using principal components analysis.

Variations in X_3 are exhibited as 'sub-clouds' (most clearly visible in Figure 4.17 (3D plot)) present at sites A, E and F. The variations in X_3 at location A increase and decrease regularly and linearly with time. It is possible that these were related to the sonar from the passing ship, or marine mammal vocalisations (below 1 kHz) (e.g. de Ruiter, in Lurton, 2010) early in the recording. At location E, the sub-cloud shows a combination of lowest and highest frequencies. Small icebergs were seen less than 20 metres away when recording and could explain the high-frequency component. The sub-cloud in F could be associated to a number of factors, because at this location the hydrophone was only ~2 km from a cruise ship at the harbour.

Closer inspection of the sub-clouds related to the third component, X_3 gave more detailed information on the possible causes. The PCA plot (Figure 4.17) shows that the sub-clouds correspond to values of X_3 below -2.47, with just a few values being above 4.3.

Position A

The histogram of X_3 shows a bimodal distribution. The first peak is centred on $X_3 = -8$ and varies from -25 to -2 with a width of approximately 10 units. The second peak is centred on 1 and is just 2 units wide, similarly to the peaks of other files. Each interval corresponds to almost half of the total number of measurements (44% and 56%). Variations of X_3 with time show that the second interval is typical of the whole file, whereas the first interval (corresponding to $X_3 < -2.47$) can be divided into three distinct regimes (Figure 4.20).

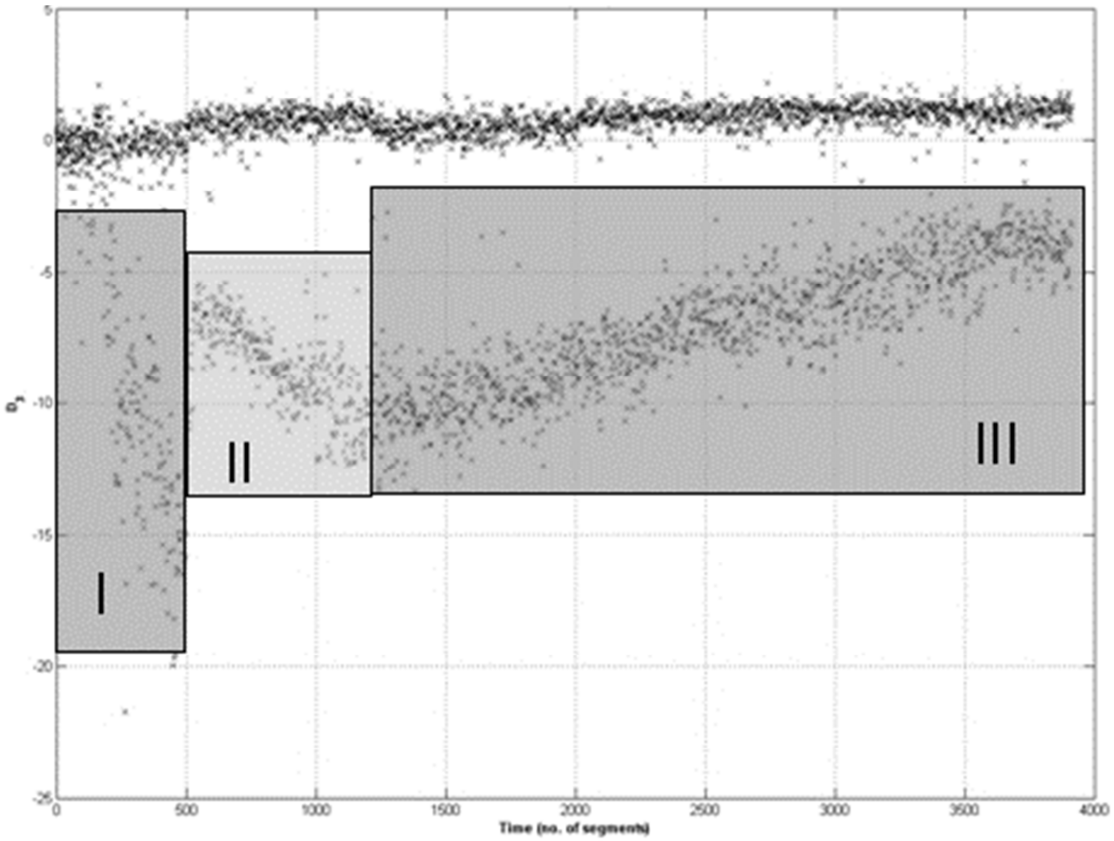

Figure 4.20 Variation of X_3 as a function of time.

Regime I corresponds to increasingly low values of X_3, which decrease sharply with time (over 500 segments in approximately 40 seconds). Regime II corresponds to higher values of X_3 which decrease slowly to a minimum of -14 after approximately 55 seconds (~700 segments) and increasing again for roughly the next 215 seconds.

All of the segments for which the values of X_3 are low include one or several very short, high-amplitude transients (typically 1-2 ms long, 10 times higher intensity than average, with strongest frequencies around 40 kHz), which is consistent with

the definition of X_3, mostly influenced by frequencies above 40 kHz. A preliminary explanation of these transients could be noise on the supporting boat as it turned to align itself with the main wave direction. However, this would not explain the fact that the transients were almost regular, or how the amplitudes of X_3 vary. Therefore, a second explanation could be that they were clicks from a neighbouring whale (for echolocation or feeding). However, the high regularity of the transients is not consistent with the movements of the whale when surfacing or with the intervals commonly observed for these clicks in other circumstances (Au and Hastings 2008). Therefore instead these transients were tentatively attributed to the echosounder from the ship visible on the horizon. The time between the transients matches the two-way travel time for echoes from the seabed below the ship (200-300 m). The decrease in X_3 would correspond to increasing amplitudes at high frequencies as the ship sails towards the hydrophones and away again. The mode of transmission of sound from the ship 5 km away in open sea to the hydrophones 10 m below the water surface in the fjord is unclear, but it could include the existence of a waveguide (as mixing of fresh water from the fjord with sea water leads to temperature variations (Cottier et al. 2005)). The transients generally occurred in pairs, which could be explained by multipath propagation. Generally, the type of vessel observed also generates noise in the 100 Hz region (Figure 4.21, (Kipple and Gabriele 2003)). Even if this noise can propagate over large distances, its main frequencies are below 1 kHz and would therefore be filtered out during processing. The frequency contributions above 1 kHz would experience propagation losses over ~5 km (the distance to the boat in the recordings) of up to 40 dB (10 kHz) meaning that at an original sound level of ~80 dB (as given in Figure 4.21), these higher frequency contributions would undergo propagation losses large enough that they would not be separable from the background noise at such a distance.

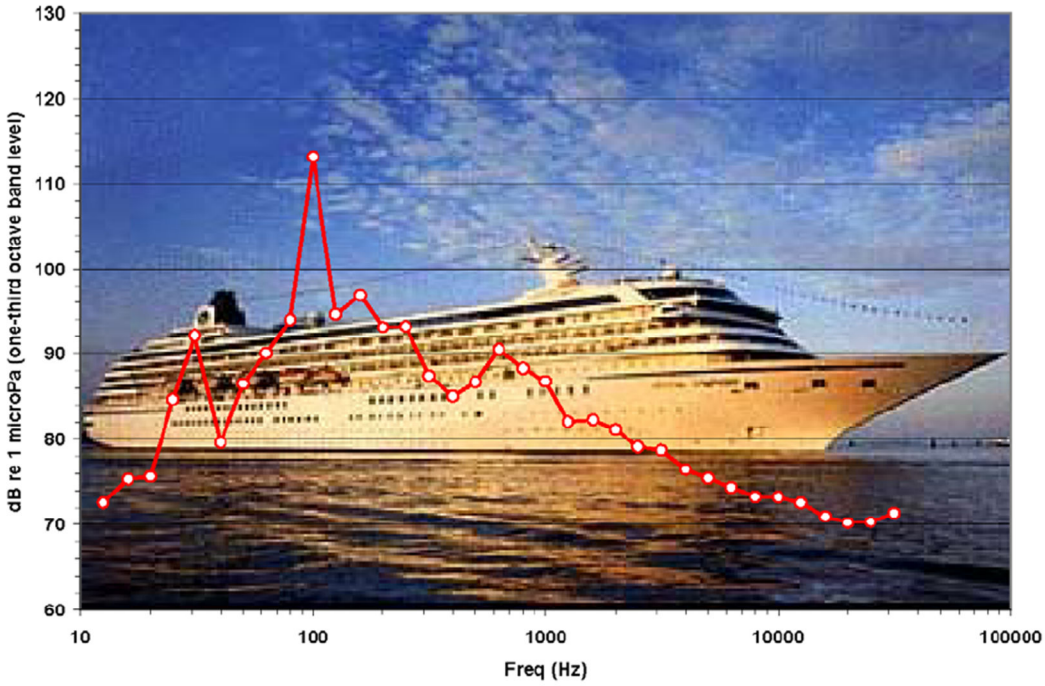

Figure 4.21: Representative large marine vessel noise spectrum (Kipple and Gabriele 2003)

Some segments in Regime I also show distinct pulse trains (Figure 4.22). These segments were analysed further using the freeware *Audacity*^{TM}, with the power spectrum computed with a Hamming window and FFT on 8192 points when available (depending on the number of points in the selection). All of the segments seem to correspond to whale vocalisations, since the main frequencies were around 680 – 700 Hz for the principal peak and 1.5 – 1.6 kHz for the secondary peak, with generally 1 vocalisation train but up to 3-4 vocalisation trains for a maximum duration of 60 ms. This is consistent with the observations of Mellinger et al. (2000) for minke whales but not with those of McDonald and Fox (1999) for fin whales. These calls show high amplitudes at low frequencies, which would result in high X_1 and slightly lower X_3, depending on which frequencies are present in the segment and contributing to the PCA components. Analysing *all* of the segments for position A more closely shows similar pulse trains, not associated to extreme values of X_3 but visually similar to the ones previously mentioned. The amplitude variations of these pulse trains are consistent with the observed behaviour of the whale, circling the boat at varying distances.

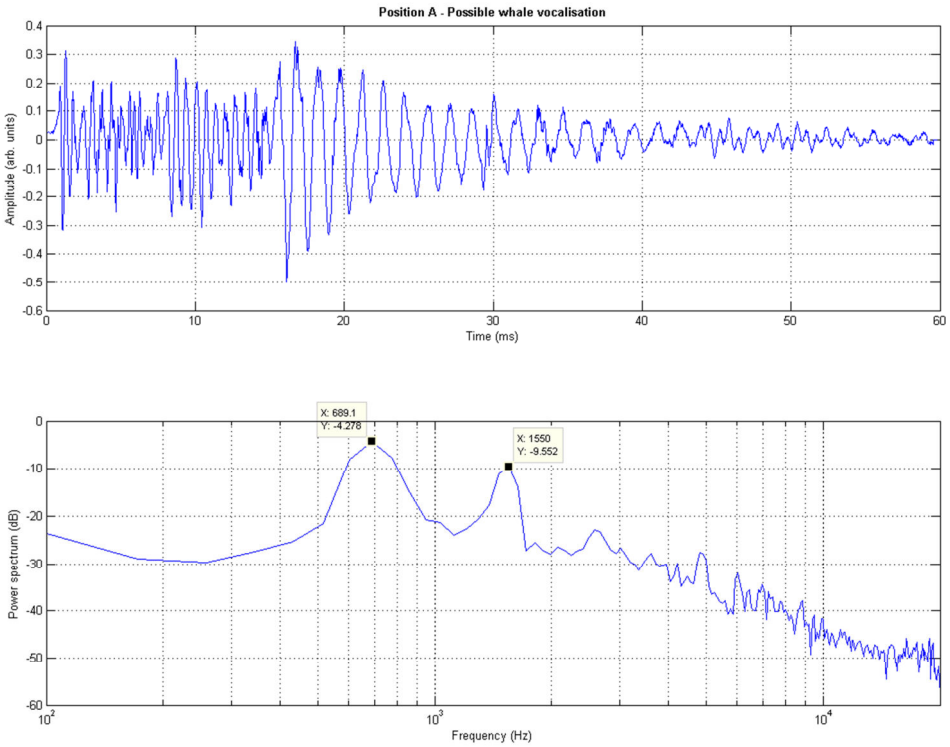

Figure 4.22: Plots of possible whale vocalisation. Top: time-domain data. Bottom: frequency-domain data.

Position B

The measurements in files B_1, B_2 and B_3 show X_3 histograms with a single, very narrow peak (2 units wide) centred on 1 or 2. There are no extreme values of X_3. Whale vocalisations can also be seen in file B.

Position C

The measurements in files C_1, C_2 and C_3 show X_3 histograms with a single, very narrow (about 3 units wide) peak centred on 0 or 1. There are no extreme values of X_3.

Position D

The measurements in files D_1 and D_2 show histograms for X_3 with one very narrow peak (3 units wide) centred on 1 or 2, with no extreme values of X_3

Position E

The histogram of X_3 for position E shows a bimodal distribution. The first peak is centred on $X_3 = -5$ and is 7 units wide. The second peak is slightly asymmetric (with a skew towards lower values of X_3), centred on $X_3 = 2$ and is 6 units wide. The first interval does not contain many segments (415 out of 1574, i.e. 26%) and does not exhibit clear patterns. The lowest values of X_3 also show high levels at lower frequencies (i.e. high values of X_1, the first principal component). Due to the method of calculation of X_3, these peaks at lower frequencies further lower the value of X_3. The physical reason for the sub-clouds here was not immediately clear. Additional recordings were taken close to the growlers and bergy bits but were lost due to battery failure related to the cold conditions. They showed that the frequency contents were typical of areas containing growlers – generally, growlers make the ambient noise more 'clinky'. It was possible that the noise was being caused by the melting of the icebergs, or by waves against the icebergs (but not surf noise as it is too low-frequency). The noise relating to different icebergs could interfere, and the fact that the icebergs were drifting in the wind (at approximately 1 km/h) could have added to the noise. Urick (1971) states that, 'The level of the noise of icebergs doubtless depends on many factors, such as size, depth, air content and rate of melting in the surrounding water'. He observed noise up to 10 kHz. Finally, it is important to bear in mind that there may be extra noise related to increased biological activity around the icebergs, since they are ideal places for fish to hide and forage as well as observation points for sea birds (some of whom forage underwater, e.g. Szczucka (2009)).

Position F

Plotting the histogram of X_3 at position F shows a bimodal distribution. The first peak is centred on $X_3 = -5$ and is 7 units wide. The second peak is centred on $X_3 = 2$, is slightly asymmetric (with a skew towards lower values of X_3) and is 5 units wide. The bimodal histogram for position E is very similar to the one for position F. Lower values of X_3 (below -2.47) are measured for 309 segments out of 1573 (19.6%). These values are influenced by the frequency content above 40 kHz, where higher

contributions from frequencies between 35 and 40 kHz decrease X_3 to its lowest values (roughly < -6). However, there is no visible pattern.

CHAPTER 5 – TANK EXPERIMENTS AND DATA ANALYSES

5.1. TANK EXPERIMENTS

The analysis of the Arctic experiments confirmed the conclusions of previous studies (Knudsen et al. 1948; Wenz 1962; Lemon et al. 1984; Nystuen 1986; Buckingham 1987; Nystuen and Farmer 1987; Scrimger et al. 1987; Pumphrey et al. 1989; Leighton 1994; Ramji et al. 2008) and enabled the establishment of a more rigorous method of selecting frequency combinations to use to separate different types of weather within a large dataset. However, in order to better interpret the Arctic measurements and the combination of different processes (such as both wind and rain in a field of melting icebergs), a series of laboratory experiments were carried out which enabled the measurement of weather-related noise in a fully controllable setting.

5.1.1. SMALL TANK EXPERIMENTS

The same hydrophone used in the Arctic experiments (Cetacean Research Technology SQ26-07) was placed less than 1 metre deep in the centre of a tank sized 1.8 m x 1.2 m x 1.2 m deep at the University of Bath. Several different types of weather were simulated; a desktop fan with variable speed settings was used to simulate wind, and a hose with a variable output was used to produce a fine mist of small droplets (the 'cloud' setting) and larger drop sizes (the 'spray' setting). The flow rate was varied using the tap on the wall of the laboratory and measured each time using a beaker. Finally, to simulate an iceberg calving from a glacier, the method described in Barker and Timco (2002) was used to create a 0.05 m^3 block of ice. Fresh water was frozen, cut into blocks, ground to small pieces, sieved and refrozen with added icy water. This method mimics the actual formation of a glacier. This ice block was placed in the tank and the hydrophone was again used to record

the ambient noise as it melted, and individual episodes of sub-blocks breaking off and capsizing were identified acoustically and visually.

In this case, the data was recorded directly onto a laptop using Audacity™ and the computer's soundcard which meant that frequencies could only be sampled up to 44 kHz (as opposed to 96 kHz in the Arctic). Therefore it was not possible to use all three of the acoustic discriminants identified in the Principal Components Analysis. However, it was possible to use the lower two peak frequencies (~5 and ~15 kHz); and consequently to distinguish the different processes simulated (Figure 5.1).

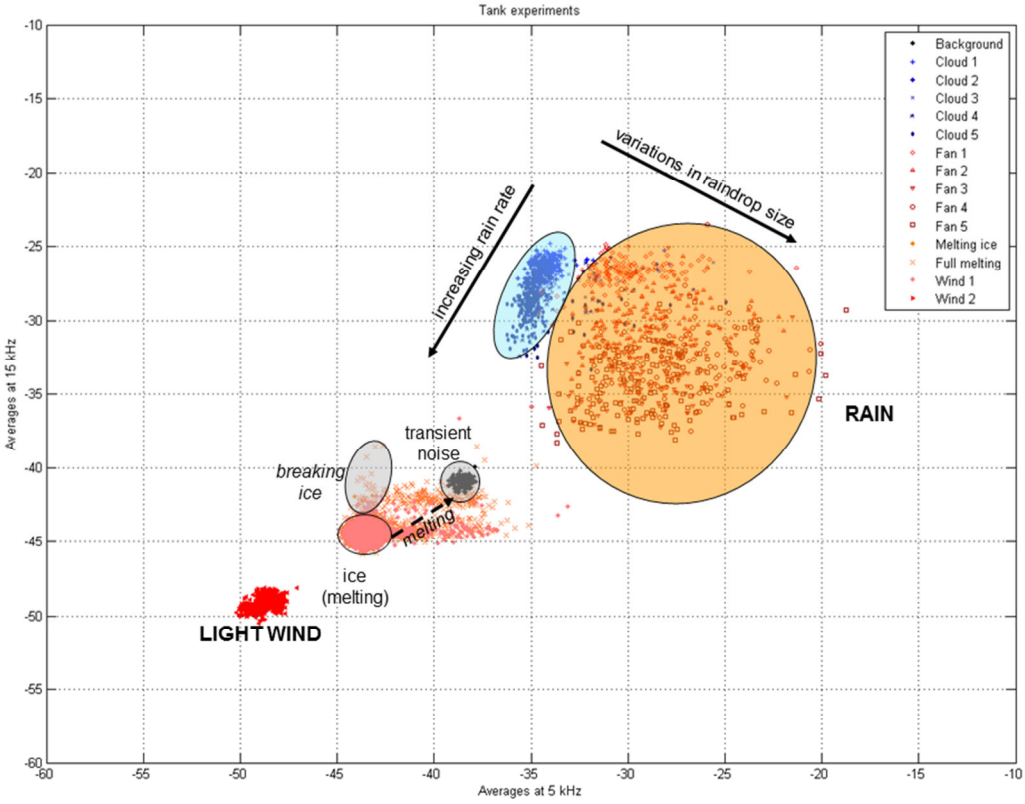

Figure 5.1: Acoustic classification of the tank measurements using averaged levels at 5 and 15 kHz. Individual processes can be clearly distinguished, including the melting of ice (with associated break-up and capsizing of sub-blocks) and variations in rainfall types.

Figure 5.1 shows acoustic measurements for 1-kHz frequency bands centred on 5 kHz and 15 kHz respectively. The blocks of melting ice correspond to a tight cluster of measurements, and the relative acoustic levels of melting ice are lower at 5 and 15 kHz than those of the breaking-ice blocks. The latter showed levels different from the transient

(background) noise, wind and rain. Logically, as the ice melted, this became more similar to the transient (background) noise. The measurements of wind and two different types of rain are also distinguishable and it is possible to notice variations in rainfall rate and droplet size. Wind and ice levels appear lower than the transient (background) noise at these particular frequencies. Normally an acoustic source such as wind or ice should be louder than the background noise; otherwise the implication is that it is not audible. However, it is possible that the background noise levels were high enough at these frequencies that the wind and ice were not audible. These levels were therefore investigated more closely.

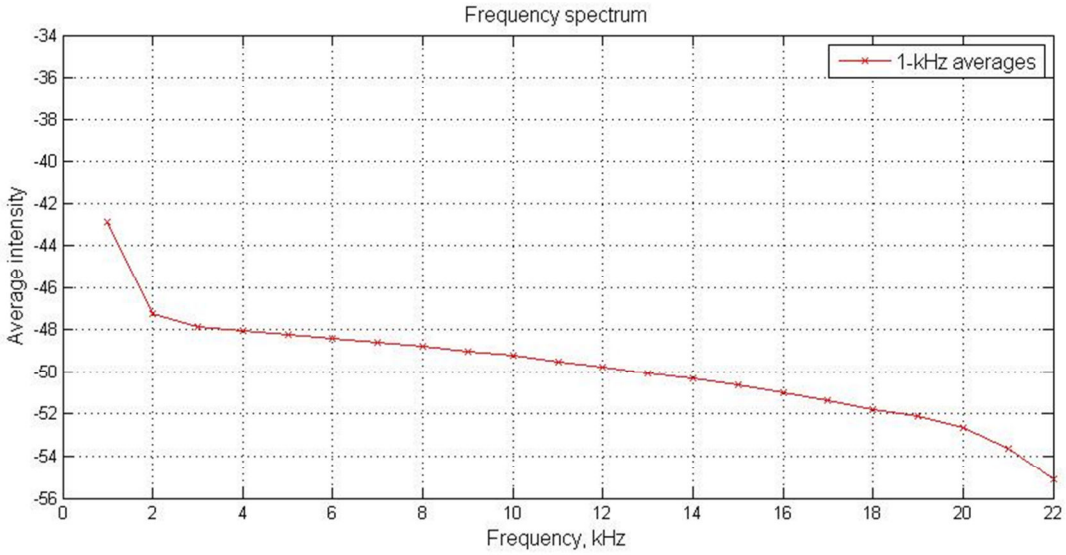

Figure 5.2: Relative sound intensity (in dB) averaged across 1-kHz bands from 1-22 kHz for ALL measurements of 'background' noise These values differ from those plotted in Figure 5.1 and are explained in detail in the text.

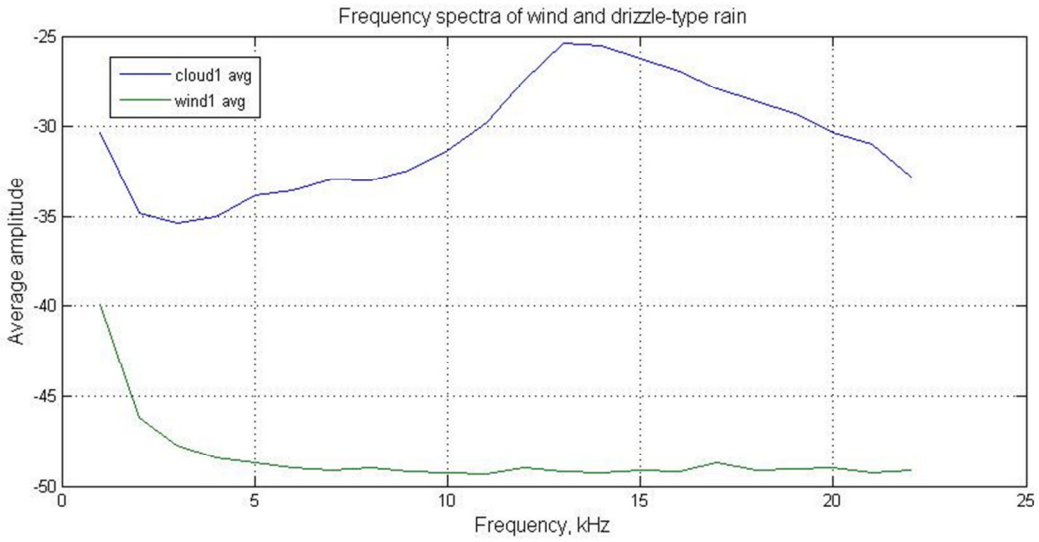

Figure 5.3: Relative sound intensity (in dB) averaged across 1-kHz bands from 1-22 kHz for rain – 'cloud' type and 'wind' measurements (smaller drop size and rainfall rate) of Figure 5.1.

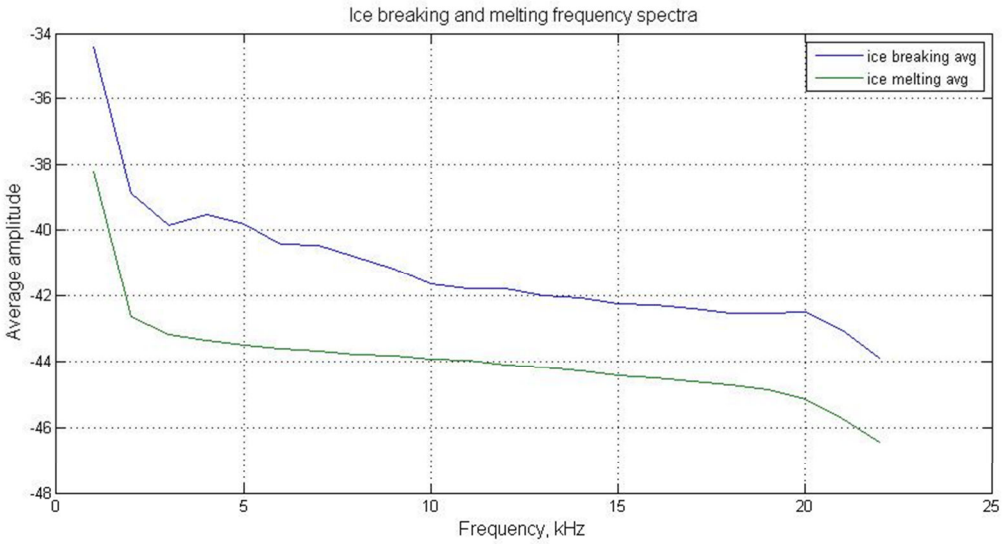

Figure 5.4: Relative sound intensity (in dB) averaged across 1-kHz bands from 1-22 kHz for measurements of ice blocks breaking and ice melting of Figure 5.1.

The sound intensities at 5 and 15 kHz for the noise sources in Figures 5.2-5.4 are summarised in Table 5.1.

Noise source	Approximate relative intensity at 5 kHz (dB)	Approximate relative intensity at 15 kHz (dB)	Time of recording
Background/transient	-48	-50	VARIOUS
Drizzle	-34	-27	Afternoon
Ice block (falling)	-40	-42	Afternoon
Ice block (melting)	-43	-44	Morning
Wind	-48	-49	Early afternoon

Table 5.1: Relative sound intensities at 5 and 15 kHz for different noise sources in tank experiments.

Figure 5.2 shows distinct background noise levels than those in Figure 5.1. Table 5.1 further shows that the transient noise levels for the file chosen for Figure 5.2 are lower than, or close to, the levels from wind and ice. Closer analysis reveals however this came from one specific recording, and the background noise recordings were taken for short periods at irregularly-spaced intervals over the days on which the experiments were conducted. These experiments were carried out with the same hydrophone and recording setup but in a smaller tank close to several intermittent and loud sources of noise (grocery shop, delivery road and cardboard compressing machine). This meant that the background noise recorded at one time could be considerably louder than at other times. These different recordings were averaged to obtain the overall representation of transient/background noise shown in Figure 5.1, and it is likely that the recordings which encompassed noisier periods could have led to the deceptively high noise levels at 5 and 15 kHz. These high levels of transient and unpredictable noise presented a considerable issue and therefore it was decided to use a larger tank further from these noise sources for the other experiments.

5.1.2. LARGER TANK EXPERIMENTS

Although the initial experiments in the smaller tank showed promising signs for separating wind from rain and ice noise using Principal Components Analysis, and distinguishing between different types of rain, the experiments were subject to several limitations. The small dimensions of the tank could not eradicate the possibility of echoes from the walls, and the background noise levels in the laboratory were quite high. More significantly, the sampling rate was lower than in the Arctic, preventing access to the third principal component (which was also the

component which did not seem to correspond to any theoretical weather-related noise), and the hydrophone's sensitivity was not consistent. Therefore the next experiments were carried out in a laboratory with lower background noise levels and a larger tank (5.1 m x 1.5 m x 1.8 m deep), again at the University of Bath. The hydrophone used in these experiments was a B&K-8103 omnidirectional hydrophone, with constant sensitivity of -211 dB re 1V/µPa between 0.1 Hz and 100 kHz.

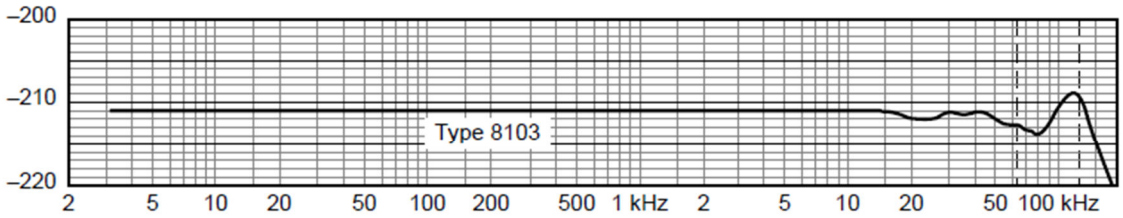

Figure 5.5. Frequency response for B&K-8103 hydrophone. From http://www.bksv.com/doc/bp0317.pdf?r=http://www.bksv.com/products/transducersconditioning/acoustictransducers/hydrophones/8103.aspx

Reliability of large tank and hydrophone

The larger tank, and a smaller tank which was later used for further experiments involving melting ice, were tested for wall echoes, and the frequency response of the hydrophone to white noise was investigated. To test for wall echoes, a single drop was released into the tank with recordings taken between 10 Hz and 100 kHz and an amplification of 50 dB. The oscilloscope was set to record for 20 ms at a time and showed a setting of 5.0 mV. A LabVIEW program written with Russell Howey was used to obtain roughly 3 recordings of 20 ms each. In the larger tank (5.1 m x 1.5 m x 1.8 m deep) the hydrophone was placed approximately in the middle of the tank, less than 1 m deep. For the experiments in the smaller tank (22 cm x 29 cm x 50 cm) the hydrophone was placed 15 cm from the narrow side, roughly in the middle, approximately 10 cm below the water surface. The plots of the raw data did not clearly show any noise from the individual drops, except in one case, and wall echoes were not visible in any of the recordings (Figures 5.6 to 5.7).

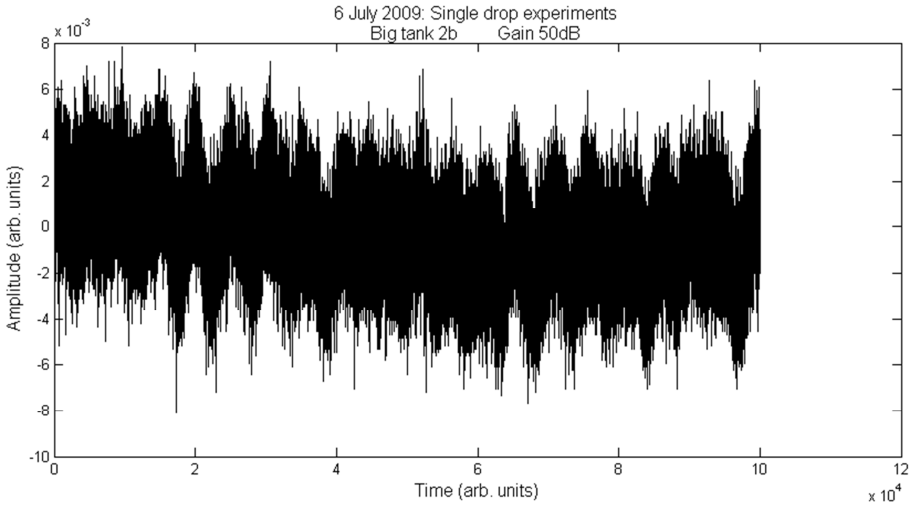

Figure 5.6: Noise from a single drop in the large tank. The drop is not visible.

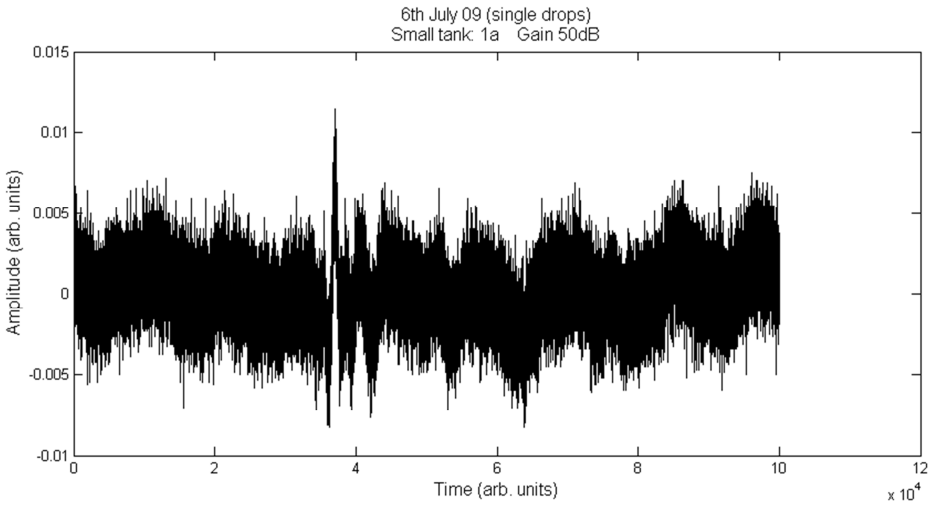

Figure 5.7: Noise from a single drop in the very small tank.

Matlab was used to perform a Fourier Transform on the time-domain data and some examples of the graphs obtained are shown in Figures 5.8 to 5.9.

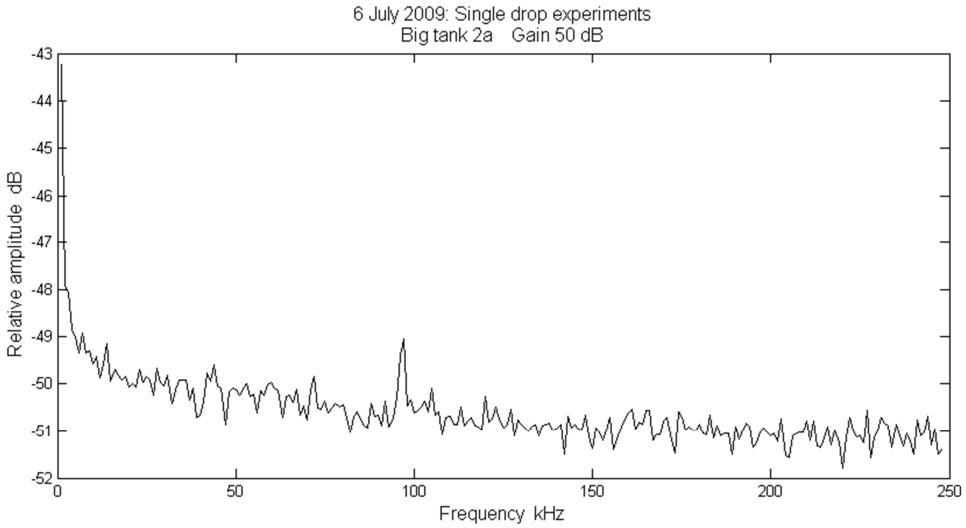

Figure 5.8: Frequency spectrum of single drop noise in a large tank.

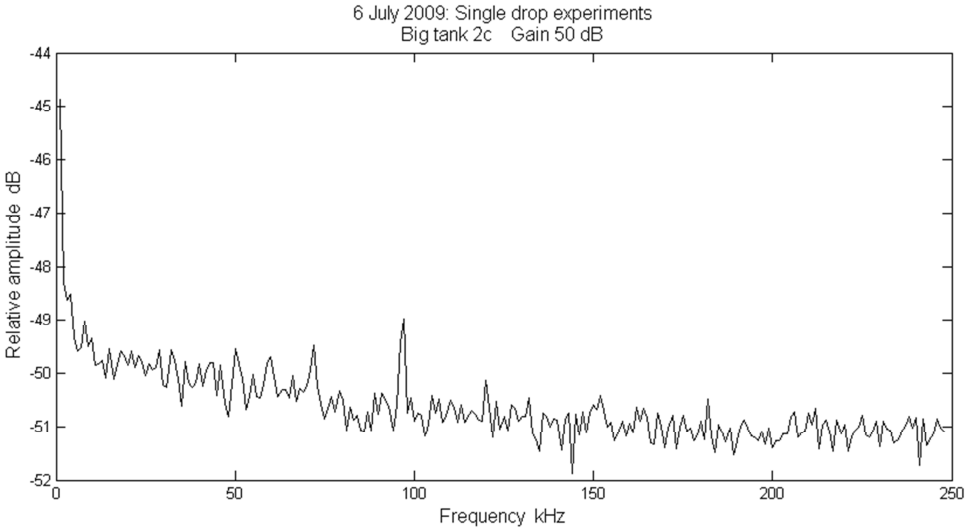

Figure 5.9: Frequency spectrum of single drop noise in a very small tank.

The lack of any clearly distinguishable wall echoes in the time-domain plots already indicated that wall echoes do not affect the measurements taken in the tanks, due to the relatively higher levels of background noise. Furthermore, the similarity of the frequency spectra indicated that wall echoes were not leading to raised amplitudes at certain frequencies. The peaks observed on the frequency spectra around 100 kHz correspond to the upper limit of the hydrophone used (B&K-8103).

To further probe any effects from wall echoes or the response of the hydrophone, a B&K white noise generator (type 1405) was used along with a Dale Electronics

2100L power amplifier and two B&K-8103 hydrophones (one to emit the white noise, one to receive it) and a Brookdeal Precision AC amplifier (type 9452, with a bandpass filter set between 10 Hz and 100 kHz) as illustrated in Figure 5.10.

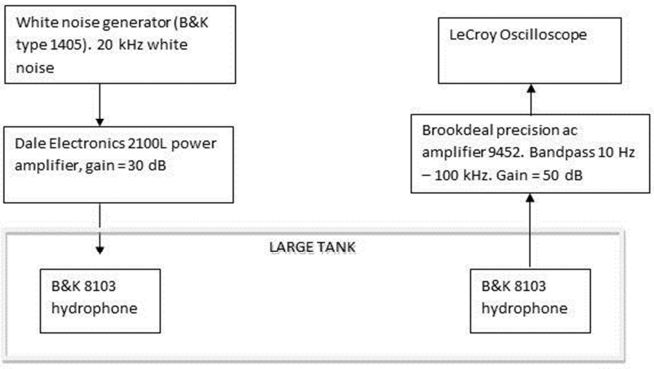

Figure 5.10. Schematic diagram of the experimental setup for the experiments to check for wall echoes and directionality of the hydrophone.

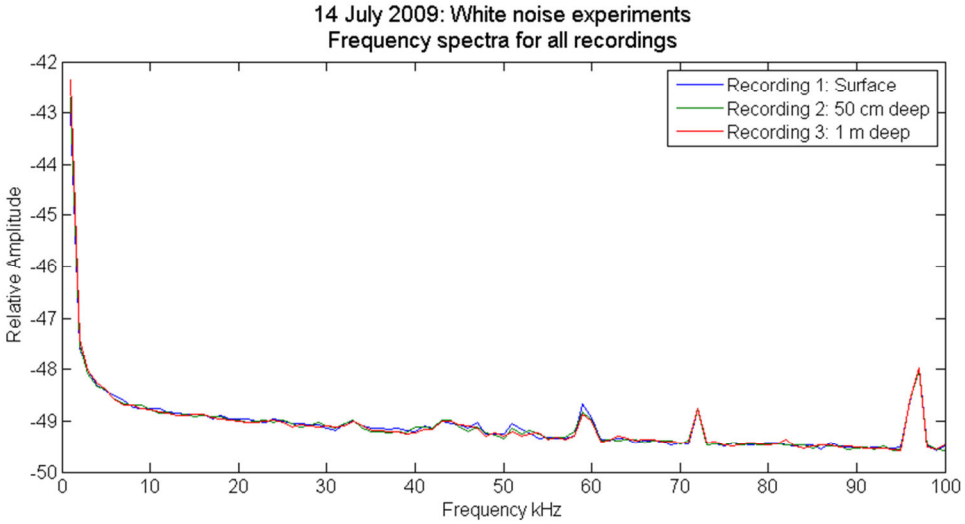

Figure 5.11. Frequency spectra for white noise emissions at three different depths.

The purpose of the white noise experiments was to test that wall echoes were not leading to false peaks at certain potential positions of the hydrophone. Three different positions were investigated; at the surface, 50 cm deep and 1 m deep. The three plots have been plotted on one set of axes in Figure 5.11. Although there are peaks at certain frequencies indicating that the hydrophone is not showing an output of the exact white noise being emitted, the peaks are at the same frequencies and of the same amplitude for all three positions. This means that the position of the

hydrophone will not adversely affect any results and these peaks cannot have been caused by wall echoes, otherwise they would vary depending on the position of the hydrophone within the tank (due to interference from reflections varying spatially).

Experiments

At first, some simple experiments were carried out where different types of rainfall were simulated. Four types of 'rainfall' were recorded along with background noise and the amplitudes were plotted at 5 kHz and 15 kHz as well as 5, 15 and 45 kHz. These plots are illustrated in Figure 5.12.

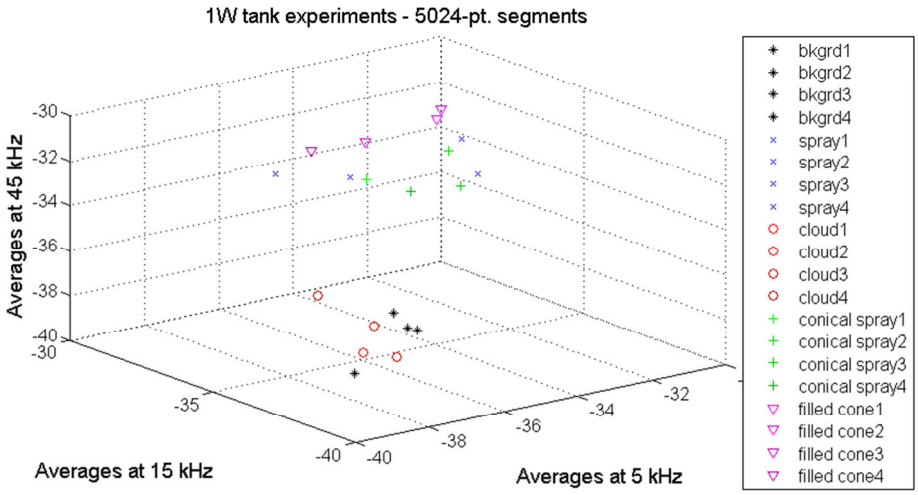

Figure 5.12. Amplitudes of noise from 4 types of rain and background noise at 5, 15 and 45 kHz.

The different types of rain were separated using the same frequencies identified in the ARCFAC dataset, and including the higher frequency of 45 kHz even showed some differentiation between the different types of rain.

To further improve the next experiments, the signal was amplified by 30 dB and band-pass filtered between 10 Hz and 100 kHz using an Ortec Brookdeal 9452 amplifier, then sampled at 500 kHz using a LeCroy LT-264 digital storage oscilloscope controlled using LabView. Figure 5.13 shows the setup of the laboratory equipment used.

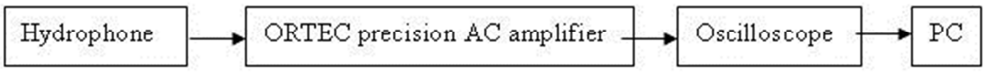

Figure 5.13: Schematic diagram showing setup of large tank experiments

The same methods used in the smaller tank were used to simulate weather processes, and recordings were taken over 3-minute periods, sampling in 0.2-second bursts every 10 seconds. Initially an ice block was created as suggested by Barker and Timco (2002) but with larger blocks of ice frozen with icy water and a hydrophone was placed approximately 75 cm away and 1 m deep, and the noise was recorded for 5 hours as the ice block melted. The amplitude was then plotted at every possible combination of frequency pairings and the noise over the entire 5 hours was inspected to try to spot frequencies which may have been useful. In this case the gain was set to 60 dB.

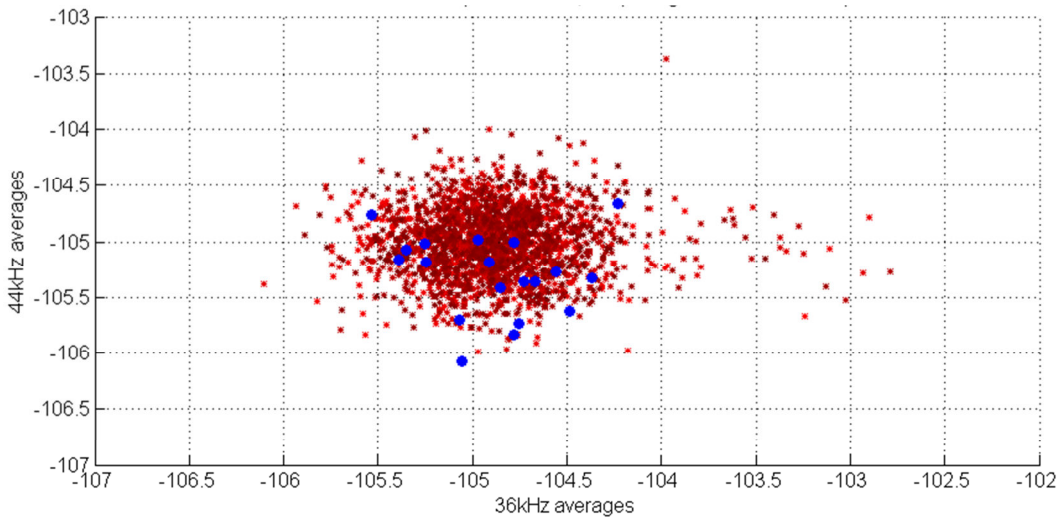

Figure 5.14. Noise from an ice block melting at a sample frequency pairing.

The distribution of points in Figure 5.14 is fairly typical of the dataset; the red points show the noise from the ice and the dark blue circles show the background noise. Although the noise recorded *with* the ice block present includes some of the same amplitudes at certain frequencies as the noise without it present, there are also slightly higher noise levels at some frequencies than for the data with the ice block.

Generally the noise from the ice block was slightly different to the background at 34 – 36 kHz.

Next, a block of ice was created by simply freezing water into a bowl, without breaking any bits of ice into smaller blocks, and the noise was again recorded as it melted over 6 hours, with a gain of 30 dB as some events seemed to be being missed from the screen of the oscilloscope due to their high amplitude. Finally a third ice block was created with small fragments of ice re-frozen with icy water. This iceberg was a similar size to the other two, at 26 cm wide x 32 cm long x 12 cm deep. For the third ice block the gain was also 30 dB. After obtaining the ice noise recordings for these three different ice blocks it was possible to compare the noise they created to check whether the Barker and Timco (2002) method of creation was necessary here.

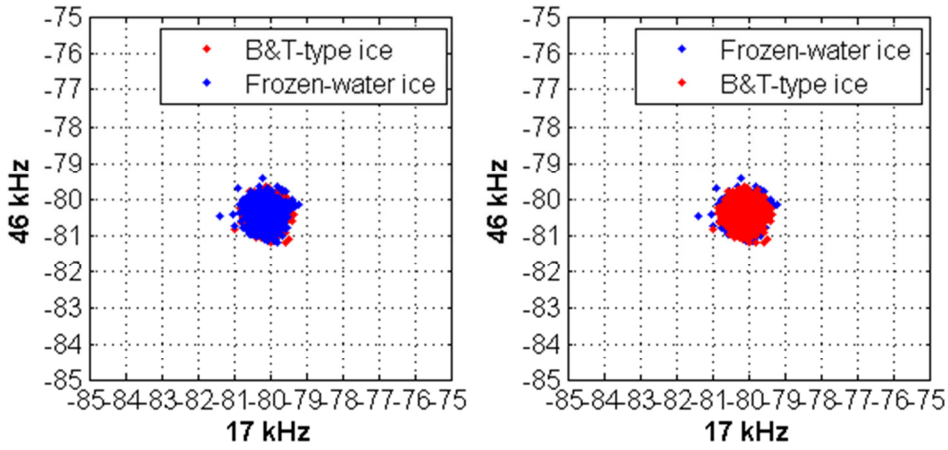

Figure 5.15. Comparison of Barker and Timco type ice to frozen water ice at 17 and 46 kHz.

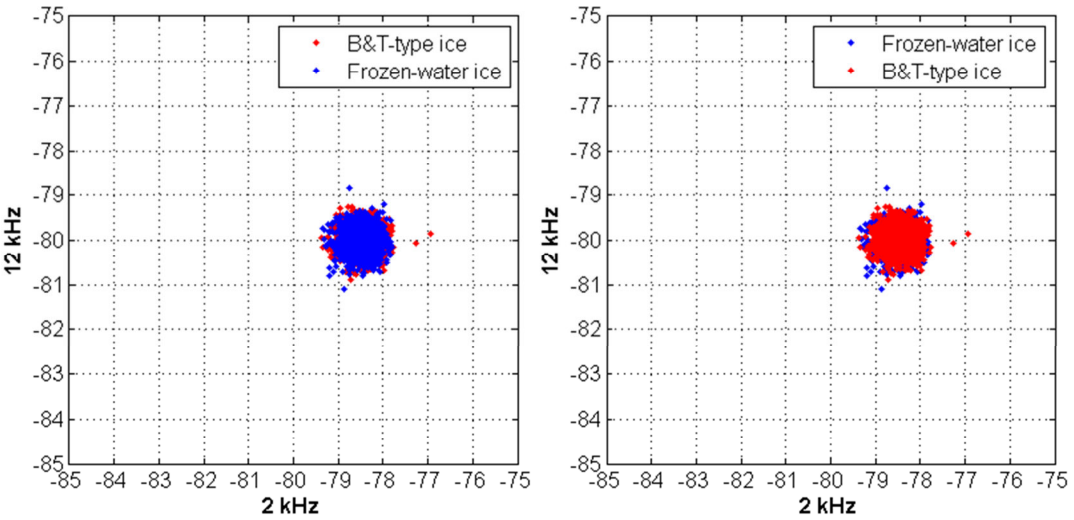

Figure 5.16. Comparison of Barker and Timco type ice to frozen water ice at 2 and 12 kHz.

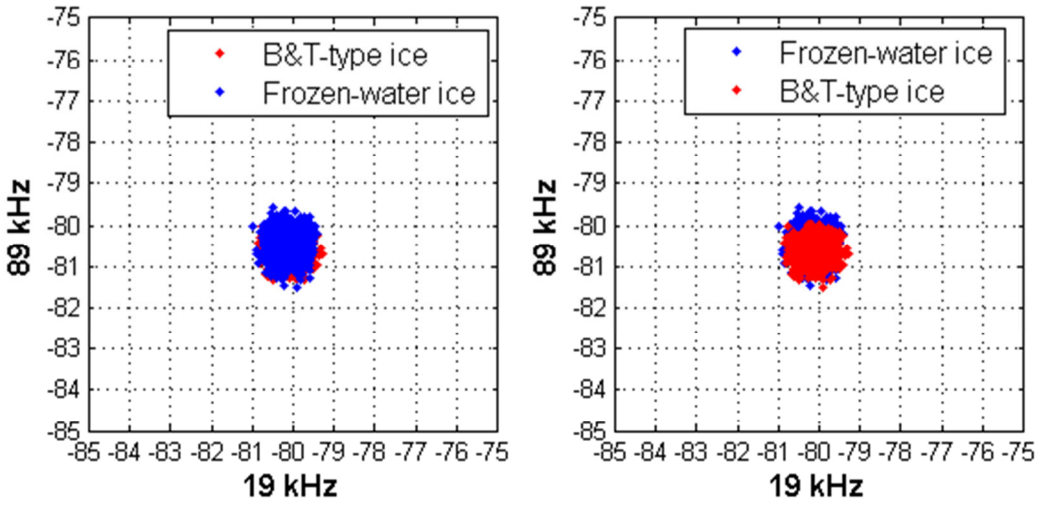

Figure 5.17. Comparison of Barker and Timco type ice to frozen water ice at 19 and 89 kHz.

Slight differences were visible in the amplitudes at certain frequencies caused by the two different types of ice – namely 89 kHz, as well as occasionally around 17 kHz, and frequently at frequencies between 1 and 5 kHz. Although these differences were not anywhere near as pronounced as the differences observed in previous laboratory experiments, the ARCFAC 2007 data or in the literature, the fact that they were visible indicated that ice created using small blocks of ice frozen with icy water made noise at different frequencies to ice created by just freezing tap water.

Another set of experiments simulating different types of rainfall were carried out, making use of the LabView program and the digital oscilloscope. Three types were simulated, a ‘cloud’ setting which produced a fine mist of small droplets, a ‘spray’ setting which created larger drops, similar to heavy rain and creating small waves and a ‘cone’ setting which gave a full spray which created some small bubbles . The hydrophone was placed less than 1 m deep in the larger tank and the spray covered roughly a 1-m diameter circle on the water surface, with the edge of the circle roughly 50 cm from the hydrophone. The gain was 40 dB for the first two experiments but reduced to 30 dB for the others, due to some peaks on the oscilloscope being too large to see on the screen. This change in gain was accounted for when processing the data. Wind was simulated by holding the fan above the

water surface approximately 1 m from the hydrophone, then the ambient noise was recorded.

To investigate the source of the noise produced by ice in the Arctic dataset further, two ice blocks were created and different types of collision were simulated in the large tank. These collisions were carried out approximately 1 m from the hydrophone and consisted of recordings taken every second for 3 minutes. One iceberg was bashed against another, then one was scraped alongside another and the noise at different frequencies caused by these collisions was investigated. The results from these tank experiments were plotted along with the data from the recording of the iceberg melting (Figure 5.18) and it was possible to observe some separation of different weather events at certain frequencies. For example, the data points from rain alone were separated from the points from the other sources of noise present at most frequency pairings involving 84 and 85 kHz with a lower frequency, particularly below 5 kHz, and also in the plot of 16 kHz against 20 kHz. Other frequency pairings, such as 36 and 84 kHz showed less obvious separation, but still some variation in amplitude from one type of 'weather' to another.

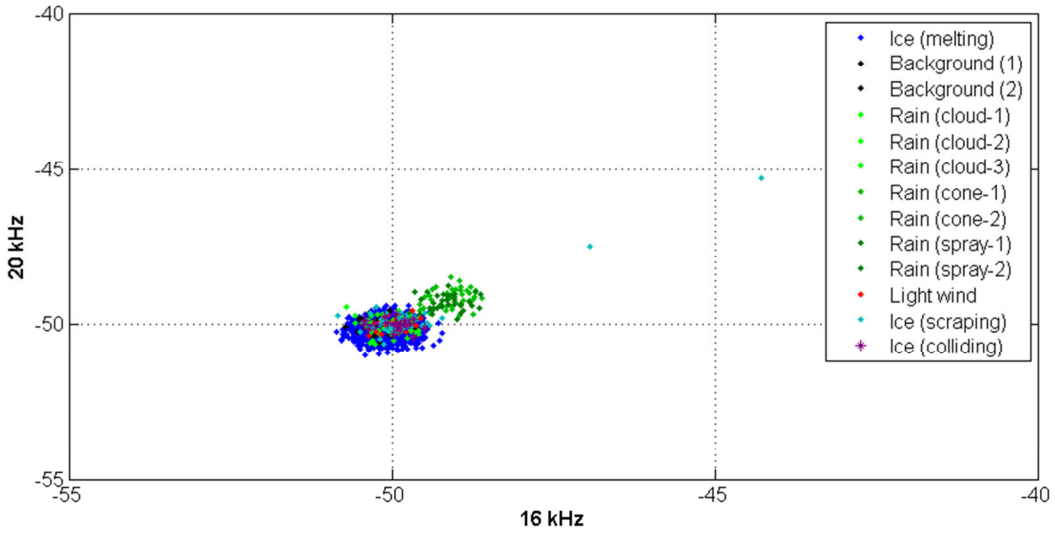

Figure 5.18. Noise amplitudes at 16 and 20 kHz for 3 types of rain, light wind, scraping, colliding and melting ice and background noise.

A larger (approximately 60 cm x 30 cm x 40 cm deep) iceberg was created using freezers belonging to the Department of Biology at the University of Bath and this

was recorded as it melted over 6 hours, and more ice blocks were recorded as they scraped and collided with each other.

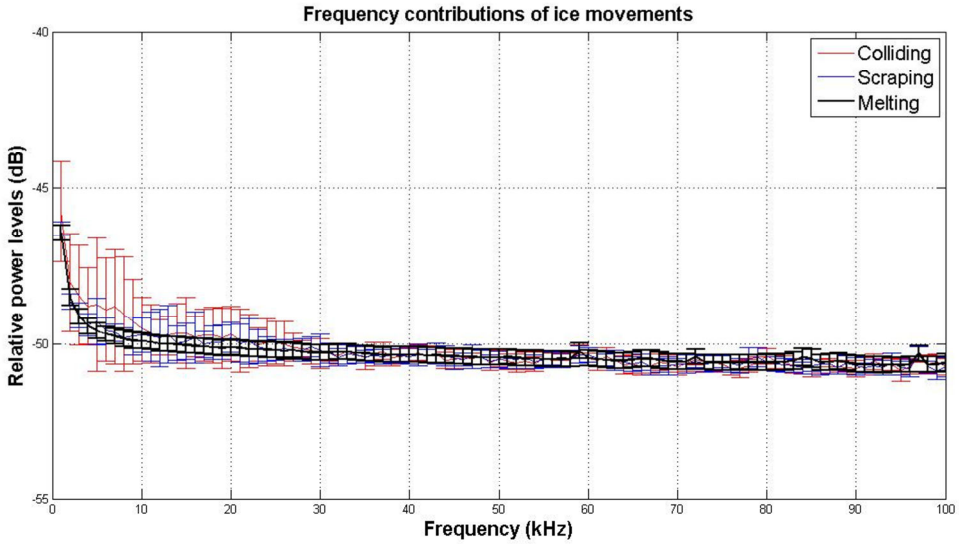

Figure 5.19. Frequency contributions of ice movements, showing peaks below 20 kHz for colliding and scraping ice.

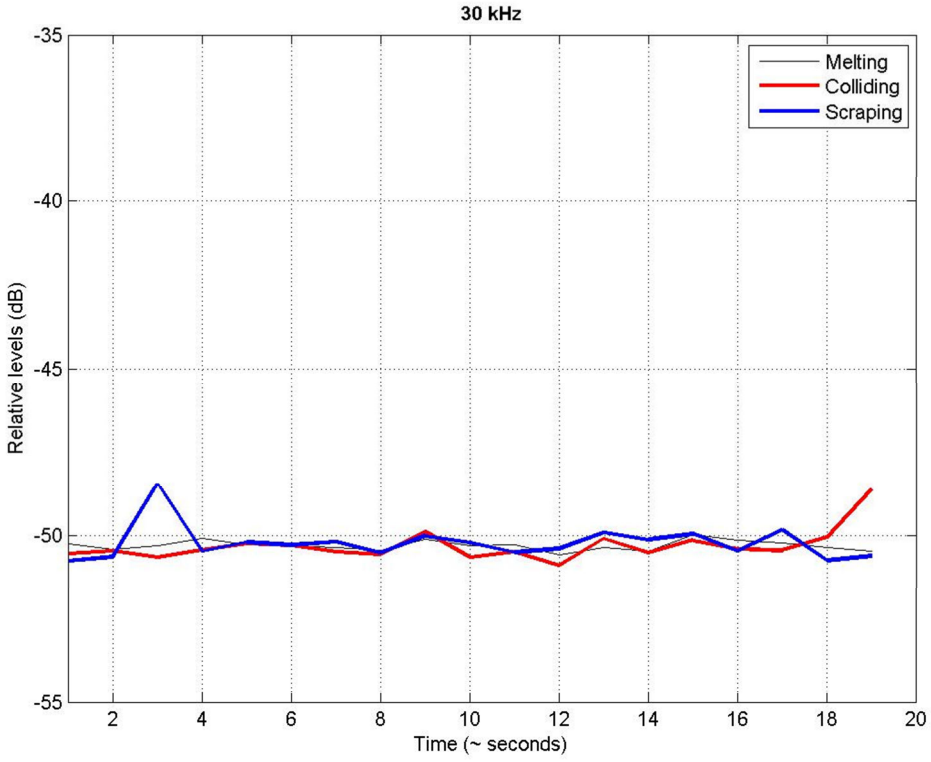

Figure 5.20. Noise levels of colliding, scraping and melting ice at 30 kHz.

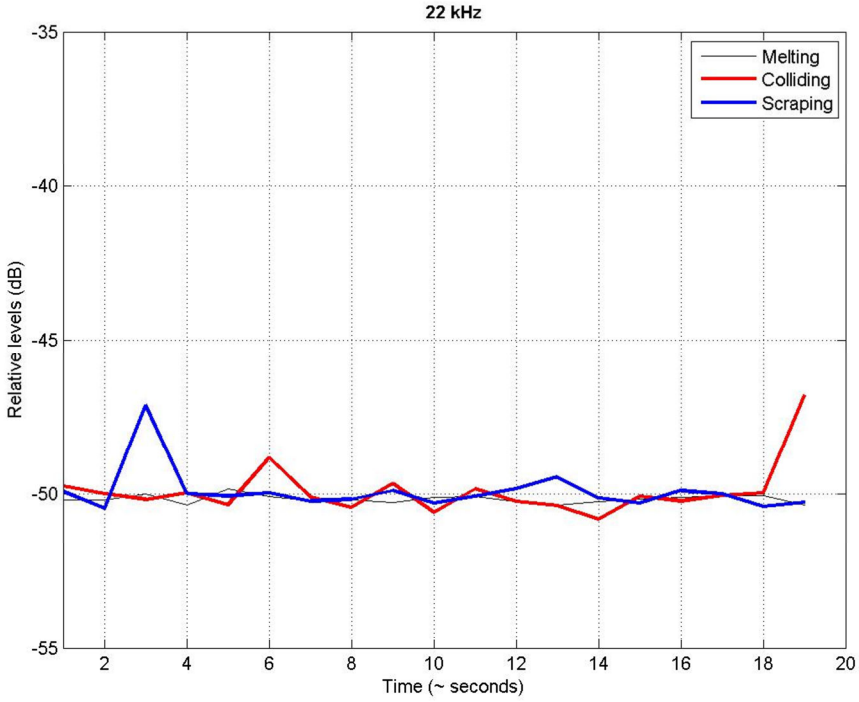

Figure 5.21: Noise levels of colliding, scraping and melting ice at 22 kHz.

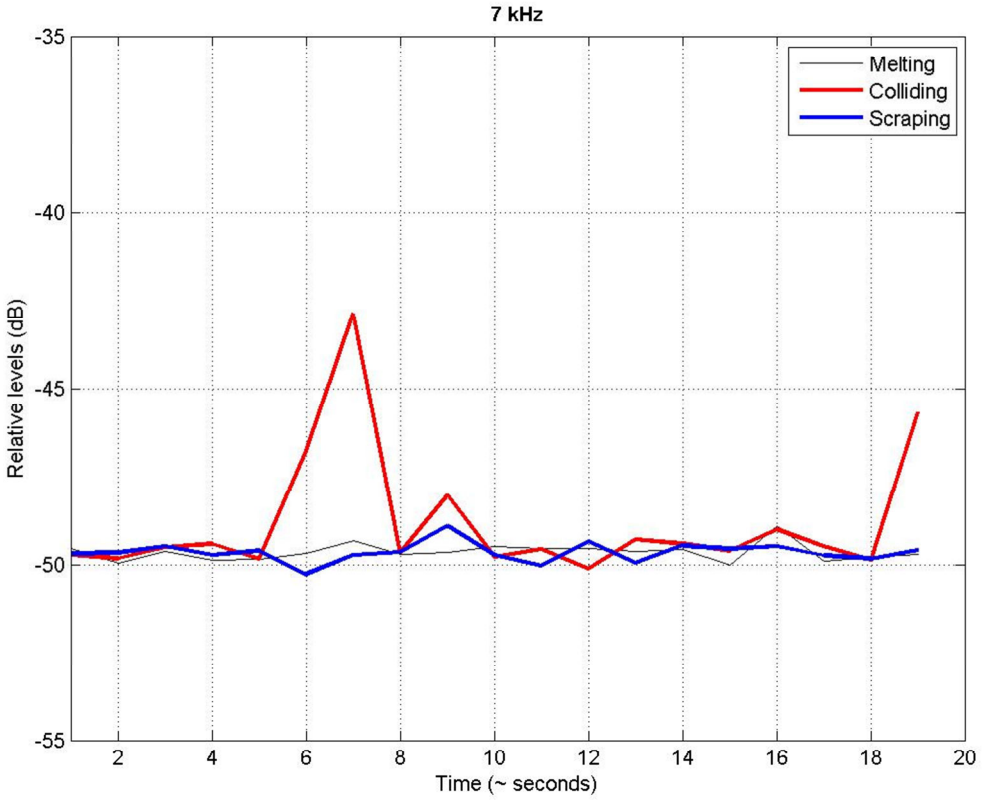

Figure 5.22: Noise levels of melting, colliding and scraping ice at 7 kHz.

At frequencies above 30 kHz the noise levels were generally the same for all three types of ice noise, e.g. 95 kHz:

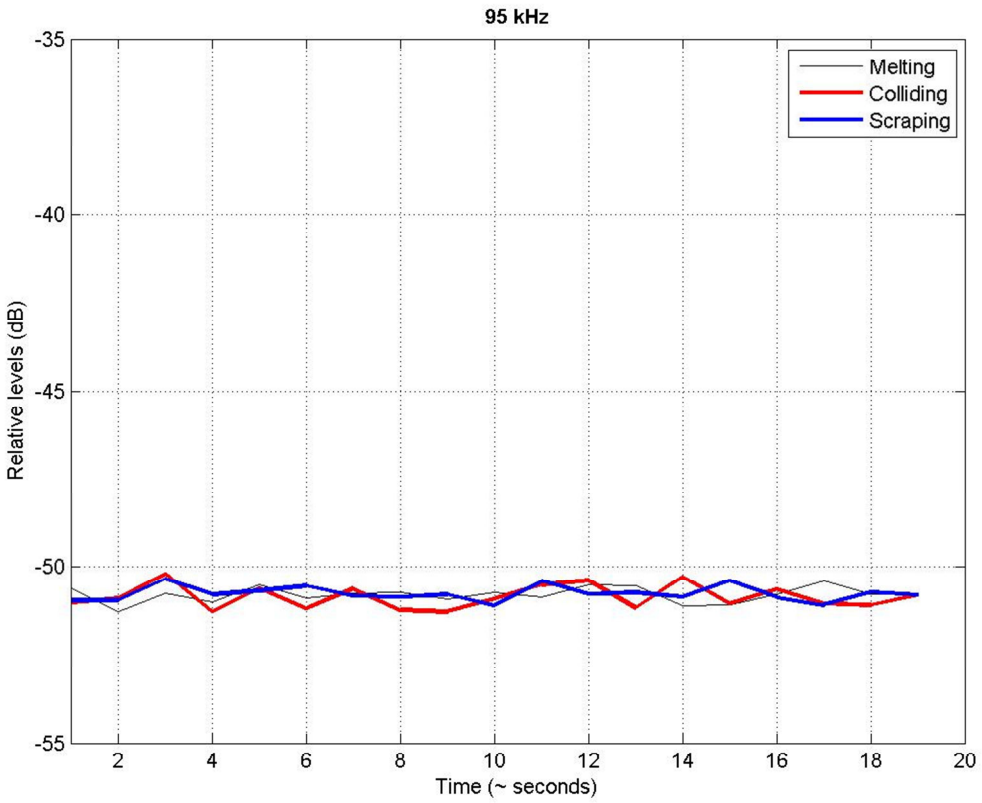

Figure 5.23: Noise levels of melting, colliding and scraping ice at 95 kHz.

Further ice experiments

Up to this point, the results from the larger tank experiments were useful in that they allowed access to the higher frequencies, and that they showed some high-frequency variation in the laboratory simulations of the different sources of noise present in the ARCFAC dataset. However, the experiments in the large tank had not made any clear explanation of the cause of the high-frequency noise observed. The role played by the formation of the ice was of interest; again, some blocks were prepared as per the method of Barker and Timco (2002) but some were simply frozen freshwater blocks. Although both types showed similar acoustic signatures, the ice blocks containing ground-up ice were several dB louder at frequencies below 3 kHz, from 85-88 kHz and above 97 kHz. It was suspected after these preliminary experiments that the difference in noise was due to the presence of air inclusions in the ground

and refrozen ice. Therefore the mode of formation of an iceberg, or the amount of heterogenities present, could influence the noise produced as the iceberg melted. The tank experiments also showed that for frequencies below 1 kHz the acoustic signature of colliding ice blocks was louder by 1-2 dB than that of the melting ice. At all other frequencies, except 8-10 kHz, 73 kHz and 97 kHz the acoustic signatures of melting ice and colliding ice blocks were the same. The acoustic recordings of the ice blocks scraping against each other showed distinct, louder (by 7 dB) events at frequencies below 5 kHz. Between 8 and 35 kHz, there were only a few distinct events in the 3-minute recording period, again up to 7 dB louder. From 89 – 91 kHz, louder (by 2 – 3 dB) events were observed where the noise from scraping ice blocks was different from the noise of melting ice and to some extent colliding ice, as well as all weather-type measurements (rain and wind). Although the ability to access higher frequencies in these experiments enabled the distinction of different types of noise produced by ice, it did not show any significant improvement on the separation of rain and wind.

The differences in the noise levels between frozen freshwater ice and ice blocks which had been ground and re-frozen implied a link between the noise produced by ice melting and the presence of heterogenities such as bubbles trapped in the ice. Furthermore, the principal components analysis had identified three components, two of which correspond to weather types which were present in the Arctic dataset (wind and rain) and a third which was not clearly attributed to wind or rain and therefore could have been related to the noise from ice, whales or shipping. Given that the differences in noise levels were at some frequencies greater than 30 kHz, and that individual events were observed above 30 kHz, further investigations were required as to whether bubbles trapped in ice could generate noise at frequencies this high.

In order to confirm that the noise as the ice melted was caused by bubbles, carbonated water was frozen into a block approximately 8 cm x 8 cm x 15 cm and melted in a small (75 cm x 30 cm x 30 cm deep) tank, and the noise was observed using the B&K-8103 hydrophone. As the ice block melted, the noise produced sounded similar to a carbonated drink fizzing. This noise is known as the ‘Bergy Seltzer Effect’ (Urick 1971). The ice block initially floated at the surface of the water and the experiment was then repeated with the ice block fixed at the bottom of

the tank using rods and nylon wire and the noise observed showed peaks around 7 – 15 kHz, showing higher noise levels than the background noise up to 29 kHz (Figures 5.24 – 5.27).

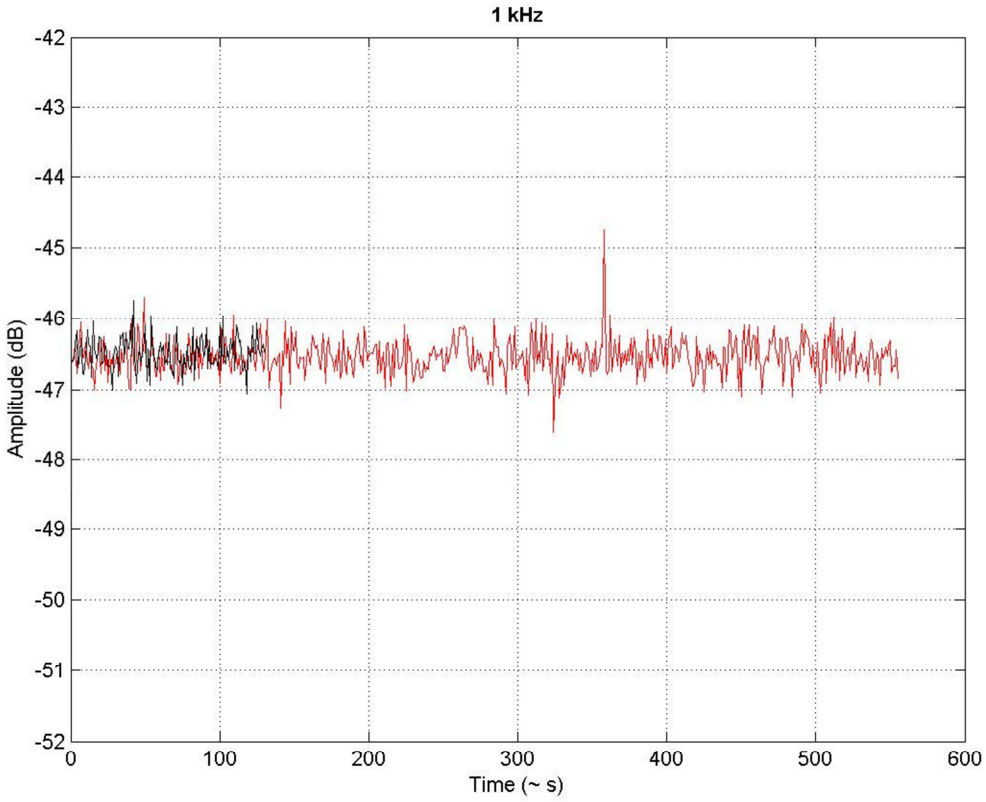

Figure 5.24: Fizzy ice block at the surface (red line), showing few peaks at frequencies below 4 kHz, with the background noise recording shown in black.

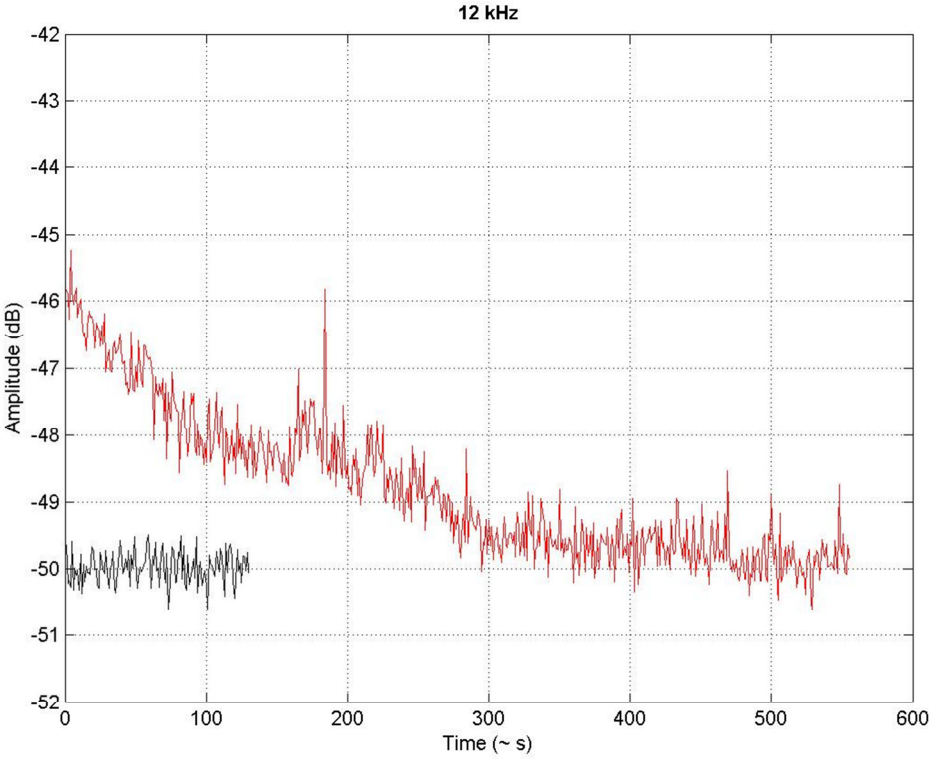

Figure 5.25: Fizzy ice block at the surface, showing peaks in amplitude and differences between ice noise (red line) and background (black line) which are typical of frequencies from 9 kHz – 31 kHz, with the most significant differences at ~11 kHz. After 32 kHz ice noise is not noticeably different from the background noise.

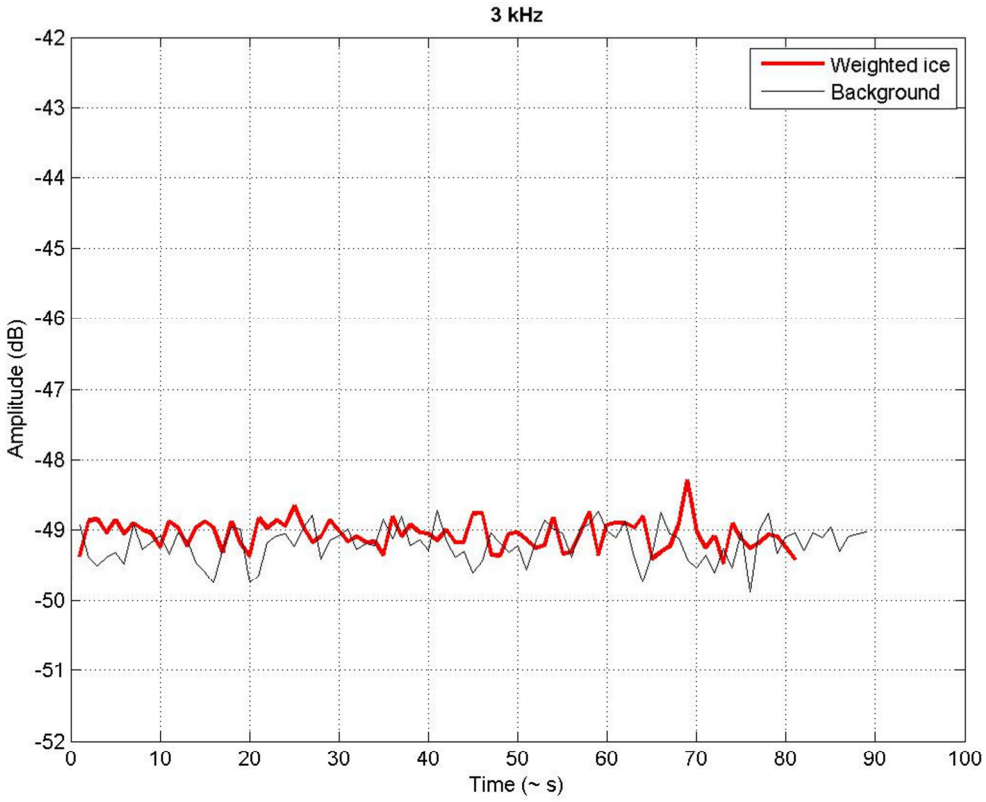

Figure 5.26: Fizzy ice (red line) weighted at the bottom with background noise (black line), showing few peaks in amplitude below 3 kHz.

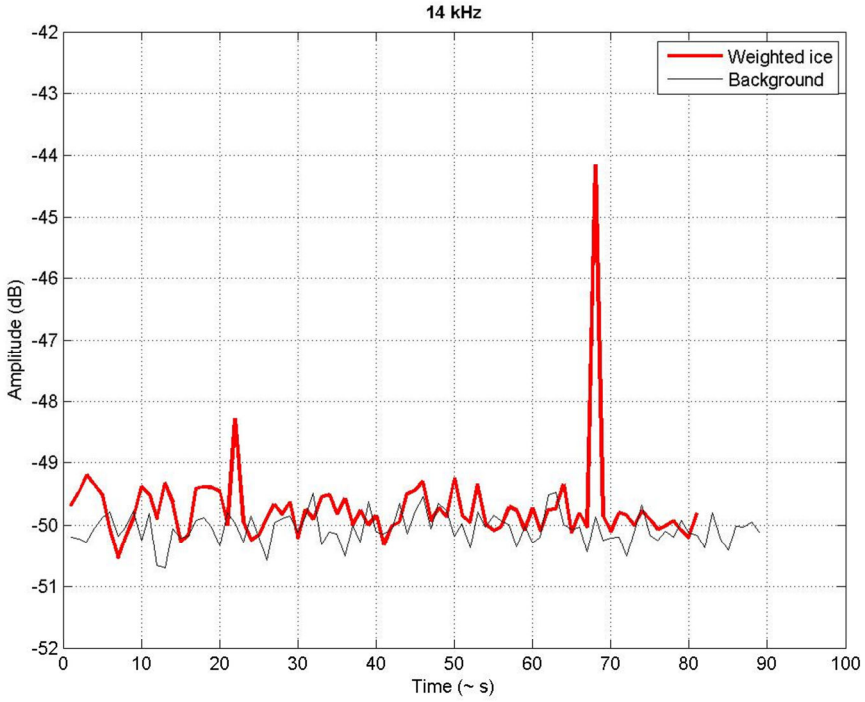

Figure 5.27: Fizzy ice weighted at the bottom (red line) with background noise (black line), where sharp peaks like this one were observed from 12-16 kHz. Nothing significant was observed at frequencies higher than 30 kHz.

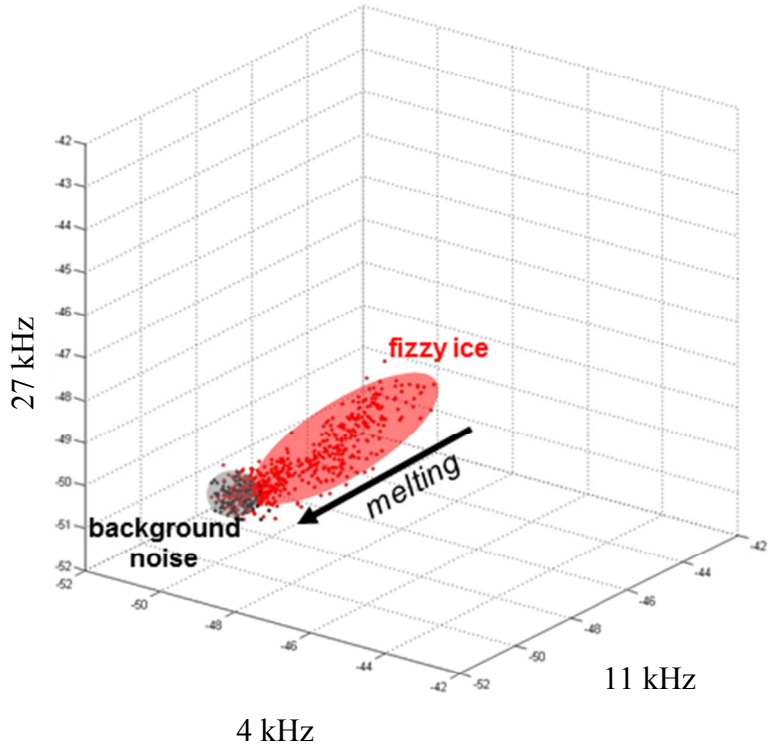

Figure 5.28: 3-component plot for unweighted fizzy ice (red points) and ambient noise (black points) using 4, 11 and 27 kHz. The frequencies were chosen by inspection of the time/amplitude plots at all frequencies.

5.2. PRINCIPAL COMPONENTS ANALYSIS OF TANK EXPERIMENTS

Acoustic measurements of different weather-related processes were taken in the large tank (Section 5.1.2). Principal Components Analyses were performed on this dataset, to assess the effectiveness of the method in a laboratory setting. The dataset included recordings of ice scraping and colliding, as well as rain of three different intensities, wind and 'background' noise, which included transient sources of noise from outside the tank, present intermittently throughout all the recordings. The principal components identified are shown in Figure 5.29.

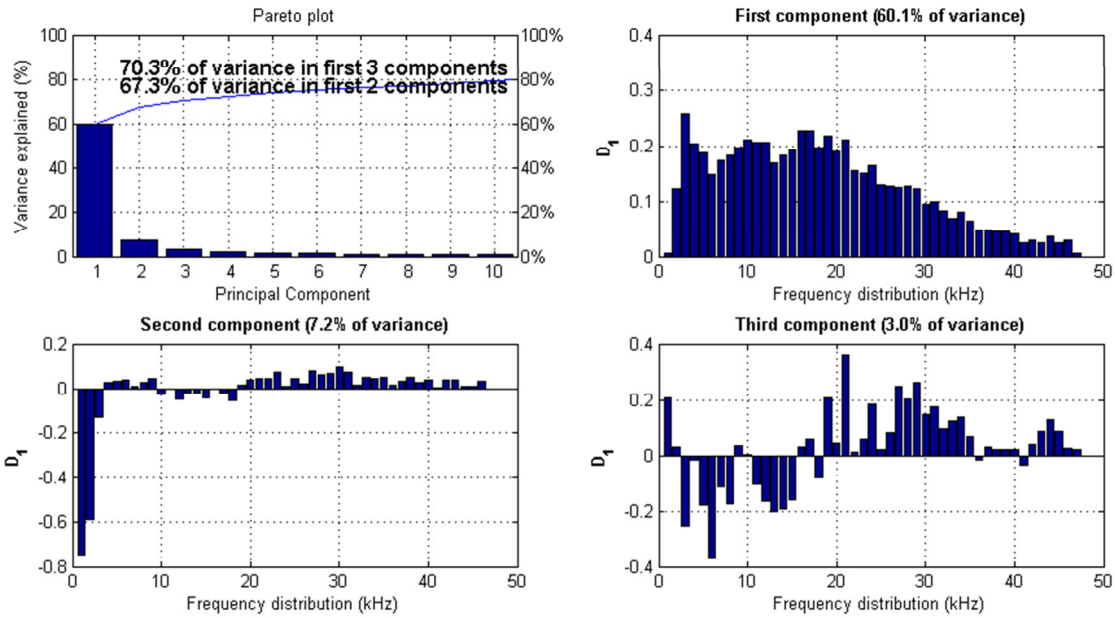

Figure 5.29: Principal Components Analysis output for laboratory data. The first three components account for 70.3% of the variance.

The first 3 components account for 70.3% of the overall variance. This is generally considered as enough of the variance for the components to represent the dataset as a whole (e.g. Lillesand and Kiefer, 2004). This value is however much less than for the Arctic dataset (91.6%).

The first component accounted for the largest part - 60.1%, with the second and third components accounting for 7.2% and 3.0%, respectively. The first (and most significant) component showed contributions from a broad distribution of frequencies up to the limit of 48 kHz. Although the peaks are less pronounced than for the first component in the Arctic dataset (Figure 4.7), there is a slight peak around 3 kHz, and the contributions become less significant beyond 20 kHz.

The second component shows a peak at frequencies below 4 kHz, and the third component shows peaks around 5, 15, 21 and 27-30 kHz, as well as a small peak around 45 kHz. These three frequency distributions were used to plot the tank dataset, as with the Arctic dataset, and the results are shown in Figure 5.30.

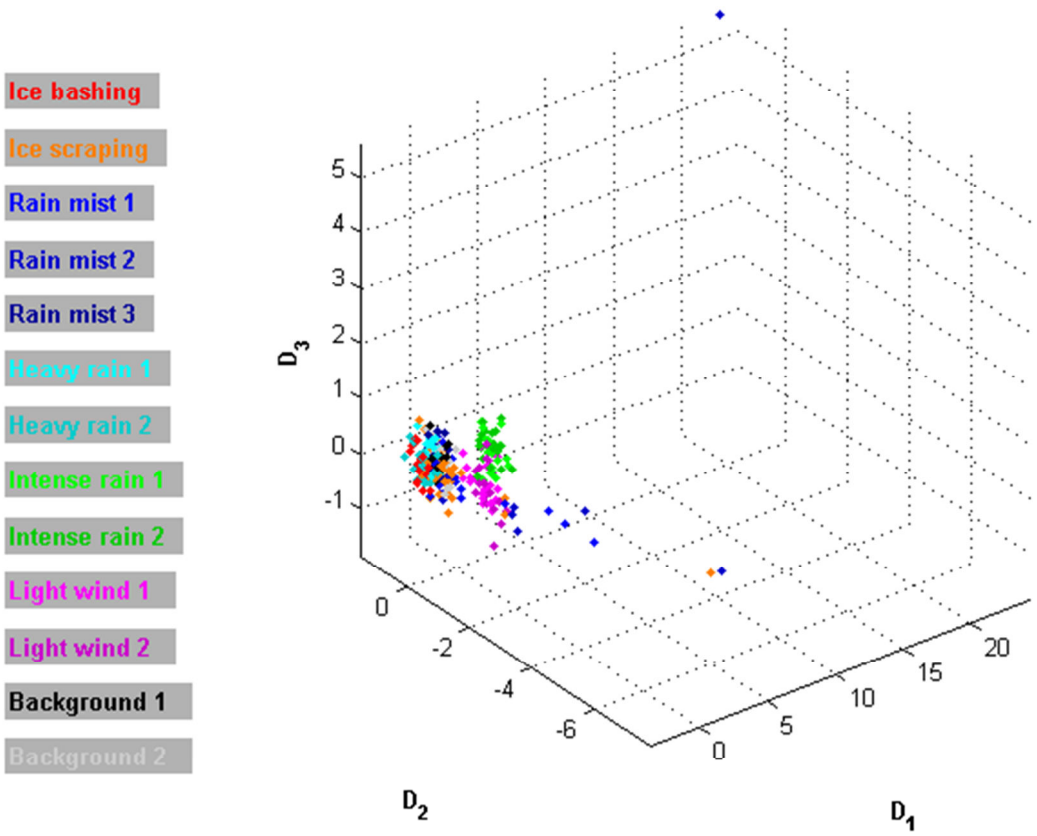

Figure 5.30: Tank experiment data plotted at the 3 frequency contributions identified using Principal Components Analysis, showing separation of heavy rain noise from other noise sources.

The separation of noise sources was not as clear with the tank data with the Arctic data. The first component (D_1) can separate the intense rain from the other types of rain. The heaviest types of rain are indeed known to 'flatten' the spectrum of drizzle noise, by leading to increased intensity levels at all frequencies (Leighton 1994), meaning that the 15-kHz "drizzle" peak becomes less pronounced. This frequency spectrum would look similar to the broad frequency contributions shown by D_1 in Figure 5.29 and this component might be considered as a 'loudness' component. The second component (D_2) shows some separation of noise from wind, scraping ice and 'mist-like' rain from other noise sources. This component's main peak was at very low frequencies, which correlates to theoretical frequency peaks for noise from wind (e.g. (Wenz 1962)) and some types of ice noise (e.g. (Macpherson 1962)). The noise from the mist-like rain varies in D_2, D_1 and D_3 (but only for a single measurement). If this rain produced bubbles. like drizzle, then the expected frequency peak would be around 15 kHz. D_3 shows a small peak around this frequency but D_1 and D_2 do not. It is possible that this type of rain did not entrain small bubbles at all and caused noise only through the impact of the droplets.

To further test the variations of PCA with the variance in the original daset, another analysis was performed by adding a recording of an ice block melting over several hours. The resulting PCA components are shown in Figure 5.31.

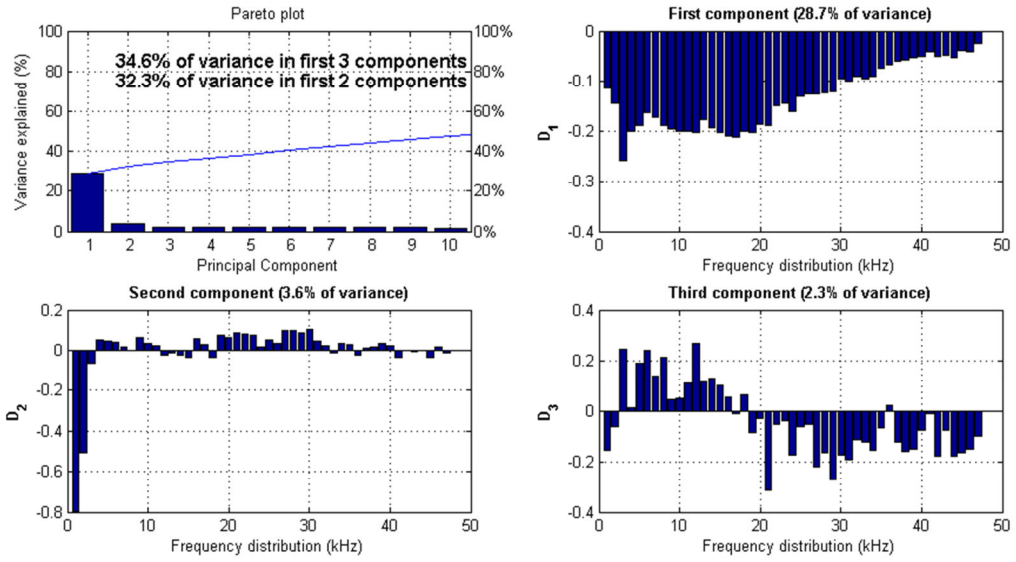

Figure 5.31: Principal Components Analysis output for a laboratory dataset, including noise from a long recording of ice melting. The first three components account for 34.6% of the variance.

The frequency contributions of each component show similarities to those of Figure 5.29. This would be expected, since the two analyses were performed on nearly identical datasets, with the addition of a long recording of ice melting here. However, the length of the ice recording (several hours) means that a significant number of data points will be acoustically similar, leading to a more homogeneous dataset. This explains why the latter Principal Components Analysis explains considerably less of the variance in the first three components (34.6% as opposed to 70.3% for the dataset without ice noise, and 91.6% for the Arctic dataset). The frequency contributions of the first and third components (D_1 and D_3) are similar in magnitude and variation to those of Figure 5.29. The second component (D_2) in Figure 5.31 is very similar to that of Figure 5.29, in terms of frequency contributions and their respective amplitudes.

As previously and as with the Arctic dataset, the amplitudes of the different noise sources were plotted for the different PCA components (Figure 5.32).

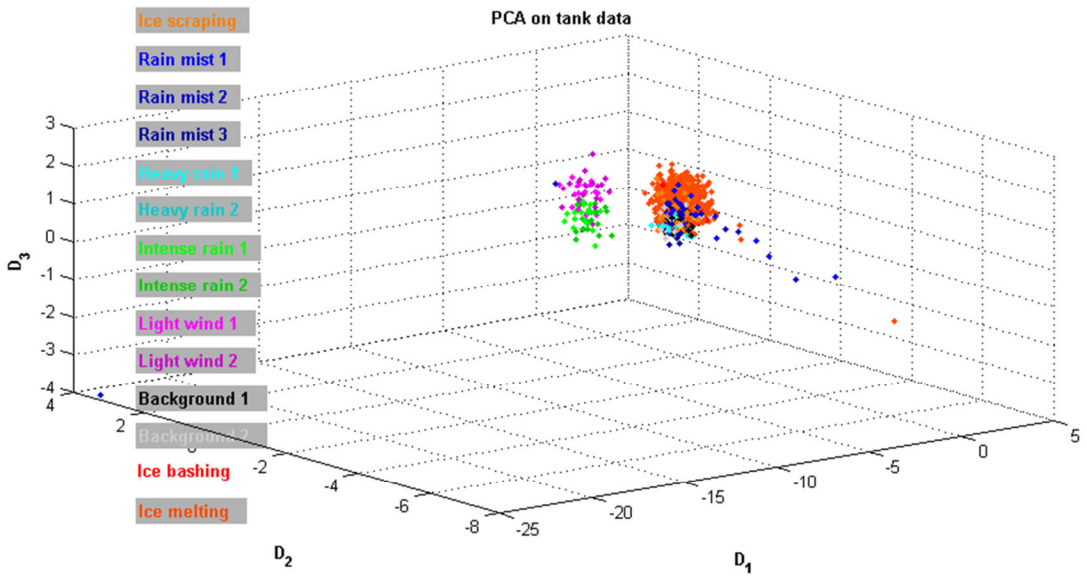

Figure 5.32: Tank experiment data (including ice melting noise) plotted at three frequency contributions identified using Principal Components Analysis, showing separation of heavy rain and wind noise from other noise sources.

As previously (Figure 5.30), plotting according to the principal components leads to some separation of the different noise sources, particularly wind and intense rain noise. This separation is mainly shown by variations in D_1, which corresponded to a broad frequency spectrum (Figure 5.31). This component could still be considered to represent 'loudness', with the possible addition now of the lower frequencies usually associated with wind noise. Drizzle and melting ice measurements show increased amplitudes at the frequencies represented by D_2. This component shows a peak at frequencies below 5 kHz, as well as smaller peaks from 20 – 30 kHz. Figure 5.32 shows that the inclusion of a large amount of background noise in a dataset does not prevent Principal Components Analysis from separating different sources visually. However, Figure 5.31 also shows that the reduction of variability, by adding a large number of similar measurements (hours of melting ice) impairs the effectiveness of Principal Components Analysis in separating sources.

To further investigate the effects of low variability on PCA results, this analysis was repeated for a dataset only made of the 'wind' noise included in the previous two analyses. The components identified are shown in Figure 5.33.

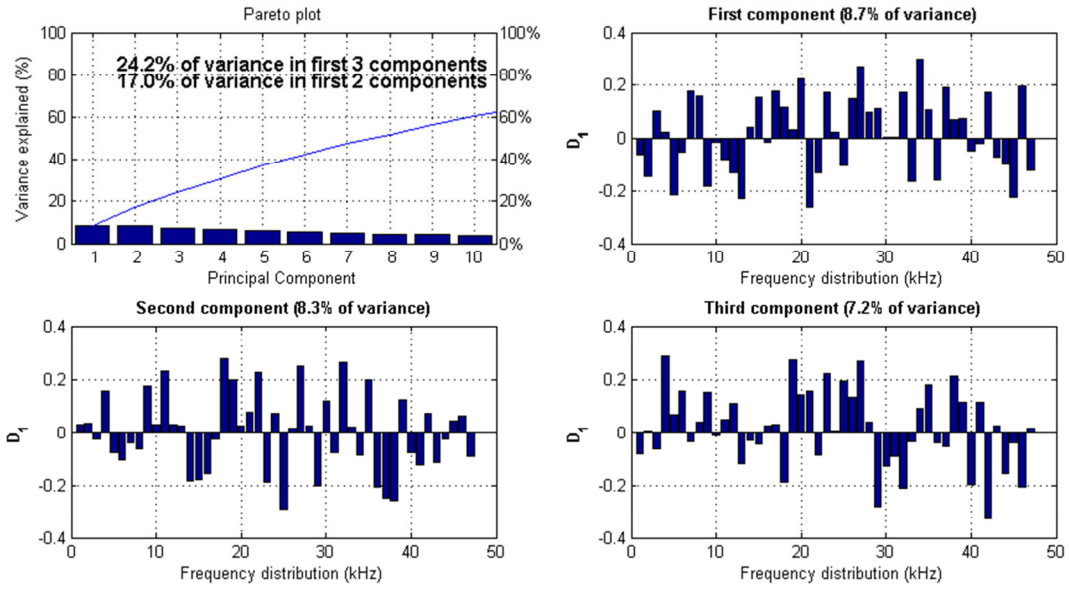

Figure 5.33: Principal Components Analysis output for a laboratory dataset of wind noise only. The first three components account for 24.2% of the variance.

Principal Components Analysis on a dataset with so little variability identifies components which explain far less of the variance – each of the first three only accounts for around 8% of the variance, so that the first three components account for only 24.2% of the overall variance (compared to 70.3% for the tank experiments and 91.6% for the field measurements). Furthermore, the frequency distributions within these components do not show a clear partitioning in specific frequency bands. Wind-related noise is generally attributed to frequencies around 5 kHz ((Lemon et al. 1984; Leighton 1994)). PCA does not identify related components because it attempts to maximise the variance explained by the dataset. Made of measurements of the same process, this dataset will have little variance, which explains the failure of PCA in identifying specific frequency contributions. As with previous analyses, measurements were plotted for the 3 components identified by PCA (Figure 5.34). This plot does not show any cluster of points, contrary to Figures 5.30 and 5.32. This is consistent with the reduction of the variability explained and totally expected.

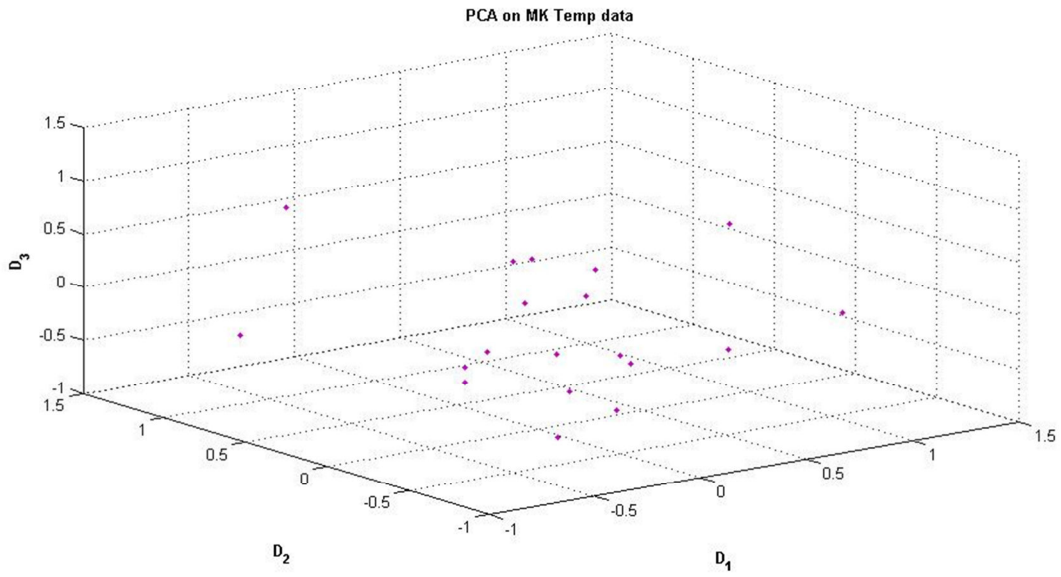

Figure 5.34: Tank experiment data of only wind noise plotted at three frequency contributions identified using Principal Components Analysis. There is no clear separation or grouping of points.

CHAPTER 6 – DISCUSSION

6.1. ANALYSIS PARAMETERS

When first analysing the data from the ARCFAC-2007 experiments, the frequency spectra for the different recordings were considered. The way in which they were calculated was considered before the processing was carried out and the parameter which were used were chosen after investigating the effects of varying their values. For example, when choosing the bandwidth over which to average the frequencies, approximately 1-kHz was initially considered an appropriate size. Decreasing this bandwidth, or analysing third or twelfth octave bands, could have given more information about the dataset, due to the increased resolution of the frequency spectra. Therefore, 0.5-kHz averages were calculated as well as 1-kHz averages and it was found that both bandwidths gave the same values. Therefore, bandwidths smaller still than 0.5 kHz would have given similar values and the same overall representation of the dataset, so would not justify the increase in computation time. Usually the work of other authors in this field used kHz bands instead of third or twelfth octave bands, a further motivation for the choice of the bandwidth, along with the current debate on the use of sub-octave centre frequencies (Blondel, pers, comm,, 2011). Therefore 1 kHz was selected as the bandwidth over which to average. The time interval over which the frequency bands were to be calculated was also investigated, by considering the sources of noise present. Segment lengths of 1 s, 100 ms and 10 ms were calculated with 1-kHz band averaged levels for each recording. On comparison, it was found that the three segment lengths showed variations of 5 dB between each successively greater segment length. Other files from different sources were also evaluated to better understand the cause of these variations, and a segment length of approximately 100 ms looked the most suitable. Finally, this segment length needed to relate to a number of data points which was a power of 2, and 8,192 points were chosen for the segment length as they

corresponded to a time of 85.33 ms. In order to ensure that events were not missed or partially excluded if they occurred at the beginning or end of an 85.33 ms segment, it was necessary to use an overlap, so a 50% overlap was compared to 10%, which showed a difference in amplitude at the different frequency bands of less than 0.001 dB, so 10% was considered long enough to include transient events at the ends of recordings, whilst minimising processing time and not losing too much information.

In other experiments for similar conditions, when these parameters were mentioned they covered a variety of values. The segment size ranged from 40.96 ms (Nystuen 2001) to 1.5 minutes (Quartly 2001). The frequency band over which to average ranged from 1 Hz (Wenz 1962) to 1 kHz (Oguz and Prosperetti 1991). Very few articles gave details of an overlap used which suggests that when data had been split into segments before analysis, overlaps to cover specific transient events had been used rarely.

If the bandwidth, segment length or overlap had been larger, it would have taken longer to process the dataset. If they had been smaller, important information could have been neglected. Therefore the values selected gave the most accurate representation of the dataset achievable for a realistic amount of computational power.

6.2. PRINCIPAL COMPONENTS ANALYSIS

Other datasets of noise from weather events had been analysed using pairs of frequencies, or frequency bands. When the band-averaged amplitudes at one frequency were plotted against those at another frequency as a scatter plot for a dataset including a variety of weather types, it was possible to see separation of the different weather types. Some of the frequency combinations used were 5 vs. 25 kHz (Nystuen and Selsor 1997; Quartly 2001) and 4-10 kHz vs. 10-30 kHz (Nystuen 2001) which separated ships, high seas, drizzle, rain and wind (Nystuen and Selsor 1997; Quartly 2001) and two events of stratiform rain from extreme rainfall (Nystuen 2001). The disagreement between authors about the most appropriate pairings as well as a lack of explanation of the method of selection of the frequencies implied a need for a more rigorous approach to choosing which frequencies best

characterised a dataset and the different weather events within it. Due to its ability to select a small number of components which represent a large dataset, a Principal Components Analysis was performed on the ARCFAC-2007 dataset. The 48 components (1-kHz bands from 1-48 kHz) were reduced to three, which explained 91.6% of the variance in the whole dataset. The three components (X_1, X_2 and X_3) consisted of varying amounts of each of the 48 1-kHz bands. X_1 mostly contained frequencies around 5 kHz, X_2 showed a peak at approximately 15 kHz but the contribution of the frequencies in X_3 was more widely distributed, exhibiting a peak between 40 and 50 kHz.

Field and tank experiments had found that typically wind creates noise underwater around 5 kHz, while rain is associated with noise around 15 kHz. Therefore it seemed that the first two components were related to noise from wind and rain, which were known to be present in some of the ARCFAC-2007 recordings. However, weather-related noise above 40 kHz was not documented and so the third component, X_3, was investigated more closely, in order to try to determine its physical cause. Similarly to the plots in the literature, the three principal components were used in their entirety (not just the peak values) to produce a three-dimensional plot of the ARCFAC-2007 dataset. This plot showed that the variations in X_3 were present in recordings from sites A, E and F, which had experienced light/very light rain and small/very small waves (sites A and E) as well as a whale less than 50 m away (site A) and a ship approximately 5 km away (site A), small icebergs approximately 20 m away (site E) and a cruise ship nearby (site F). Also, inspecting the variations in X_1 and X_2 for all of the sites further implied a link between X_1 and wind and X_2 and rain, since the sites where it was raining (A ,B, C and E) showed lower values of X_1 and the sites with wind (A, B and E) showed lower values of X_2. The variations in X_3 were inspected at sites A, E and F, and they increased and decreased regularly and linearly with time at location A. The regularity of the variations implied that they were caused by a passing ship or a vocalising marine mammal. These transients showed frequency peaks above 40 kHz, with variations in amplitude. These amplitude variations along with some small supplementary experiments proved that the noise at high frequency was not caused by the boat trying to align itself. Observations of the nearby whale proved that the transients were not consistent with clicks from it. Therefore the variations in X_3 at site A were

tentatively attributed to a distant ship's echosounder. However, the type of ship present mostly emits noise below 1 kHz, which would have been filtered out during processing.

Pulse trains in the recording at site A correspond to observations of minke whales. At location E, extra measurements a few metres from the observed growlers and bergy bits were 'clinky' sounding, which is typical of an environment containing blocks of ice. The X_3 subclouds at this point could have been related to the ice itself or to the increased biological activity associated with icebergs. The recordings from site F did not show any visible patterns in the variations in X_3.

Principal Components Analysis maximises variance when reducing a multi-variable dataset to the most characteristic components, so it will be most successful when measurements show large amounts of variance explained. This was demonstrated by its ability to separate different noise sources from within the ARCFAC 2007 dataset (Figure 4.17).

Calibrated measurements can be used to identify acoustic sources, as the absolute sound pressure levels in specific frequency bands can be compared to similar measurements elsewhere (e.g. (Nystuen and Selsor 1997; Nystuen 2001; Quartly 2001)). Uncalibrated measurements can benefit from PCA to identify weather-related acoustic sources at sea, provided the dataset over which PCA is performed exhibits enough variability. A processing algorithm to be used operationally could use a combination of these two processes, with PCA determining whether there was more than one type of weather present (e.g. wind and rain) and then deciding which would be the most appropriate algorithm to determine the wind speed or rainfall rate from their respective frequency contributions (and their respective magnitudes). This would be particularly useful in certain situations where the presence of one type of weather will change the acoustic signature of another, such as wind with rain (Ma and Nystuen 2005).

Principal-Component Analyses perform well in datasets with high variability, like the Arctic measurements (explaining 91.6% of the variance and explaining all acoustic sources, cf. Figure 4.17) and tank experiments inspired by the different processes experienced there (explaining 70.3% of the variance and identifying most

acoustic sources, cf. Figure 5.29). Further analyses with other datasets (Figures 5.31 to 5.34) showed its utility decreased with the overall variance. For example, hydrophone measurements in a lake with rainfall of constant intensity present would show poor overall variability unless other types of weather, or other acoustic sources, were present for a relatively significant amount of time. The length of time over which the data is collected, before PCA is performed, should be selected to ensure adequate variability. In the case of the Arctic measurements, overall acoustic variability was ensured by the rapidly changing weather in polar regions, and particularly Kongsfjord. Over the course of an entire day, different types of rain and different wind speeds could be experienced, sometimes in combination. The different measurement locations, from near the mouth of the fjord (closer to potential shipping) to glaciers (closer to melting and moving ice blocks) also added to the acoustic variability.

These analyses show that, although PCA worked well for the Arctic measurements and specific tank experiments, it is NOT a single and complete method for identifying weather-related acoustic sources underwater. PCA cannot separate sources in a dataset with low overall variability, for example if the weather has changed little over the recording duration. However, for datasets with more variety and with similar length recordings, PCA can be used successfully to separate and identify the different weather-related acoustic sources present.

6.3. SMALL TANK EXPERIMENTS

Once Principal Components Analysis had been used to separate the different events present in the ARCFAC-2007 dataset, further experiments were carried out in tanks at the University of Bath in order to obtain extra datasets for investigating the roles of the three components.

In the smaller of the two tanks, wind, fine mist, rain of larger droplet size and a melting iceberg were replicated and their noise was recorded. The amplitude of the noise from these events was plotted at 5 kHz against that at 15 kHz which enabled separation of the different sources. The smaller tank at the University of Bath is not sunk into the ground. This means that it was not possible to stand high enough above

it to ensure that all of the drops were falling at terminal velocity. However, this is not the only defining parameter to make the droplets realistically represent rain (Montero Martínez et al. 2009). A more significant issue with the method of replicating wind and rain is that the desktop fan used to replicate wind could have been causing the whole tank to vibrate and it could have been these vibrations which were detected by the hydrophone and not noise from the surface.

As with the ARCFAC-2007 data, the band-averaged noise levels were plotted as a scatter graph at 5 and 15 kHz, which separated wind from rain and ice. The wind noise had the smallest amplitude at both frequencies, while the noise from the rain was higher than the background noise at both frequencies. The noise from the ice block was lower than the background noise at 5 and 15 kHz but as it melted, the amplitudes at (particularly) 5 kHz and 15 kHz increased to merge with the background noise. Changes in the droplet size from smaller ('cloud') to larger ('spray') showed an increase in the noise at 5 kHz and a slight decrease at 15 kHz. This agrees with the findings of Ma and Nystuen (2005) for rain heavier than 'drizzle'.

It is important to note that, although the noise from, for example, the wind, was lower in amplitude at both 5 and 15 kHz, it was not necessarily 'quieter' than the background noise, only at those two specific frequencies. Although the first two frequency peaks identified using Principal Components Analysis had been used to separate noise sources replicating the weather events observed in the Arctic, the small tank experiments could be improved significantly. The tank's size did not eliminate wall echoes and the laboratory had high levels of background noise, the frequencies available were limited to 22 kHz and the hydrophones' sensitivity was not as high as it might have been. In order to address these issues, a larger tank was used (to reduce wall echoes) with less background noise, along with a more reliable hydrophone and the means to access frequencies up to 100 kHz, to fully investigate all three of the principal components identified.

6.4. LARGE TANK EXPERIMENTS

Since the smaller tank could have suffered from wall echoes, experiments were carried out on all subsequent tanks used to check that wall echoes were not causing false signals to be picked up, or for peaks at certain frequencies to occur. Experiments with single drops showed that the frequency spectra had very similar shapes, with the only peak at 100 kHz from the limit of the hydrophone. Echoes were also not discernible visually on the time-domain plots of the single drop. When white noise was recorded at various positions, the frequency spectra for all three positions were very similar, showing that varying the position of the hydrophone did not lead to variations in the sound received.

Next four types of rain were simulated, as in the smaller tank, and using 5, 15 and 45 kHz the different types of rain were separated from each other and from the background noise graphically. Due to the fact that the larger tank is set into the ground it was possible to achieve enough height above the water surface that all of the droplets created by the hose would fall at terminal velocity. The 'cloud' setting produced very fine droplets and the noise levels from this type of rain were similar to the background noise at 5 and 15 kHz. The noise levels were higher at 5 and 15 kHz for the different types of rain, which all produced larger droplets. The addition of the amplitudes at 45 kHz did not show much variation between the different rain types, which corresponds with the findings of other authors, who document rain noise as usually being below 25 kHz. It was interesting to discover that, as with the small tank experiments, the rain noise differed from the background noise at 5 kHz as well as at 15 kHz, which is usually the frequency attributed to rain noise. This implies that not only were some of the droplet sizes created similar to drizzle and therefore able to entrain bubbles, but also that some were larger in size, which according to Ma and Nystuen (2005) would cause noise at frequencies ranging from 1 – 30 kHz due to the impact of the droplets.

An ice block was created using large blocks of ice refrozen with icy water, and the noise was recorded as it melted and compared to the background noise. This experiment was then repeated using a solid ice block and one with smaller fragments of ice. The noise from the latter two types of ice was compared and it was found that the noise from the small-ground ice different from the solid block's noise at certain

frequencies, namely 89 kHz, 17 kHz and 1-5 kHz. Not only did this verify that it was necessary to pay attention to the method of formation of ice blocks in experiments, but it implied that noise at 89, 17 and 1-5 kHz could be related to something which was present in one type of ice and not the other. In grinding the ice into smaller blocks and re-freezing, small inclusions may have been introduced, and this was considered as a possible cause of the noise. Another possible cause of the higher-frequency component identified in the ARCFAC-2007 dataset could have been noise from icebergs either scraping against or colliding into each other. Therefore two icebergs were created (using ground and refrozen ice) and were scraped against and collided into each other. On the whole, the noise from the colliding blocks showed increased amplitudes from 0-25 kHz, particularly below 10 kHz. The noise from the scraping blocks only differed from the noise of the melting ice by approximately 1 dB around 10-20 kHz. Furthermore, individual 'spikes' in amplitude were observed at 3 kHz for scraping ice and at 19 and 7 kHz for colliding ice. The melting ice did not show any such significant spikes in amplitude. These values do not agree with the literature, where reports rarely consider ice-related noise at frequencies above 1 kHz. The noise of ice melting was previously considered by Urick (1971) up to 10 kHz but none of the ice melting recordings at the University of Bath had showed significantly increased noise levels from melting ice at 1-10 kHz. In the work extending the listening range for melting ice to 10 kHz (Urick 1971) the inclusion of air bubbles trapped in the ice was cited as a possible cause of ice-related noise. Therefore, to recreate these bubbles in glacial ice, a bottle of carbonated water was frozen and the noise it created as it melted was recorded. The noise caused by this ice block showed amplitude peaks from 7-15 kHz, but was louder than the background noise at frequencies up to 29 kHz.

Icebergs can be formed from layers of compressed snow, with density increasing with depth. Close to the top, where the density is lower, air and water can pass between crystal grains. As the density increases the channels through which air could pass become closed off and form isolated bubbles. This depth is approximately at the same level as the waterline (Wadhams 2000). Deeper than this the bubbles are compressed, and in Greenland icebergs the bubbles are typically elongated with lengths of up to 4 mm and diameters between 0.02 and 0.18 mm (Scholander and Nutt 1960) while Antarctic glaciers and icebergs feature bubbles which are spherical

or ellipsoidal and have diameters of 0.33-0.49 mm (Gow 1968; Gammon 1983). However, bubbles in growlers freshly calved from a large glacier were observed visually to have diameters of approximately 0.3 – 1 mm (Tegowski, pers. comm., 2011). As ice melts, the edge of the ice block will move closer to the trapped bubbles and they will escape (Figure 6.1) (Urick 1971)

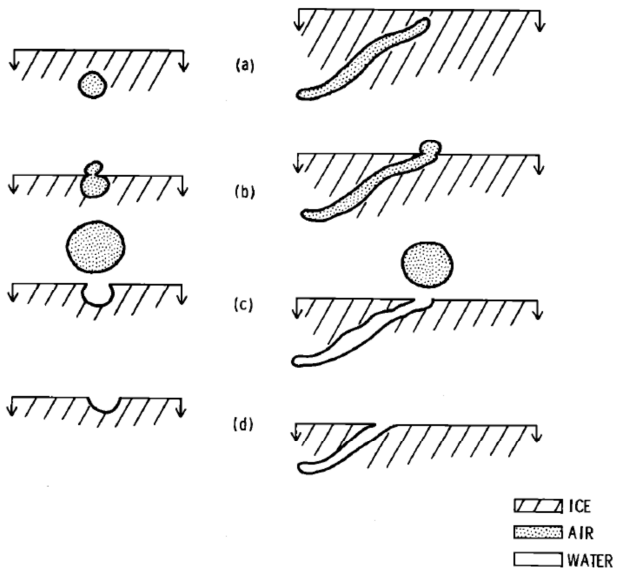

Figure 6.1 (from (Urick 1971)). An illustration of air escaping an ice cavity as the ice wall position varies. A spherical cavity is shown on the left and a tubular cavity on the right. It was suspected that a burst of noise would occur between diagrams (b) and (c), when the air bubble escaped.

Recalling the Minnaert equation, which relates the frequency at which a bubble resonates to its radius, it was possible to calculate the theoretical resonance frequency of them after they have escaped from the ice made from the carbonated water, as well as the theoretical resonance frequency of bubbles which have escaped from Arctic ice:

$$f_M = \frac{1}{2\pi R_0}\sqrt{\frac{3\,\gamma\,p_0}{\rho}} \tag{6.1}$$

Where f_m is the Minnaert frequency, R_0 is the radius of the bubble, γ is the ratio of heat capacity of the gas inside the bubble at constant pressure to that at constant volume, p_0 is the hydrostatic pressure and ρ is the density of water.

Using the values p_0 = 101.325 x 10^3 Pa, γ = 1.403, ρ = 1000 kg/m^3 and R_0 = 0.01 – 0.09 mm (Scholander and Nutt 1960) gives values of f_m between 36 and 330 kHz. Recalling the third principal component this range includes the position of the peaks observed, but is so broad (due to the large variation in theoretical bubble sizes) that it is difficult to draw any firm conclusions. This implies a need for further investigation of the range of bubble sizes in ice to see if the distribution really is that broad. The derived range of frequencies does not correspond to any of the observed peaks in frequency for the ice blocks created in the laboratory and melted in the tanks. This could be due to the impurities present in the ice blocks created in the laboratory – they could have been of different sizes to those in real Arctic ice, or the ice blocks could have not contained full bubbles and the noise produced as they melted could have been from cracks forming under stress or water lapping against the edge of the block instead of bubbles escaping. If the noise was not caused by bubbles then the peaks in frequency would not be determined by the Minnaert equation.

Keeping in mind that the gas trapped in carbonated water bubbles is different to the gas trapped in ice formed by grinding up and re-freezing tap water, and that the bubbles are of different diameters (0.5 mm (Cleary et al. 2007)), the Minnaert frequency for the frozen carbonated water bubbles is 12 kHz. The peak in frequency observed for this ice type was between 7 and 15 kHz which includes the theoretical resonance frequency of 12 kHz. The agreement between the experimental and observed noise confirmed that the noise created by bubbles escaping as ice melted had a frequency determined by the Minnaert equation.

6.5. EFFECTS OF SALINITY

The measurements in the Arctic were made in cold and salty water (Figure 4.1) whereas the tank experiments were performed in warmer, fresh water. Could it have affected the results, or rather the comparisons of the field and tank measurements?

Experimental constraints justified these choices. In the Arctic, the short time available and the lack of equipment deployable from a small boat prevented direct measurements of salinity and temperature at depth, over the entire fjord. The only published oceanographic

study of Kongsfjord (MacLachlan et al., 2007) presents measurements at a handful of locations along the fjord, done in April and September 2005. Figure 6.2 presents a simple extrapolation from these measurements, with water temperatures between 1.5°C (at the surface) and 2.75°C and salinities varying between 31.5 psu (at the surface) and 34.5 psu (at depth). The conditions in August 2007 were relatively close to those of September 2005, with surface water temperatures measured as close to 2°C, and it can be reasonably expected that, in similar conditions, salinity and temperature were similar overall. The tank experiments, however, had to be conducted in warmer, fresh water. It was not possible to cool down the large (> 5 m^3) volume of water of the tank used to temperatures close to 2°C and maintain its stability well enough. The presence of metal frames at the bottom of the tank also prevented the use of corroding, salty water.

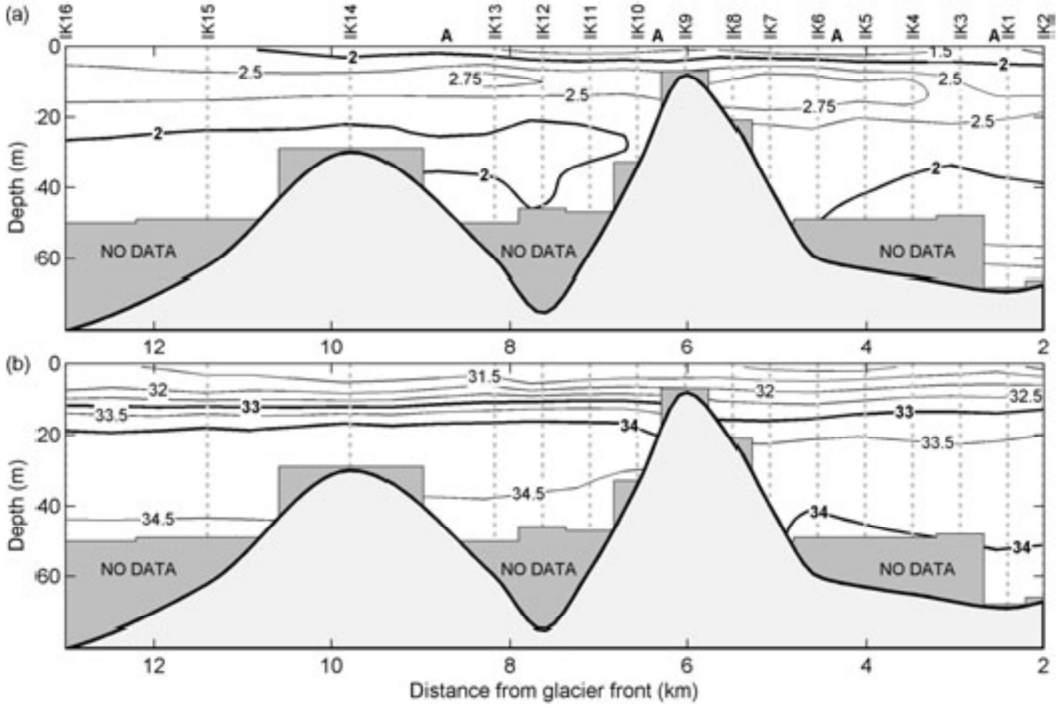

Figure 6.2: Measurements of salinity (a) and temperature (b) in Kongsfjorden in September 2005, by MacLachlan et al. (2007). Bathymetry is estimated from CTD drops and charts. Station locations are indicated by the dashed vertical lines.

The effects of temperature and salinity on sound propagation and absorption are well constrained, benefiting from a series of laboratory and sea experiments as well as theoretical calculations (see Chapter 2 of Lurton, 2010 and references therein).

Absorption in saltwater increases with frequency because of the effects of Magnesium Sulphate and Boric Acid (Figure 6.3). For pure water the relationship is linear. Attenuation values in the tank experiments were derived from the 'pure water' curve in Figure 6.3.

Figure 6.4 shows the variation of attenuation with frequency for salinities of 20, 27, 35 and 42psu, at a temperature of 15°C and a depth of 0 m. The salinity in the Arctic experiments can be inferred as 33 psu from Figure 6.2. Figure 6.4 shows that a variation of 2 p.s.u. will not lead to a large variation in attenuation, therefore the salinity can be approximated to 35 psu.

As ice measurements showed the highest frequencies, they were used to estimate the highest attenuations expected in each case. Using the hydrophone depths of 10 m in the field experiments and 1 m in the tank experiments, and approximate distances from the ice of 20 m in the field and 1 m in the tank leads to attenuations of 0.34 dB for the field experiments and 0.001 dB for the tank experiments, at 50 kHz. Although these values differ by several orders of magnitude, these differences in attenuation are still small enough that they cannot affect the comparison of the Arctic measurements with the field experiments.

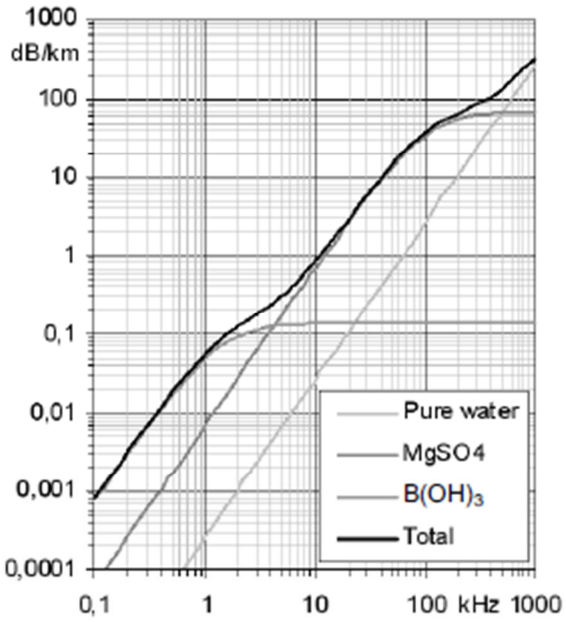

Figure 6.3 (Repeated from Figure 2.9): Sound absorption in sea water and pure water, showing the effects on attenuation of Magnesium Sulphate and Boric Acid. From Lurton (2010).

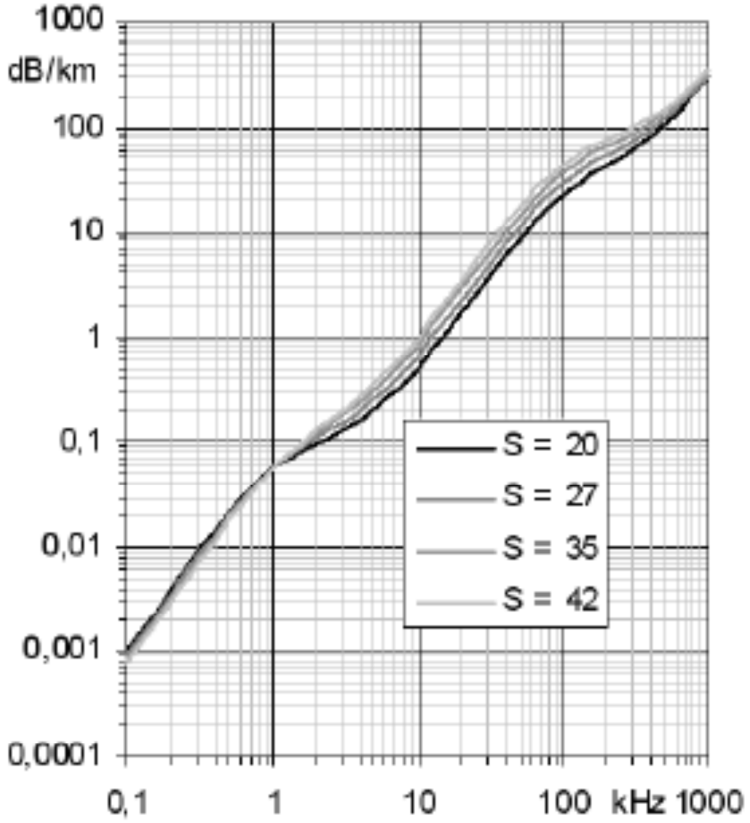

Figure 6.4 (Repeated from Figure 2.9): Sound absorption in sea water as a function of frequency, showing the influence of salinity, for a reference temperature T=15°C and depth z=0. From Lurton (2010).

Water temperature and salinity also have direct effects on sound speed. For depths less than 1000 m, the agreed formula for sound velocity is (Medwin 1975):

$$c = 1449.2 + 4.6T - 0.055T^2 + 0.00029T^3 + (1.34 - 0.01T)(S - 35) + 0.016z \quad (6.1)$$

where c is the sound velocity, in m/s, T is the temperature, in °C, z is the depth, in m and S is the salinity, in p.s.u.

Figure 4.1 shows the variations in temperature and salinity in Kongsfjord. Between the surface and water layers less than 20 m deep, the salinity would change by 0.5 p.s.u (31.5 p.s.u to 32.0 p.s.u) and the temperature by 0.5°C (2°C to 2.5°C). This would yield a change in sound velocity of 3 m/s (from 1456.5 m/s to 1453.5 m/s), i.e. 0.2% between the surface and 20 m deep.. Using the sound speed equation of Medwin (1975) to investigate the effects of fresh water (S = 0.5 p.s.u) and the near-constant temperature of the water in the laboratory

(T = 15°C), the sound velocity is c = 1474.6 m/s at z = 1 m. This is less than 20 m/s faster than in the field experiments (i.e. 1.2%). These changes in sound velocity affect the time at which different acoustic sources would be measured. This might be significant if using several hydrophones to estimate ranges or directions (the largest sound velocity difference of 20 m/s would, at distances of 20 m for the growlers in the ice fields, correspond to 0.2 ms differences in potential arrival times, i.e. 19 samples when measuring at 96 kHz). Because the times of arrival were not used in this study, these small depth, temperature and salinity variations are considered small enough that they cannot affect the comparison of the Arctic measurements with the field experiments.

CHAPTER 7 – CONCLUSIONS

7.1. SUMMARY OF FINDINGS

The specific aims of this PhD project were:

- Review the acoustic contributions of specific weather patterns to ambient noise in the ocean and how they can be used in monitoring efforts, in particular in polar regions;

  A significant body of literature was found relating to the noise of weather patterns underwater. The frequency range of such processes was found to be 1 – 50 kHz, with corresponding audible ranges of 1 km to tens of kilometres. Other sources of underwater noise were investigated. Around the frequencies applicable to weather-related noise, potential noise sources include seismic and volcanic activity, wave turbulence and biological noise. The extensive body of literature on acoustic noise underwater is based on theory as well as tank experiments and field measurements in a variety of conditions and locations. The basic physical mechanisms for rain, wind and shipping are well understood, even if the exact frequency ranges and amplitudes vary significantly. Biological sources of ambient noise are increasingly better constrained, as shown in the recent review by de Ruiter (in Lurton, 2010). Conversely, noise caused by ice has been studied mostly at lower (< 1 kHz) frequencies, concentrating on pack ice. And the combination of all these processes in regions such as the Arctic has been poorly studied. The findings of this review formed part of a chapter in Lurton (2010) which is included in Appendix A.3.

- Analyse a dataset acquired in the Arctic (Kongsfjord, Svalbard) in varied conditions and identify the different acoustic processes;

  A collection of recordings of ambient noise were obtained using a single hydrophone in the summer of 2007 in Kongsfjord, covering varying levels of rain, wind, ice, shipping and animal activity. Weather-focused analyses of ambient noise carried out by other teams had used the comparison of noise levels at pairs of frequencies (or frequency bands) in order to separate the different weather types present, similarly to the rainfall classification algorithms used in laser disdrometers. These methods were used successfully but rarely included a rigorous justification of the selection of the frequencies used. This, along with the size of the dataset implied that Principal Components Analysis could be a useful tool to select the most appropriate frequencies.

  When a Principal Components Analysis was performed on the Arctic dataset, three components were identified which successfully separated the different weather events. These frequency bands were also shown to work with some success on tank experiments but the method of Principal Components Analysis was less successful on a further dataset obtained in a temperate fjord in British Columbia. It is suspected that it was less successful here because there was less noise variation between the different sound files in this dataset, which implies that the ideal solution to a present weather classification algorithm could include a combination of the identification of the noise levels at particular frequencies used by other authors in less variable areas, with a Principal Components Analysis method to identify the weather in a more repeatable manner in a variety of different environments.

- Identify and distinguish the contribution of ice-related processes to the overall ambient noise

  The third component identified showed frequency contributions at a range of frequencies, including some as high as 45 kHz. At first it was suspected that this contribution was due to noise from ice, shipping or marine animals such as the whale spotted nearby. After further analyses of the sound files and tank experiments attempting to recreate the ice observed, it was discovered that ice melting, scraping and colliding can cause noise at frequencies as high as 30 kHz, which is considerably higher than the frequencies previously associated with noise from ice. It was also found that the method of creation of an ice block will affect its noise (confirming the work of others) at frequencies from 1-5 kHz, as well as 17 and 89 kHz. Noise from colliding ice blocks showed increased amplitudes from the background noise at 0-25 kHz, in particular below 10 kHz. Noise from scraping ice blocks produced increases in amplitude compared to the background noise of around 1 dB at 10 – 20 kHz. Spikes in amplitude were also observed at 3 kHz for scraping ice and at 19 and 7 kHz for colliding ice, whereas the melting ice did not show any significant spikes in amplitude. After investigations into the sound created by melting ice with bubbles present, it was found that the noise recorded has peaks in amplitude at frequencies which were in the broad range given theoretically by the Minnaert equation.

7.2. FUTURE WORK

The present study has focused on the analysis of a broadband dataset acquired in an Arctic fjord (Kongsfjord, Svalbard), in summer 2007. Analyses at higher than usual frequencies show the potential for identifying specific processes associated to the melting of glaciers and icebergs. This was checked using laboratory measurements of specific processes, in particular the melting of ice blocks with bubble inclusions, their scraping and their colliding in controlled conditions.

These results paved the way for the design of measurements at other glaciers in Svalbard (Hornsund Fjord and Murchison Fjord) in summer 2009 (Tegowski et al. 2011). The field work was done by the University of Gdansk (PI: Prof J. Tegowski), using a calibrated

omnidirectional broadband hydrophone and digital recorder (designed by Dr G. Deane, Scripps Institution of Oceanography, USA) and in collaboration with the University of Bath (Dr Ph. Blondel). The data recorded was made available in October 2010, after I had left the University of Bath, and therefore could not be analysed during this PhD. The setup and mode of deployment drew heavily on the ARCFAC-2007 experience. The main differences were *in situ* calibration of the recorder and gain settings (with a white noise generator), longer recording times (ca. 2 hours each time) and continuous GPS monitoring (because of the drifting induced by very strong currents and affecting the stationarity of the measurements).

Both sets of measurements highlighted key issues to be factored in the design of an experiment to improve understanding of sound sources in an Arctic fjord:

- Portability

  Proximity to sound sources means the ability to navigate in shallow water, between growlers or close to glaciers. The equipment used therefore needs to be small enough to fit on a small boat (e.g. **rigid-**hulled **inflatable** boat) and portable enough to be deployed from this boat and easily recovered (for safety reasons, as Arctic weather can change very rapidly). Alternately, it could be attached to a drifting or moored buoy, or deployed at depth for later recovery (requiring adequate battery power and pressure housing). The current setup of one (or several) hydrophones and a digital recorder seems well suited. One can note it is also the type of setup adapted by commercial instruments (e.g. JASCO Research, Canada).
- Calibration

  Calibration is a very important issue. The equipment used for ARCFAC 2007 was not fully calibrated: although the hydrophone manufacturer issued a generic calibration curve, the recording equipment was not fully calibrated. Individual hydrophone calibration can be checked in the laboratory, although calibration at lower frequencies (< 1 kHz) would require large ranges, only achievable in calibration ranges such as those of the National Physical Laboratory (NPL, UK). Recorder calibration can be achieved using a white noise generator replacing the hydrophone(s).
- Recording lengths and analysis times

Long recording times are preferable to look at long-lasting processes, or to make sure short, transient events, like the calving of a glacier front, are not missed. They lead however to very large datasets (2 hours of high-quality 16-bit recording, sampled at 96 kHz, would yield over 1 GB of uncompressed data) and might not be compatible with the amount of storage available. Conversely, short recording times save on power and storage requirements but need careful tailoring of the duty cycles to the processes of interest (e.g. rain episodes vs. glacier melting). The duration of the acoustic segments also needs to be related to the sampling frequency (to get enough samples for valid statistical analyses) and the process observed. Many of the current efforts use segment lengths of 0.1 to 1 second, over recording times varying between minutes and hours or even weeks.

- Processing methodology

  The use of sound pressure levels at specific frequencies requires accurate calibration of the hydrophones and a good understanding of the ambient noise field in the area being considered, so these would need to be considered before the experiments. Processing would ideally combine these identification methods with techniques such as Principal Component Analyses if there is enough acoustic variability in the entire dataset. For example, the sound pressure levels could be used to identify whether the main source of noise originated from wind, rain or ice etc., the spectrum shape and slope would assess wind speed or droplet size, and Principal Components Analyses could be used to further characterise these and other sources like those related to floating ice or glaciers.

- Identification of sound sources

  Sound sources can be identified from their absolute source pressure levels (if calibrated) and from their frequency spectrum (e.g. for rain or wind speed). More localised sources, like melting growlers or colliding ice blocks, can also be identified from their frequency spectra, but identification is often desirable in terms of range and bearing. Directional hydrophones are available but run the risk of missing events just outside their “field of view”. Omnidirectional hydrophones, cheaper and more versatile, are generally preferred. They can be arranged as 1-D, 2-D or 3-D arrays, and at least 3 are

required to estimate directions in the X-Y (bearing) and X-Z (depth difference) planes. Time differences between hydrophones can also be used to determine the ranges of the different sources. Hydrophones in these arrays need to be accurately positioned in water (to avoid angular offsets, for example) and their angle/time resolutions affect how far they need to be deployed to resolve specific events. In the case of independent hydrophones (e.g. on separate buoys), relative positions and timestamping will become additional issues, along with sound propagation underwater. Finally, the presence of several hydrophones will also affect data storage requirements.

- Environmental information

  Section 6.5 showed the effects of salinity and temperature on sound propagation and attenuation underwater. Ideally, these parameters should be measured regularly through the recordings, close to the recording station(s) and further afield.

  Other measurements of interest include the sea state and weather. This can be done via photo/video evidence, as in ARCFAC 2007, where the wave heights could be related to specific sea states, rain levels could be qualitatively compared between one measurement and the next, and ice cover/types could also be estimated. In the case of glaciers, video can show whether acoustic events are related to physical changes at the front of the glacier (calving, fall of one large block of ice or several smaller blocks) or other changes (e.g. strong currents produced by melting at the base of the glacier). Another advantage of attaching the system to a buoy is that it may contain an automated weather system. This would enable a more accurate value of the wind speed at that precise location. Perhaps the system could also contain some way of recording the rainfall rate and drop size distribution, and if this was not deemed to be possible then satellite data could be used for the comparison for a thorough assessment of the effectiveness of the processing algorithms.

7.3. POTENTIAL APPLICATIONS

Principal-Component Analysis is shown to be a valuable and rigorous tool for identifying weather processes at sea, especially in complex combinations of wind, rain, ice and other factors. Analyses at frequencies higher than generally used also offer the potential of identifying specific processes associated to the melting of glaciers and icebergs. This has paved the way for field measurements at glaciers around Svalbard in summer 2009. The approach presented here is now considered by the Meteorological Office (UK) for inclusion on operational present-weather sensors attached to moored or drifting buoys in polar and high-latitude regions in general.

REFERENCES

M. A. Ainslie (2010). Principles of Sonar Performance Modelling. Berlin, Springer.

T. Alsarayreh and L. Zedel (2009). Snow falling on water, does it really make noise? Underwater Acoustic Measurements: Technologies & Results, Greece.

W. Au and M. Hastings (2008). Principles of marine bioacoustics, Springer.

A. Barker and G. Timco (2002). "Laboratory experiments of ice scour processes: rigid ice indentor." Cold Regions Science and Technology **35**: 196.

R. G. Barry and R. J. Chorley (1998). Atmosphere, Weather and Climate. London, Routledge.

D. J. Bartholomew, et al. (2008). Analysis of multivariate social science data London, CRC Press.

P. G. Black, et al. (1997). "Oceanic rainfall detection and classification in tropical and subtropical mesoscale convective systems using underwater acoustic methods." Monthly Weather Review **125**(9): 2014.

P. Blondel and B. J. Murton (1997). Handbook of seafloor sonar imagery, PRAXIS - Wiley & Sons.

M. J. Buckingham (1987). "Theory of 3-Dimensional Acoustic Propagation in a Wedge-Like Ocean with a Penetrable Bottom." Journal of the Acoustical Society of America **82**(1): 198.

M. J. Buckingham (1997). "Sound speed and void fraction profiles in the sea surface bubble layer." Applied Acoustics **51**(3): 225.

M. J. Buckingham (2005). Acoustical remote sensing of the sea bed using propeller noise from a light aircraft. Sounds in the Sea: from Ocean Acoustics to Acoustical Oceanography. H. Medwin. Cambridge, Cambridge University Press**:** 581.

P. W. Cleary, et al. (2007). "Bubbling and frothing liquids." ACM Transactions on Graphics **26**(3): 97.

F. Cottier, et al. (2005). "Water mass modification in an Arctic fjord through cross-shelf exchange: The seasonal hydrography of Kongsfjorden, Svalbard." Journal of Geophysical Res. **110**.

G. B. Deane (2000). "Long time-base observations of surf noise." Journal of the Acoustical Society of America **107**(2): 758.

O. I. Diachok and R. S. Winokur (1974). "Spatial variability of underwater ambient noise at the Arctic ice-water boundary." Journal of the Acoustical Society of America **55**: 750.

R. F. Dwyer (1981). FRAM II single channel ambient noise statistics. Naval Underwater Systems Centre Tech. Doc**:** 6583.

D. M. Farmer and Y. Xie (1989). "The sound generated by propagating cracks in sea ice." Journal of the Acoustical Society of America **85**(4): 1489.

S. Farooq. "Spectral reflectance of land covers." Retrieved 5/2/2011, 2011, from http://www.cps-amu.org/sf/notes/m1r-1-8.htm.

C. Fowler, et al. (2003, July 2008). "AVHRR Polar Pathfinder Twice-Daily 5 km EASE-grid Composites." 3. Retrieved 05/02/2011, 2011, from http://nsidc.org/data/docs/daac/nsidc0066_avhrr_5km.gd.html.

G. J. Franz (1959). "Splashes as sources of sound in liquids." Journal of the Acoustical Society of America **31**: 1080.

Gammon (1983). Proceedings of Offshore Technology Conference OTC.

R. D. Gaul, et al. (2007). "Ambient noise analysis of deep-ocean measurements in the northeast pacific." IEEE Journal of Oceanic Engineering **32**(2): 497.

O. A. Godin (2006). "Anomalous transparency of water-air interface for low-frequency sound." Physical Review Letters **97**(16): 164301.

A. J. Gow (1968). Bubbles and bubble presusres in Antarctic glacier ice. US Army Cold Regions Res. and Engng. Lab. Hanover N.H.
C. R. Greene and B. Buck (1964). "Arctic Ocean ambient noise." Journal of the Acoustical Society of America **36**: 1218.
M. G. Gross (1990). Oceanography. Ohio, Merrill Publishing Company.
J. G. Harvey (1982). Atmosphere and Ocean - Our Fluid Environments. London, Artemis Press.
H. Hop, et al. (2002). "The marine ecosystem of Kongsfjorden, Svalbard." Polar Research **21**: 167.
J. A. Howe, et al. (2003). "Multibeam bathymetry and the depositional environments of Kongsfjorden and Krossfjorden, western Spitsbergern, Svalbard." Polar Research **22**(2): 301.
J. Hulbert (1973). The World's Weather. Oxford, Pergamon.
R. T. Iwase, Kikuchi, T. Tsuchiya, K. Mizutani (2008). Long-term deep seafloor ambient noise observation by a cabled observatory off Hatsushima Island in Sagami Bay, Central Japan. Proc. 8th European Conference on Underwater Acoustics, Portugal.
M. Keogh and P. Blondel (2008). "Passive acoustic monitoring of ocean weather patterns." Proceedings of the Institute of Acoustics **30**(5).
M. Keogh and P. Blondel (2009). Underwater monitoring of polar weather: Arctic field measurements and tank experiments. Proc. 3rd Underwater Acoustic Measurements Conference (UAM-2009), Nafplion, Greece.
B. Kipple and C. Gabriele (2003). Glacier Bay Underwater Noise - August 2000 Through August 2002: Technical Report NSWCCD-71-TR-2004/521, Naval Surface Warfare Center.
D. P. Knobles, et al. (2008). "Analysis of wind-driven ambient noise in a shallow water environment with a sandy seabed." Journal of the Acoustical Society of America **124**(3): EL157.
V. O. Knudsen, et al. (1948). "Underwater Ambient Noise." Journal of Marine Research **7**: 410.
A. Kruss, et al. (2008). "Estimation of macrophytes using single-beam and multibeam echosounding for environmental monitoring of Arctic fjords (Kongsfjord, West Svalbard Island)." Journal of the Acoustical Society of America **123**(5(2)): 3213.
NOAA AOML. "Real time current measurement system." Retrieved 04/08/2010, 2010, from http://www.aoml.noaa.gov/themes/CoastalRegional/cr_coastal_regional_adaptive_control.html.
F. Laville, et al. (1991). "Underwater Sound Generation by Rainfall." Journal of the Acoustical Society of America **89**(2): 715.
T. G. Leighton (1994). The acoustic bubble. London, Academic Press.
D. D. Lemon, et al. (1984). "Acoustic Measurements of Wind-Speed and Precipitation over a Continental-Shelf." Journal of Geophysical Research-Oceans **89**(Nc3): 3462.
T. M. Lillesand, et al. (2004). Remote sensing and image interpretation. Hoboken, N.J., John Wiley & Sons.
X. Lurton (2004). An Introduction to Underwater Acoustics. Chichester, Praxis Publishing.
X. Lurton (2010). An Introduction to Underwater Acoustics. Chichester, Praxis Publishing.
B. A. Ma, et al. (2005). "Prediction of underwater sound levels from rain and wind." Journal of the Acoustical Society of America **117**(6): 3555.
B. B. Ma and J. A. Nystuen (2005). "Passive Acoustic Detection and Measurement of Rainfall at Sea." Journal of Atmospheric and Oceanic Technology **22**(8): 1225.
J. D. Macpherson (1962). "Some under-ice acoustic ambient noise measurements." Journal of the Acoustical Society of America **34**: 1149.
V. Makarov. (2002). "Barentsburg, Russian settlements on Svalbard." Retrieved 12/02/2011, 2011, from http://www.russia.no/regional/svalbard/svalbard-map-4.jpg.

D. F. Mccammon and S. T. Mcdaniel (1985). "The Influence of the Physical-Properties of Ice on Reflectivity." Journal of the Acoustical Society of America **77**(2): 499.
S. O. Mcconnell, et al. (1992). "Ambient noise measurements from 100 Hz to 80 kHz in an Alaskan fjord." Journal of the Acoustical Society of America **91**(4 Pt 1): 1990.
M. A. Mcdonald and C. G. Fox (1999). "Passive acoustic methods applied to fin whale population density estimation." Journal of the Acoustical Society of America **105**(5): 2643.
H. Medwin and M. M. Beaky (1989). "Bubble sources of the Knudsen sea noise spectra." Journal of the Acoustical Society of America **86**(3): 1124.
H. Medwin, et al. (1988). "Low-Frequency Backscatter from Arctic Leads." Journal of the Acoustical Society of America **83**(5): 1794.
H. Medwin and C. S. Clay (1998). Fundamentals of Acoustical Oceanography. London, Academic Press.
H. Medwin, et al. (1990). "Impact and bubble sound from raindrops at normal and oblique incidence." Journal of the Acoustical Society of America **88**(1): 413.
D. K. Mellinger, et al. (2000). "Characteristics of minke whale (Balaenoptera Acutorostrata) pulse trains recorded near Puerto Rico." Marine Mammal Science **16**(4): 739.
Met Office UK (1999). "The Beaufort Scale of wind force." Retrieved 14/09/08, 2008, from http://www.stvincent.ac.uk/Resources/Weather/Charts/beaufort.html.
A. R. Milne (1967). "Sound propagation and ambient noise under sea ice." Underwater acoustics **2**: 120.
M. Minnaert (1933). "On musical air-bubbles and sounds of running water. ." Phil. Mag. **16**: 235.
G. Montero Martínez, et al. (2009). "Do all raindrops fall at terminal speed?" Geophysical Research Letters **36**(11).
National Park Service. (2011, 05/02/2011). "Glacier Bay Park and Reserve - Sounds Recorded in Glacier Bay." Retrieved 05/02/2011, 2011, from http://www.nps.gov/glba/naturescience/soundclips.htm.
National Weather Service. (2004). "National Weather Service Observing Handbook No. 1." Retrieved 06/08/10, 2010, from http://www.nws.noaa.gov/om/marine/handbk1.pdf.
J. A. Nystuen (1986). "Rainfall Measurements Using Underwater Ambient Noise." Journal of the Acoustical Society of America **79**(4): 972.
J. A. Nystuen (2001). "Listening to Raindrops from Underwater: An Acoustic Disdrometer." Journal of Atmospheric and Oceanic Technology **18**(10): 1640.
J. A. Nystuen and D. M. Farmer (1987). "The influence of wind on the underwater sound generated by light rain." Journal of the Acoustical Society of America **82**: 270.
J. A. Nystuen and B. M. Howe (2005). Ambient Sound Budgets. Underwater Acoustic Measurements: Technologies & Results, Crete, Greece.
J. A. Nystuen and H. D. Selsor (1997). "Weather classification using passive acoustic drifters." Journal of Atmospheric and Oceanic Technology **14**(3): 656.
H. N. Oguz and A. Prosperetti (1991). "Numerical-Calculation of the Underwater Noise of Rain." Journal of Fluid Mechanics **228**: 417.
F. A. Payne (1964). "Effect of ice-cover on shallow water ambient sea noise." Journal of the Acoustical Society of America **36**: 1943.
F. A. Payne (1967). "Further measurements on the effect of ice cover on shallow-water ambient sea noise." Journal of the Acoustical Society of America **41**: 1374.
K. W. Peters (1979). Ambient noise levels in the marginal sea-ice zone east of Greenland, Naval postgraduate school, Monterey CA. **Master's Thesis**.
W. Press (1999). Numerical recipes in C: the art of scientific computing, Cambridge University Press.
H. C. Pumphrey (1989). Sources of ambient noise in the ocean: an experimental investigation, University of Mississipi. **PhD Thesis**.
H. C. Pumphrey (1991). "Underwater rain noise - the initial impact component." Proceedings of the Institute of Acoustics **13**: 192.

H. C. Pumphrey, et al. (1989). "Underwater Sound Produced by Individual Drop Impacts and Rainfall." Journal of the Acoustical Society of America **85**(4): 1518.
H. C. Pumphrey and A. J. Walton (1988). "Experimental study of the sound emitted by water drops impacting on a water surface." European Journal of Physics **9**: 225.
Quartly (2010). "Improving the altimetric rain record from Jason-1 and Jason-2." Journal of geophysical research **115**(C3).
G. D. Quartly, Gregory, J.W., Guymer, T.H., Birch, K.G., Jones, D.W., Keogh, S.J. (2001). "How reliable are acoustic rain sensors?" Proceedings of Acoustical Oceanography 2001: 142.
S. Ramji, et al. (2008). "Wind dependence of ambient noise in shallow water of Bay of Bengal." Applied Acoustics **69**(12): 1294.
R. Reynolds (2006). Guide to Weather. London, Philip's.
I. Robinson (2004). Measuring the Oceans from Space – The Principles and Methods of Satellite Oceanography. Chichester, Praxis Publishing Ltd.
SCAR (2004). SCAR report on marine acoustic technology and the Antarctic environment (Information Paper IP 078). XXVII Antarctic Treaty Consultative Meeting ATCM. Cape Town, South Africa**:** 17.
H.-W. Schenke. (2011). "Alfred Wegener Institute for Polar and Marine Research (AWI) Fram Strait - Bathymetry." Retrieved 08/02/2011, 2011, from http://www.awi.de/en/research/research_divisions/geosciences/marine_geology_and_paleontology/research_themes/bathymetry_and_geodesy/bathymetric_chart_of_the_fram_strait_bcfs/fram_strait_bathymetry.
P. F. Scholander and D. C. Nutt (1960). "Bubble pressure in Greenland icebergs." Journal of Glaciology **3**(28): 671.
J. A. Scrimger, et al. (1987). "Underwater Noise Due to Rain, Hail, and Snow." Journal of the Acoustical Society of America **81**(1): 79.
M. C. Serreze, Francis, J. A., (2006). "The Arctic on the fast track of change." Weather **61**(3): 65.
D. Stansfield (1991). Underwater Electroacoustic Transducers, Bath University Press and Institute of Acoustics.
J. Szczucka (2009). Acoustic studies of diving birds in the Arctic. Underwater Acoustic Measurements: Technologies & Results, Greece.
J. Tegowski (2004). "A laboratory study of breaking waves." Oceanologia **46**(3): 365.
Tegowski, J. G.B. Deane, A. Lisimenka, Ph. Blondel (2011), "Detecting and analysing underwater ambient noise of glaciers on Svalbard as indicator of dynamic processes in the Arctic", Proc. 4th Underwater Acoustic Measurements Conference, 1149-1154.
P. D. Thorne (1985). "The measurement of acoustic noise generated by moving artificial sediments." Journal of the Acoustical Society of America **78**(3): 1013.
P. D. Thorne (1993). Seabed saltation noise. Natural physical sources of underwater sound, . Dordrecht, Kluwer Academic**:** 721.
S. T. Thoroddsen, et al. (2003). "Air entrapment under an impacting drop." Journal of Fluid Mechanics **478**: 125.
R. J. Urick (1971). "Noise of Melting Icebergs." Journal of the Acoustical Society of America **50**(1): 337.
R. J. Urick (1972). "Noise Signature of an Aircraft in Level Flight over a Hydrophone in the Sea." Journal of the Acoustical Society of America **52**(3B): 993.
Urick (1975). Principles of Underwater Sound, McGraw Hill.
R. J. Urick (1986). Ambient noise in the sea. Los Altos, California, Peninsula Publishing.
P. Wadhams (2000). Ice in the Ocean, Gordon and Breach.
G. M. Wenz (1962). "Acoustic Ambient Noise in the Ocean: Spectra and Sources." Journal of the Acoustical Society of America **34**: 1936.

J. D. Wilson and N. C. Makris (2008). "Quantifying hurricane destructive power, wind speed, and air-sea material exchange with natural undersea sound." Geophysical Research Letters **35**(10).
O. B. Wilson (1988). Introduction to Theory and Design of Sonar Transducers. CA, USA, Peninsula Publishing.
Y. B. Xie and D. M. Farmer (1991). "Acoustical Radiation from Thermally Stressed Sea Ice." Journal of the Acoustical Society of America **89**(5): 2215.